



U.S. Department
of Transportation
**Federal Highway
Administration**

Publication No. FHWA-RD-89-084
August 1989

Instrumentation for Flexible Pavements

Research, Development, and Technology
Turner-Fairbank Highway Research Center
6300 Georgetown Pike
McLean, Virginia 22101-2296

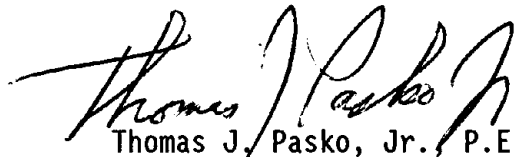
REPRODUCED BY
U.S. DEPARTMENT OF COMMERCE
NATIONAL TECHNICAL
INFORMATION SERVICE
SPRINGFIELD, VA 22161

FOREWORD

Pavement design is largely based on past experience and empirical data. More reliable data on the performance of current designs are needed for improving and optimizing future designs. One important indicator of pavement performance is the deflection under load. Numerous devices for applying loads to the pavement and measuring the resulting deflections are in use. Magnitude and mode of load application are different from the different devices. But pavement response depends on the mode and rate of load application. Therefore, interpretation of the measured deflections to derive the structural properties of the pavement layers is complex and the resulting data are highly variable. The primary advantages of deflection testing are the relative simplicity and the non-destructive nature of these tests.

Another way of measuring pavement performance is by gauges installed in the pavement. The obvious advantage is that pavement response is measured under real exposure conditions, i.e. traffic and environmental exposure. Such installations were made over the last 20 years but no completely satisfactory methods have been developed. Major difficulties are in the survivability of the gauges and the connections under the harsh conditions and the variability and inhomogeneity of the pavement structure which affect the readings. These problems can be partially overcome by installing redundant gauges. This increases the cost and the amount of data to be recorded.

This report describes the state-of-art of pavement instrumentation. It is based on a literature survey conducted under a research contract for "In-Situ Instrumentation for Resilient Moduli Measurement." The contract objectives are to investigate and test new concepts of pavement sensors suitable for large-scale field installation.



Thomas J. Pasko, Jr., P.E.
Director, Office of Engineering
and Highway Operations
Research and Development

NOTICE

This document is disseminated under the sponsorship of the Department of Transportation in the interest of information exchange. The United States Government assumes no liability for its contents or use thereof. The contents of this report reflect the view of the contractor, who is responsible for the accuracy of the data presented herein. The contents do not necessarily reflect the official policy of the Department of Transportation. This report does not constitute a standard, specification, or regulation.

The United States Government does not endorse products or manufacturers. Trade or manufacturers' names appear herein only because they are considered essential to the object of this document.

TECHNICAL REPORT STANDARD TITLE PAGE

1. Report No. FHWA-RD-89-084		PB91-162909		3. Recipient's Catalog No.	
4. Title and Subtitle INSTRUMENTATION FOR FLEXIBLE PAVEMENTS				5. Report Date August 1989	
				6. Performing Organization Code	
7. Author(s) Peter Sebaaly, Nader Tabatabaee, and Tom Scullion				8. Performing Organization Report No. PTI 8913	
9. Performing Organization Name and Address Pennsylvania Transportation Institute Pennsylvania State University Research Building B University Park, PA 16802				10. Work Unit No. 3C32312	
				11. Contract or Grant No. DTFH61-88-R00052	
12. Sponsoring Agency Name and Address Office of Engineering & Highway R & D Federal Highway Administration 6300 Georgetown Pike McLean, VA 22101-2296				13. Type of Report and Period Covered Interim Report July - September 1988	
				14. Sponsoring Agency Code	
15. Supplementary Notes FHWA Contract Manager (COTR): R. R. Hegmon (HNR-20)					
16. Abstract This report documents the findings of the literature search on instrumentation used in flexible pavements. The search covered areas such as strain, stress, deflection, temperature, moisture, load location, load magnitude, performance models, and backcalculation techniques. Each group of instrumentation was evaluated in terms of the design feasibility, cost, availability, and field performance.					
17. Key Words H-gauges, Bison coils, pressure cells, LVDT, geophone, accelerometer, SLD, MDD, thermocouples, RTD			18. Distribution Statement This document is available to the public through the National Technical Information Service, Springfield, VA 22161.		
19. Security Classif. (of this report) Unclassified		20. Security Classif. (of this page) Unclassified		21. No. of Pages 166	22. Price

SI* (MODERN METRIC) CONVERSION FACTORS

APPROXIMATE CONVERSIONS TO SI UNITS

Symbol	When You Know	Multiply By	To Find	Symbol
--------	---------------	-------------	---------	--------

LENGTH

in	inches	25.4	millimetres	mm
ft	feet	0.305	metres	m
yd	yards	0.914	metres	m
mi	miles	1.61	kilometres	km

AREA

in ²	square inches	645.2	millimetres squared	mm ²
ft ²	square feet	0.093	metres squared	m ²
yd ²	square yards	0.836	metres squared	m ²
ac	acres	0.405	hectares	ha
mi ²	square miles	2.59	kilometres squared	km ²

VOLUME

fl oz	fluid ounces	29.57	millilitres	mL
gal	gallons	3.785	litres	L
ft ³	cubic feet	0.028	metres cubed	m ³
yd ³	cubic yards	0.785	metres cubed	m ³

NOTE: Volumes greater than 1000 L shall be shown in m³.

MASS

oz	ounces	28.35	grams	g
lb	pounds	0.454	kilograms	kg
T	short tons (2000 lb)	0.907	megagrams	Mg

TEMPERATURE (exact)

°F	Fahrenheit temperature	5(F-32)/9	Celsius temperature	°C
----	------------------------	-----------	---------------------	----

APPROXIMATE CONVERSIONS FROM SI UNITS

Symbol	When You Know	Multiply By	To Find	Symbol
--------	---------------	-------------	---------	--------

LENGTH

mm	millimetres	0.039	inches	in
m	metres	3.28	feet	ft
m	metres	1.09	yards	yd
km	kilometres	0.621	miles	mi

AREA

mm ²	millimetres squared	0.0016	square inches	in ²
m ²	metres squared	10.764	square feet	ft ²
ha	hectares	2.47	acres	ac
km ²	kilometres squared	0.386	square miles	mi ²

VOLUME

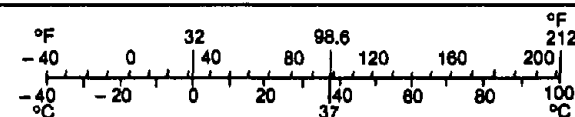
mL	millilitres	0.034	fluid ounces	fl oz
L	litres	0.264	gallons	gal
m ³	metres cubed	35.315	cubic feet	ft ³
m ³	metres cubed	1.308	cubic yards	yd ³

MASS

g	grams	0.035	ounces	oz
kg	kilograms	2.205	pounds	lb
Mg	megagrams	1.102	short tons (2000 lb)	T

TEMPERATURE (exact)

°C	Celsius temperature	1.8C + 32	Fahrenheit temperature	°F
----	---------------------	-----------	------------------------	----



* SI is the symbol for the International System of Measurement

(Revised April 1989)

TABLE OF CONTENTS

	<u>Page</u>
1. INTRODUCTION	1
2. DESCRIPTION OF VARIOUS TEST FACILITIES	3
Linear Test Tracks	3
FHWA ACCELERATED LOADING FACILITY	3
AUSTRALIAN ACCELERATED LOADING FACILITY	5
TRANSPORT AND ROAD RESEARCH LABORATORY	6
SOUTH AFRICA HEAVY VEHICLE SIMULATOR	6
DANISH ROAD TESTING MACHINE	6
SHELL TEST FACILITY	10
Circular Test Tracks	11
Test Roads with Controlled Loadings	11
VIRTAA TEST FIELD	11
NARDO TEST TRACK	11
PENNSYLVANIA TEST TRACK	13
TRRL FULL-SCALE EXPERIMENT	16
ALBERTA RESEARCH COUNCIL TEST PAVEMENT	16
3. STRAIN MEASUREMENT	19
Types of Strain Gauges	19
MECHANICAL DEVICES	19
OPTICAL DEVICES	20
ELECTRICAL DEVICES	20
UNBONDED METALLIC-FILAMENT STRAIN GAUGE	21
BONDED METALLIC-FOIL STRAIN GAUGE	21
SEMICONDUCTOR STRAIN GAUGE	21
Strain Measurement in Flexible Pavements	23
Strain Gauges for Bonded Layers	23
H-GAUGES	23
FOIL STRAIN GAUGES ON CARRIER BLOCK	32
FOIL STRAIN GAUGES CEMENTED TO CORES	36
STRAIN COILS	38
Methods of Installation	39
INSTALLATION OF H-GAUGES	39
INSTALLATION OF INSTRUMENTED CORES	40
Data Acquisition	41
Strain Measurement in Unbonded Material	42
BISON COILS	42
TRRL SOIL STRAIN GAUGE	44
INSTALLATION	44
Cost and Availability	47
Performance of Strain Gauges	47
4. PRESSURE MEASUREMENT	62
Basic Design Requirement	62
Types of Pressure Cells	69
TRRL/LVDT PRESSURE CELL	72
TRRL PIEZOELECTRIC PRESSURE CELL	72
NOTTINGHAM PRESSURE CELLS	75

	SE PRESSURE CELL	75
	WES SOIL PRESSURE CELLS	79
	KULITE PRESSURE CELL	79
	SOPT PRESSURE CELLS	79
	Installation	83
	PRESSURE CELLS IN THE SUBGRADE	86
	PRESSURE CELLS IN THE SUBBASE LAYER	86
	PRESSURE CELLS IN THE BASE LAYER	87
	Cost and Availability	88
	Performance of Pressure Cells	88
5.	DEFLECTION MEASUREMENT	93
	Acceleration-Measuring Devices	93
	Velocity-Measuring Devices	94
	Deflection-Measuring Devices	97
	SINGLE-LAYER DEFLECTOMETER	97
	MULTIDEPth DEFLECTOMETER	100
	Installation Procedure	100
	ACCELEROMETERS AND GEOPHONES	100
	BONDED LAYERS	104
	SINGLE-LAYER DEFLECTOMETER (SLD)	105
	MULTIDEPth DEFLECTOMETER	106
	Data Acquisition	106
	ACCELEROMETER	106
	GEOPHONES	107
	SINGLE-LAYER DEFLECTOMETER	107
	MULTIDEPth DEFLECTOMETER	108
	Cost and Availability	108
	ACCELEROMETERS AND GEOPHONES	108
	SINGLE-LAYER DEFLECTOMETER (SLD)	108
	MULTIDEPth DEFLECTOMETER	108
	Repeatability of Multidepth Deflectometer	110
6.	TEMPERATURE MEASUREMENT	112
	Types of Temperature Gauges	112
	THERMOCOUPLES	112
	METAL FILM RTDs	114
	THERMISTOR PROBES	116
	MONOLITHIC INTEGRATED CIRCUITS	117
	Installation of Temperature Transducers in Flexible Pavements.	117
	Cost and Availability	119
	Performance	119
7.	MOISTURE MEASUREMENT	122
	Moisture Content Sensor	122
	INSTALLATION	123
	CALIBRATION	123
	Suction Measurement Sensor	123
	INSTALLATION	125
	CALIBRATION	125
	Recommendation	125
8.	AXLE LOAD MEASUREMENT	126

9.	VEHICLE TRANSVERSE LOCATION SENSORS	132
	Types of Transverse Location Sensors	132
	PHOTOELECTRIC SYSTEM	132
	LASER-GUIDED SYSTEM	134
	ULTRASONIC SYSTEM	136
10.	PAVEMENT PERFORMANCE MODELS	140
	PDMAP Pavement Performance Models	141
	Texas Transportation Institute Pavement Performance Model	142
	Vesys Pavement Performance Model	144
11.	GENERALIZED MODULUS BACKCALCULATION PROCEDURE	147
12.	REFERENCES	153

LIST OF FIGURES

<u>Figure</u>	<u>Page</u>
1. Photo of ALF	4
2. TRRL loading machine	7
3. View of the HVS machine	8
4. Plan and section view of Danish Road Testing Machine	9
5. Plan of Nardo test track	14
6. View of the Pennsylvania test track	15
7. Plan and cross section of Alberta Research Council test section	17
8. A typical wire strain gauge	22
9. A typical foil strain gauge	22
10. A typical semiconductor gauge	22
11. TRRL H-gauges	25
12. H-gauge designed by NIRR	26
13. H-gauge used by Australian team at Nardo Road Test	28
14. H-gauge used by French team at Nardo Road Test	29
15. H-gauges used by Swiss team at Nardo Road Test	30
16. H-gauge used by Danish team at Nardo Road Test	31
17. Different layers of modified Danish H-gauges	33
18. Design details and specifications of modified Danish H-gauges	34
19. Encapsulated strain gauge or strip gauge (all dimensions in millimeters)	35
20. Block-type strain gauge transducer used by researchers from Finland at Nardo Road Test	35
21. Block-type strain gauge transducer used by researchers from Germany at Nardo Road Test	37
22. Early TRRL soil strain gauge	45
23. Recent TRRL soil strain gauge	46
24. Ratio of measured to calculated strains for the Nardo Road Test	54
25. Strain measured during load-up study for testing of section 2.3	56
26. Comparison of measured and calculated peak stress and strain values for different climatic conditions	61
27. Stress distribution around embedded pressure cells	63
28. Variation of pressure cell registration with flexibility factor	65
29. Comparison of theoretical pressure cell registration for zero stress ratio	66
30. Comparison of theoretical pressure cell registration at various stress ratios	67
31. Typical diaphragm-type pressure cells	71
32. Two versions of hydraulic pressure cells	71
33. TRRL plan view and cross-sectional views of a TRRL/LVDT pressure cell	73
34. Cross sections of MK.I and MK.II piezoelectric pressure cells	74

35.	Plan and cross-sectional views of the Nottingham pressure cell	76
36.	Plan and cross-sectional views of an SE pressure cell . . .	77
37.	Kulite LQ-080U soil pressure cell	78
38.	Plan and cross-sectional views of a WES soil pressure cell	80
39.	Soil pressure cell type 0234	81
40.	SOPT soil pressure cell	84
41.	Comparison between measured and calculated vertical stresses and strains	92
42.	A typical accelerometer used for pavement instrumentation .	95
43.	Schematic of a geophone	96
44.	LVDI single layer deflectometer	98
45.	WES-designed soil deflection gauge	99
46.	The multidepth deflectometer	101
47.	Details of MDD installation	102
48.	MDD response under FWD loading (section 12)	103
49.	Typical thermocouple element assemblies	113
50.	A platinum RTD	115
51.	A solid-state temperature sensor	118
52.	Pavement temperature at the FHWA ALF site	121
53.	Cross section of the thermal moisture sensor	124
54.	Sketch of the loading plate for measuring the total load under dual tires	127
55.	Truck tire tester	129
56.	Wheel force transducer	130
57.	A high-intensity halogen bulb mounted under the test vehicle	133
58.	Two configurations for photo cell arrays	135
59.	Sketch of a laser beam attached to the side of a test truck	137
60.	Transmitting and receiving a sound pulse	138

LIST OF TABLES

<u>Table</u>		<u>Page</u>
1.	Properties of different circular testing machines.	12
2.	Specifications of Bison coils	43
3.	Cost and availability of strain gauges	48
4.	Variation of the required force versus thickness of strip .	52
5.	Strain gauge measurements during testing under ALF wheel load of 19,000 lb	57
6.	Long-term repeatability of Kyowa gauges	60
7.	Major factors affecting pressure cell registration	70
8.	Design specifications of type-0234 soil pressure cells . . .	82
9.	Specifications of SOPT pressure cells	85
10.	Cost and availability of pressure cells	89
11.	Cost and availability of accelerometers and geophones	109
12.	Cost and availability of temperature measuring devices . . .	120

1. INTRODUCTION

Full-scale pavement testing and in-situ instrumentation have received considerable attention recently. Various factors have driven the momentum into this area of research; among these are that (1) in-situ pavement responses can be used to verify mathematical models, (2) mechanistic design procedures can be developed based on the full-scale pavement response, and (3) in-situ material properties can be evaluated under various environmental conditions.

To verify mathematical models it is necessary to have multiple response measurements such as stresses, strains, or deflections. If a single response parameter is compared, then a perfect agreement can always be obtained by selecting the appropriate material properties. A certain type of response parameter should be used to evaluate the materials' properties, such as deflection. Then the other response parameters should be compared with the theoretical values. If the predicted material properties are realistic, the comparison between what is measured and what has been predicted should still be valid.

Mechanistic design procedures are needed to be able to transfer design methodologies from one region to another under different materials, load, or climatic conditions. An ideal mechanistic design procedure should be capable of predicting the response and the performance of pavement structures from the measured fundamental properties of the materials. The role of in-situ instrumentation is critical in developing and calibrating these mechanistic design procedures.

Material properties play an important role in any pavement design method. The determination of the materials' correct in-situ resilient modulus is a critical task. By examining the new AASHTO design equations, one can see that any small change in the resilient modulus of the subgrade or base course, on the order of 1 percent, would create a 2-percent change in the resulting structural number (SN). Whether the change in the SN is significant cannot be determined unless one looks at the resulting layers' thicknesses.

Considering all of these factors, one can conclude that not only better instrumentation is needed, but more effective methods of installation, calibration, protection against environmental effects, and better data acquisition techniques are necessary as well. This report reviews a large number of the existing instrumentation techniques applicable to flexible pavements.

2. DESCRIPTION OF VARIOUS TEST FACILITIES

Numerous test facilities have been built around the world to study the response of pavement structures under simulated or actual traffic loading. The majority of these facilities are aimed to conduct accelerated loading of pavements, which is usually achieved by increasing the load level beyond the legal load limit or increasing the frequency of load repetition on a given section. The advantages of these facilities are the capabilities of controlling the various test parameters such as load, tire pressure, tire type, material type, and material properties. Another advantage, which comes with the indoor loading devices, is the control of climatic conditions whereby the temperature and moisture content of the test section are controlled variables.

The various active test facilities around the world may be classified into three separate groups:

- Linear test tracks.
- Circular test tracks.
- Test roads with controlled loadings.

The following is a brief description of some facilities exemplifying the various groups. The selected facilities are the ones that have used some kind of instrumentation in the test sections.

LINEAR TEST TRACKS

FHWA ACCELERATED LOADING FACILITY

In 1985 the Federal Highway Administration (FHWA) sponsored a research program to develop a U. S. version of the Accelerated Loading Facility (ALF).^[11] The FHWA ALF is an outdoor loading device with an all-weather, computer-controlled operation and unassisted movement of the machine in a transverse direction. A photograph of the ALF is shown in figure 1. The

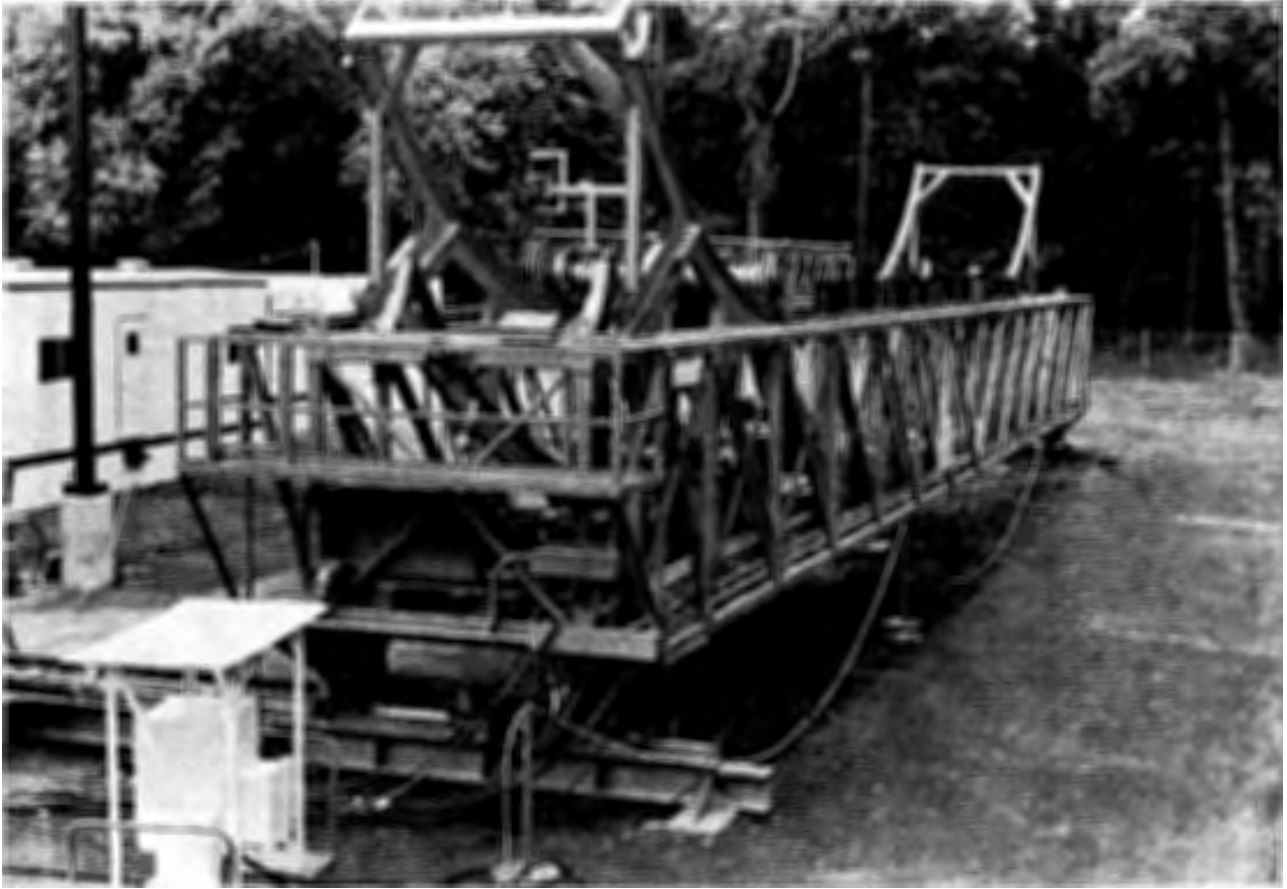


Figure 1. Photo of ALF.

machine is 105 ft (32 m) long, 13 ft (4 m) wide, and 19 ft (5.8 m) high, and weighs 120,000 lb (537.6 kN) fully assembled. The ALF requires little external power to operate because gravity is used to accelerate and decelerate the trolley assembly.

The test section is 40 ft (12.2 m) long and 13 ft (4 m) wide. Since the facility is outdoors, there are no restrictions on the thicknesses of the test sections and normal highway construction equipment can be used. The ALF applies load to the pavement through one set of dual truck tires. Investigations to retrofit a single wheel are underway by the FHWA. The load is applied through dead weights of steel plates placed on top of the loading wheels. The load that can be applied to the tires ranges from 9,400 to 22,500 lb (42 to 100 kN). The test wheels travel at 12.5 mi/h (20.1 km/h) over the entire test section. Loads are applied to the pavement only in one direction of wheel travel. The transverse position of the wheels can be varied across a 48-in (1.2-m) wheelpath.

The instrumentation in the pavement test section may be installed during the construction or retrofitted after the construction is completed. The test section may be instrumented with strain gauges, pressure cells, deflection gauges, or temperature and moisture gauges.

AUSTRALIAN ACCELERATED LOADING FACILITY

The Australian Accelerated Loading Facility (ALF) was designed and built by the Department of Main Roads in New South Wales.^[2] The overall dimensions of the machine are similar to the FHWA ALF. The load is applied through wheels at 12.5 mi/h (20.1 km/h). The load ranges between 9,000 and 18,000 lb (40.3 and 80.6 kN) and can be transversely varied across a 16- to 24-in (40.6- to 61-cm) wheelpath. The total length of the test section is about 40 ft (12.2 m) and could be either a special test section or a section of an inservice pavement.

TRANSPORT AND ROAD RESEARCH LABORATORY

The Transport and Road Research Laboratory (TRRL) built a linear motion machine that can traffic individual test sections.^[3] The load is applied through a single- or dual-wheel configuration traveling at a speed of 12.5 mi/h (20.1 km/h). The facility is housed inside a laboratory, and the test temperature can be controlled with the aid of infrared heaters. The machine can load sections in either one or both directions of motion. The test section is 33 ft (10 m) long, 8 ft (2.5 m) wide, and 10 ft (3 m) deep. The maximum load that can be applied is 22,500 lb (10 kN). Figure 2 shows a view of the TRRL loading machine.

SOUTH AFRICA HEAVY VEHICLE SIMULATOR

The National Institute for Road Research at South Africa has developed the Heavy Vehicle Simulator (HVS).^[4] This mobile machine can be driven under its own power from site to site and can be used to test both inservice roads and specially constructed experimental sections. It is 23 ft (7 m) in length, 12 ft (3.7 m) in height, and 8.3 ft (2.5 m) in width. The load is applied to the pavement through dual tracking wheels which accommodate various tire sizes. The HVS machine, shown in figure 3, is capable of loading in the forward and backward directions. The test section is 20 ft (6.1 m) long and 12 ft (3.7 m) wide. The load can be varied between 4,500 and 18,000 lb (20 and 80 kN). The lateral position of the wheel can be automatically changed during the testing to give a desired lateral distribution over 3.3 ft (1 m). The speed of the loading wheels is 9 mi/h (19.2 km/h); 800 wheel passes per hour or 18,000 wheel passes per day can be applied. The pavement section can be instrumented with various types of strain, deflection, and stress gauges.

DANISH ROAD TESTING MACHINE

The Danish Road Testing Machine (RTM) is a linear-tracked loading device designed in the early 1970's.^[5] It is a full-scale facility, with a width of 8.2 ft (2.5 m) and a length of 89 ft (27 m). A plan and a section view of the machine are shown in figure 4. The facility consists of (1) a test pit with automatic water-level control, (2) a wheel-loading system, (3) a climate

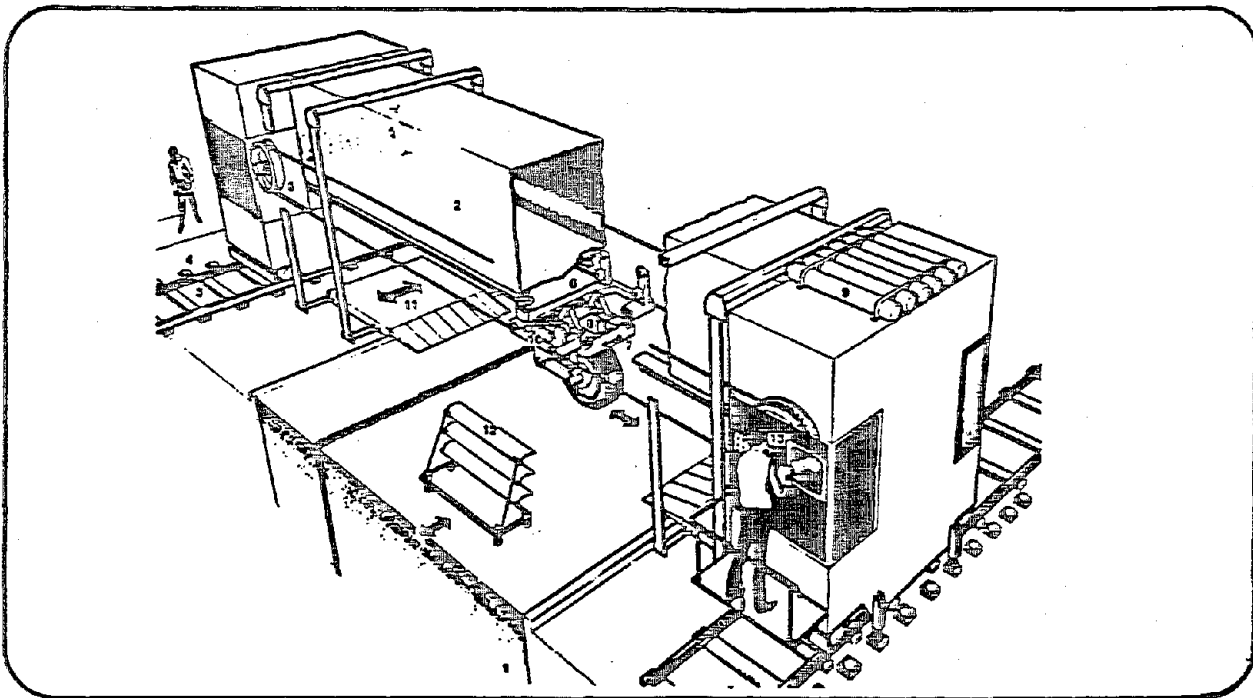
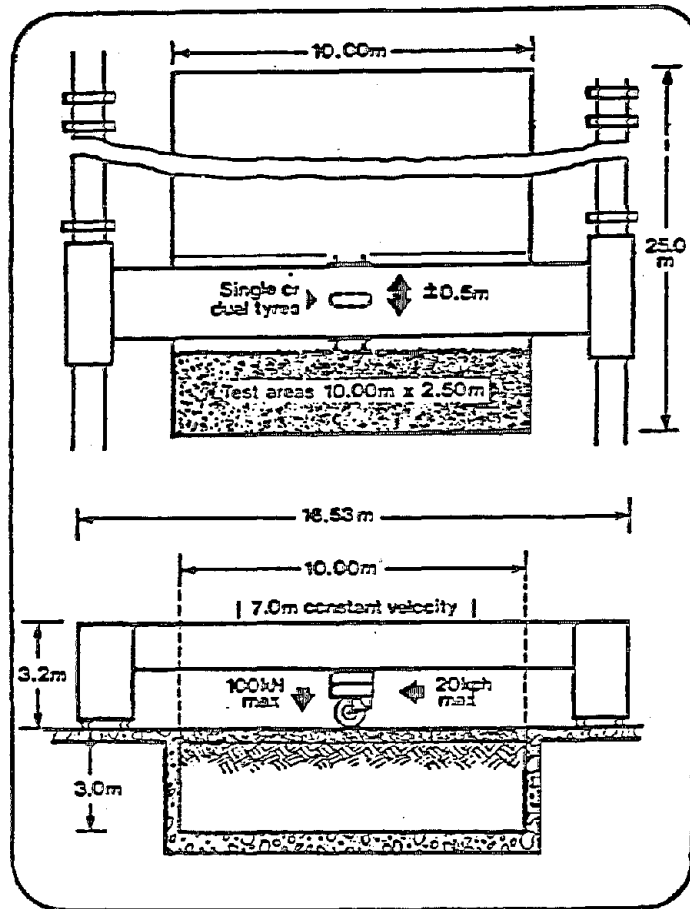


Figure 2. TRRL loading machine. [3]

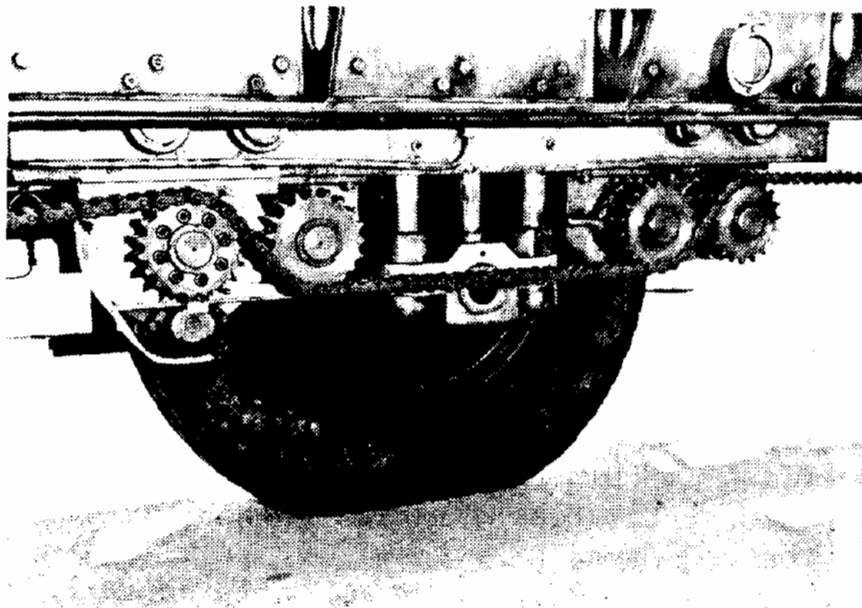
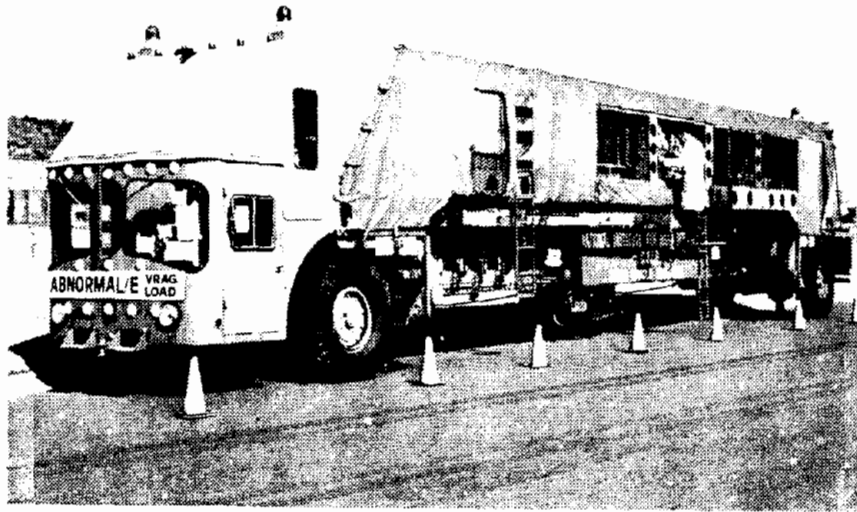


Figure 3. View of the HVS machine.^[4]

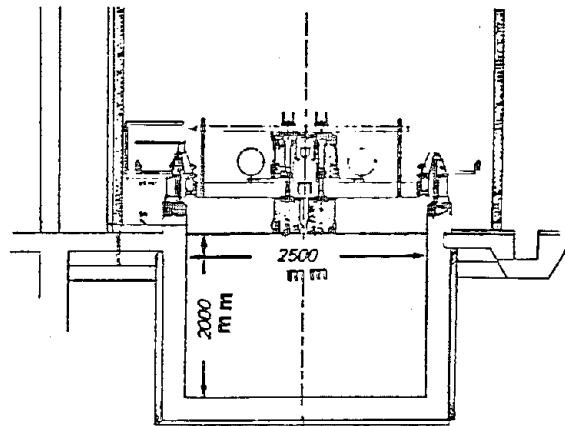
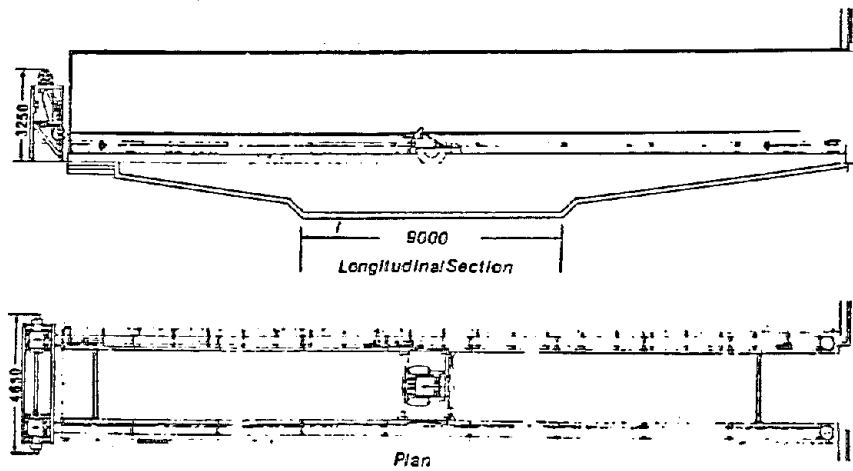


Figure 4. Plan and section view of Danish Road Testing Machine (RTM).^[5]

chamber, and (4) a system of transducers, amplifiers, and a data logger for measuring and recording stresses and strains. The RTM is enclosed in a climate chamber that is 13 ft (4 m) wide and 12.5 ft (3.8 m) high. Therefore, ordinary construction equipment can be used to construct the test pavements. The temperature range inside the climate chamber is between 14 °F and 104 °F (-10 °C and +40 °C).

The test section is 30 ft (9 m) long, 8.2 ft (2.5 m) wide, and 6.6 ft (2 m) deep (figure 4). The wheel load is hydraulically applied and may consist of a single or a dual wheel. The maximum dual wheel load is 14,600 lb (65 kN) and the maximum velocity is approximately 16 mi/h (25 km/h). The loads are applied in both directions. The lateral position of the wheels can be automatically changed during testing to give a desired lateral load distribution; 10,000 wheel passes may be applied during one 24-hour day.

During testing the pavements are instrumented with pressure cells, soil strain gauges, strain gauges in bonded materials, deflection gauges, and gauges for measuring temperature, frost penetration and, sometimes, soil suction.

SHELL TEST FACILITY

In the late 1960's, the Shell Laboratory at Hamburg, West Germany, constructed a straight road test track which permits variations in the road test construction as well as the control of the load and the speed of one wheel or twin wheels.^[6] The test area is 33 by 33 ft (10 by 10 m), with an additional 45-ft (13.6-m)-long track on both sides for the acceleration and deceleration of the loading equipment. The wheel load ranges between 1,000 and 4,000 lb per single wheel. The speed of the loading tire is between 0 and 30 mi/h (50 km/h). The 33- by 33-ft (10- by 10-m) test area can be constructed of two different test sections. Instrumentation such as strain gauges may be placed throughout the depth of the asphalt layers or pressure cells may be placed in the unbonded layers.

CIRCULAR TEST TRACKS

Circular tracking machines exist in a number of countries. In these, the experimented sections are constructed to form circular tracks with radii varying between 6.6 and 66 ft (2 and 20 m). A loading wheel, or bogie, anchored at the center of the track, is then propelled around the track. These circular tracking machines have the advantage that a number of different pavement structures can be tested simultaneously, and since the machines run practically unattended, the cost per section is relatively low. However, their disadvantage is that, when one of the sections fails, the entire operation must be brought to a halt while that section is replaced. Table 1 shows the various properties of different circular testing machines.

TEST ROADS WITH CONTROLLED LOADINGS


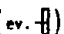


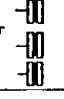

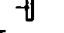



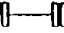

VIRTTAA TEST FIELD

The Virttaa test field is a temporary airfield in Finland. The overall length of the track is 1.9 mi (3 km). Regular truck traffic can easily attain a 50-mi/h (80-km/h) speed.^[3] The circulating time for a fully loaded truck is about 6 min, which means that the load can be applied at a rate of 10 passes per hour. The two instrumented flexible pavement sections, which have bituminous layers of thicknesses 3 and 6 in (80 and 150 mm), are instrumented with strain gauges, pressure cells, and temperature sensors. The load is applied through either single- or tandem-axle trucks at regular highway speeds and various load levels.

NARDO TEST TRACK

In March 1983 the Organisation for Economic Cooperation and Development (OECD) started its full-scale pavement testing activity with Switzerland as the pilot country and active participation by delegates from Australia, Canada, Denmark, Finland, France, Germany, Italy, Japan, Britain, and the United States.^[7] The purpose of the program was to verify the comparability

Table 1. Properties of different circular testing machines.^[3]

CIRCULAR TEST TRACKS	construction year	construction costs	diameter centerline (m)	pavement width (m)	structure depth (m)	number of arms	wheel disposition	loading ¹⁾ (kN)	transversal movement (mm)	max. speed (km/h)	max. frequency loadings/h	OBSERVATIONS
CANADA Dept. of Highways and Transportation Research Branch 1610 Park Street REGINA, Saskatchewan, S4P 3V7	1977	0.4-10 ⁶ Can\$	12	3.7	1.25	1	 (ev. )	max. 55 6	± 660	36	1 000	indoor track with temperature control (-40°C / +50°C), partial control of water table, artificial rain.
GERMANY Institut für Strassenbau und Eisenbahnwesen Universität Karlsruhe	1928 (mod. later)	-	20	3.0	0.1- 0.7	4		22 + 17 6	± 400	35	2 200	status of activity unknown, open-air facility
FINLAND Neste Oy, Research Centre SF - 06850 Kulloo	1971	2-10 ⁶ Fmk	3.70	2.0	2.0	2		3 - 100 F	± 100	30	5 200	insulated chamber with temperature control (-40°C / +40°C) and water table control.
FRANCE Laboratoire des Ponts et Chaussées Centre de Mantes les bauches du désert, B.P. 19 F-44340 BOUGUENAI	1977	10.6-10 ⁶ FF	35	5	-	4	or 	140 G	± 520	100 (70 kW)	3 600	test pavements directly on the existing subgrade
SWITZERLAND Institut für Strassenbau ETH Hölgerberg CH - 8093 Zürich Test-Track: Dübendorf	1978	1-10 ⁶ SFr.	32	2.5	2.0	3		50 - 80 G	± 400	80 (60 kW)	2 400	pavements in a concrete pit with possibi- lity of regulation of the water table
UNITED KINGDOM Transport and Road Research Laboratory Old Mokingham Road Crowthorne, Berkshire RG11 6AU Road Machine No.3 in Harmondsworth	1936 mod. 1958/ 1960	-	33.6	3.0	1.8	1	or 	- 67 F	± 200	32	300	Possible surface heating by infra-red lamps, with noticeable reduction of loading frequency.
U.S.A. Washington State University Pullman, Washington	1963/ 64	100'000 US\$	25.4	2.5	0.5- 1.0	3		45 - 90 G	± 1000	88	3 300	also used for pavement wear tests; status of activity unknown.
MEXICO Instituto de Ingenieria Universidad Nacional Autonoma de Mexico Mexico City, D.F.	1970	600'000 Mex.Pesos	10	4.0	1.5	3		41 to 50 G	± 1000	40	3 800	indoor facility, active
NEW ZEALAND University of Canterbury Canterbury	1970	-	19.7	1.3	0.3- 0.4	2		13 to 40 G	± 650	19	600	open-air facility, under reconstruction
POLAND Instytut Badawczy Dróg i Mostów WARSAW	1972	-	40	9.4	2.0	2		80 - 120 G	± 600	70	1 100	open-air facility, active
CZECHOSLOVAKIA VUIS, Res. Institute for Construction Bratislava	1962	-	32	6.0	1.5	2		100 - 150 G	± 1500	65	1 300	open-air facility, extended from 1-arm to 2-arm type in the mid-70 ies, active

OECD RTR member countries

1) G : by gravity

F : by force

Other circular test tracks also exist in Brazil (new), Soviet-Union (Leningrad and Kiev), Rumania (Bucarest), The Netherlands (Arnhem); very reduced information is available and it is believed that some of those facilities are inactive.

of strain values measured with different techniques under the same boundary conditions and with a sufficient number of single measurements.

The Nardo test track was selected to conduct the strain measurement experiment. The track, located in the southeastern part of Italy, is owned and operated by the company Soceta Autopiste Specimentali Nardo (SASN). The facility is a ring road with a radius of 1.25 mi (2 km), the main ring of which is divided into four lanes for cars and two lanes for trucks. In 1979 it was decided to use the facility also for particular pavement tests. For this purpose an additional road was constructed inside the main ring. The total length of the road is approximately 1.1 mi (1.8 km) including 1,650-ft (500-m) connections to the ring and an available length of 2,640 ft (800 m) for experimental pavement sections. A plan of the track is shown in figure 5.

The area chosen for the OECD test program is in the central portion of the experimental pavements. A pavement section with a total length of 131 ft (40 m) was reconstructed after partial removal of an existing flexible pavement. The loading of the pavement is accomplished through regular truck traffic at normal highway load and speed conditions. The pavement section was instrumented by strain gauges located at the bottom of the asphalt concrete layer and temperature sensors located throughout the asphalt layer.

PENNSYLVANIA TEST TRACK

The Pennsylvania Transportation Research Facilities (test track) was designed in the early 1970's and expanded in 1982.^[6] The facility has the shape of an oval loop with two test sections, each about 1,320 ft (400 m) long, connected by curves of different radii. The total length of the test road is about 1 mi (1.6 km). There are 16 flexible sections with variable layer thicknesses and materials properties and 4 rigid pavement sections. Traffic loading is achieved using normal trucks with one or more trailers. The loading truck can attain a speed of 55 mi/h (88 km/h) on the straight section and 45 mi/h (72 km/h) around the curves. Various instruments can be easily installed at all of the test sections. Normal highway construction procedures and equipment can be used in the construction of any test section. Figure 6 shows a view of the test track.

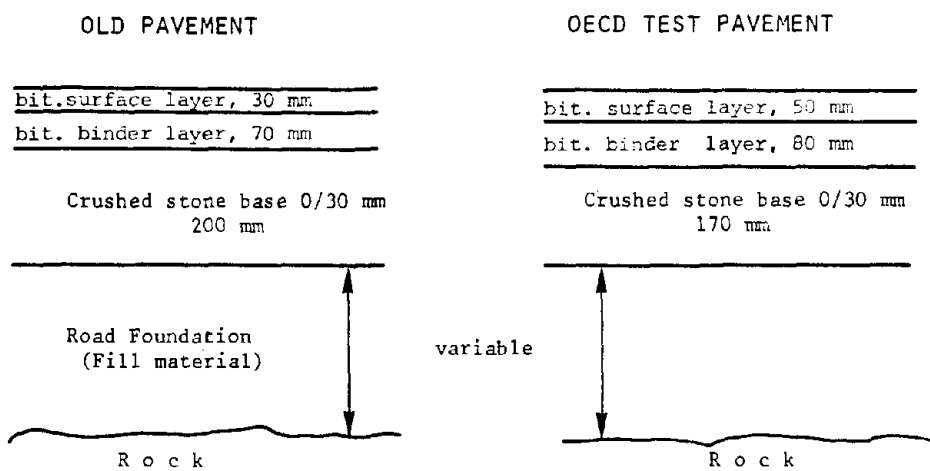
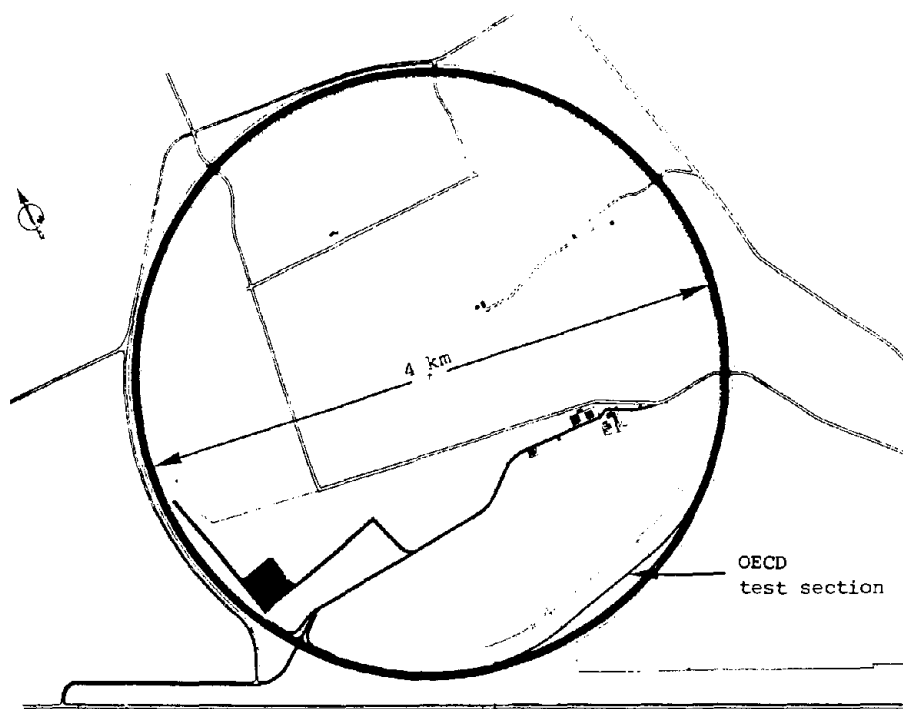


Figure 5. Plan of Nardo test track. [7]

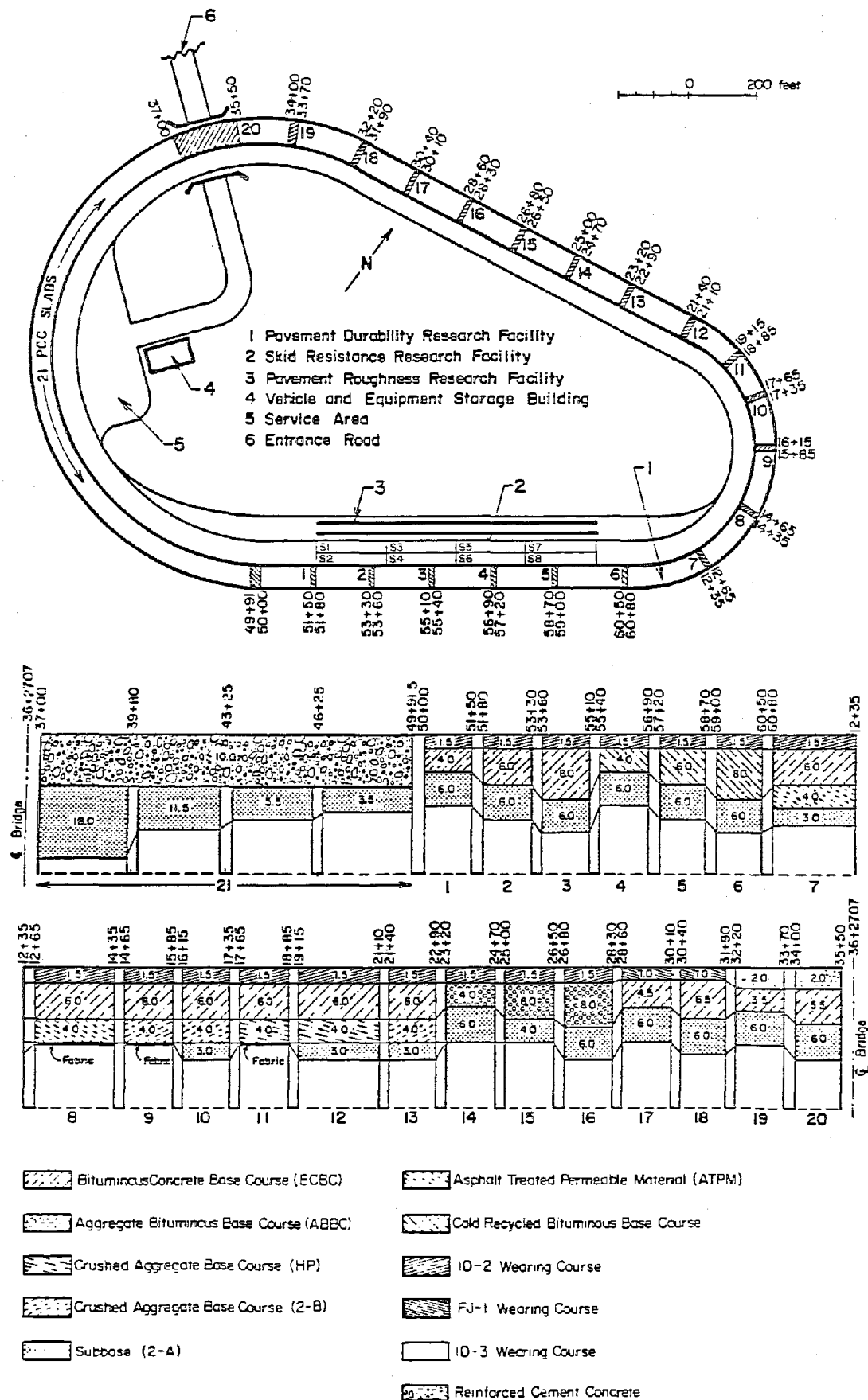


Figure 6. View of the Pennsylvania test track.

TRRL FULL-SCALE EXPERIMENT

In 1968 the Transportation and Road Research Laboratory of England built instrumented pavement sections on the southbound carriageway of the A1 trunk road at Conington, Huntingdonshire.^[9] Of the 30 different pavement sections built, 10 were instrumented with pressure cells, strain and deformation gauges, and temperature sensors. Each section was 112 ft (34 m) long and laid on a heavy clay soil. The sections were loaded by a regular truck with either a single- or tandem-axle configuration. The objective of the experiment was to compare the performance of various gravel aggregates used in the base and subbase layers in conjunction with bitumen and tar binders.

ALBERTA RESEARCH COUNCIL TEST PAVEMENT

In 1973 the Alberta Transportation Department constructed two full-depth asphalt pavement test sections. The test site is located on Secondary Road 794, northwest of the City of Edmonton.^[10] The thickness of the full-depth asphaltic concrete was chosen to be 11 in (280 mm) for the inbound lane and 7 in (178 mm) for the outbound lane. The need for different designs in the inbound and outbound layers is a result of the fact that the inbound lane is trafficked by loaded gravel trucks while the outbound lane traffic consists of unloaded trucks. The instrumented sections are in a relatively low-lying, flat tangent, and to accommodate special vehicle testing, a by-pass lane was added for diversion of through traffic. A plan and cross section of the test pavement are shown in figure 7.

The total length of the test section is 400 ft (122 m). The load is applied through regular truck traffic at normal highway speed. The following instrumentation was installed at the test sections:

- Single-layer deflectometer to measure total deflection.
- Elastic-diaphragm pressure cells to measure pressure at the subgrade interface asphalt.

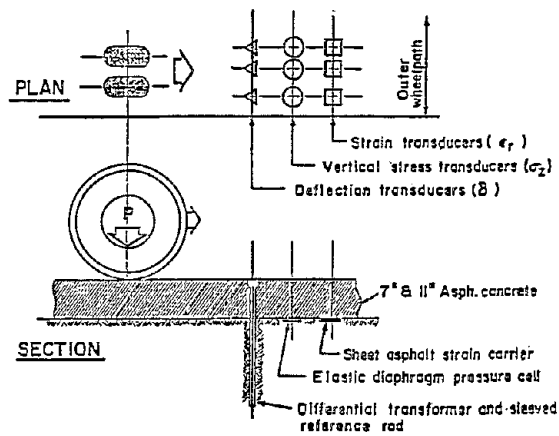
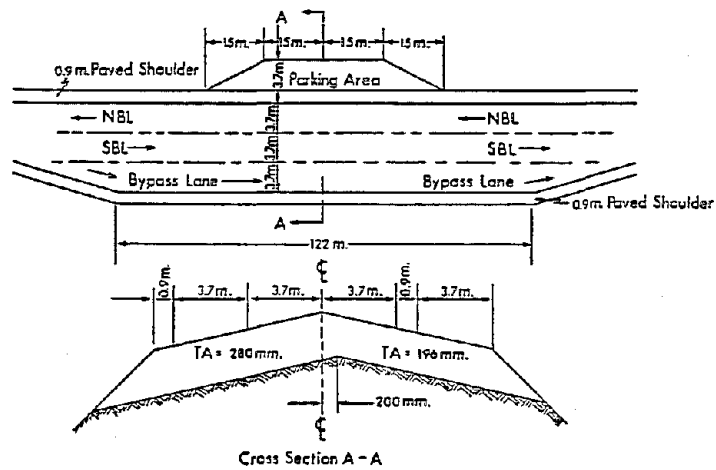


Figure 7. Plan and cross section of Alberta Research Council test section. [10]

- Strain gauges to measure longitudinal strains at the bottom of the asphaltic concrete.
- Temperature sensors.

3. STRAIN MEASUREMENT

Strain is defined by the ratio of induced deformation or the change in length to the original length (gauge length) of an element due to application of load or change in temperature. The relation can be written as:

$$\epsilon = \frac{\delta L}{L} \quad (1)$$

Many engineering structures are designed to undergo relatively small deformations, involving only the straight line of their stress-strain diagram. Hooke's law states that, for the straight portion of the stress-strain diagram, the stress is directly proportional to the strain as follows:

$$\sigma = \epsilon E \quad (2)$$

This relation is important since stress in a material cannot be measured directly. Thus the measured strains in conjunction with other properties of the material can be used for stress analysis.

Different methods of measuring strain are based on various mechanical, optical, acoustical, pneumatic, and electrical phenomena.^[11] The underlying principle for all of these methods is the measurement of displacement between two points some distance apart (gauge length) and then the determination of strain using equation 1.

TYPES OF STRAIN GAUGES

MECHANICAL DEVICES

Mechanical devices are the earliest type of equipment used for strain measurement. Extensometers are a class of mechanical devices. With a purely mechanical device, the gauge length must be at least 0.5 in (12.5 mm) and will have a resolution of about 10 microstrain.^[11]

OPTICAL DEVICES

This method employs interference fringes produced by optical flats to measure strain. This type of device is sensitive and very accurate but requires a laboratory setting for its use.^[11]

ELECTRICAL DEVICES

The underlying theory for this category is that, when a wire (foil) is mechanically stretched, the cross section of the wire is reduced; therefore, the electrical resistance across that wire is increased. This may be written as:

$$\frac{\Delta R}{R_0} = k \cdot \epsilon \quad (3)$$

where k is the gauge factor and is a characteristic value of the gauge.

In 1856 Lord Kelvin described the results of his experiments in which he found that the resistances of copper wire and iron wire change when subject to strain.^[12] Probably the first unbonded wire resistance strain gauge was that made by Carlson in 1931.^[13] The first bonded-type strain gauge used was a carbon resistor gauge developed by Bloach.^[14] This device consisted of a carbon film applied to the surface of the member in which the strain was to be measured.

In 1938 Edward Simmons used a bonded wire strain gauge in a study of stress-strain relations under tension impact. At about the same time, A. C. Ruge of M.I.T. decided to make a preassembly of the gauge by mounting the wire between thin pieces of paper. Simmons and Ruge were later jointly credited with inventing the gauge, and the "SR" in the SR-4 trademark honors the co-inventors.^[15]

Types of resistance strain gauges currently used as transducer elements include the unbonded metallic-filament strain gauge or wire strain gauge, the

bonded metallic-foil gauge, and the bonded piezoresistive or semiconductor gauge.

UNBONDED METALLIC-FILAMENT STRAIN GAUGE

This type of gauge, also called a wire strain gauge, is often used as a secondary electromechanical element in other transducers (i.e., accelerometers and pressure sensors). One or more (usually four) filaments of resistance wire stretch between supporting insulators. Transducers using unbonded gauges are available, but because of their fragility they are not commonly used. Figure 8 shows a typical wire strain gauge.

BONDED METALLIC-FOIL STRAIN GAUGE

This type of gauge, also called the foil strain gauge, was developed mainly by William T. Bean.^[16] The gauge consists of a thin foil grid element on some type of support, usually an epoxy film. The gauges are manufactured by printed circuit techniques. This type of gauge is the most popular strain gauge for various engineering applications. Figure 9 shows a typical foil strain gauge.

SEMICONDUCTOR STRAIN GAUGE

Studies of piezoresistive properties of silicon and germanium in 1950's resulted in the development of semiconductor strain gauges. This type of gauge consists of a thin sliver of silicon, typically 0.005 by 0.0005 in (0.1 by 0.1 mm) in cross section. Active gauge length may range from 0.03 to 0.35 in (0.75 to 8.9 mm) and the sensitive element may be backed or unbacked.^[17] The major advantage of a silicon gauge is its high gauge factor, approximately 130, which improves the sensitivity of the strain gauge, but also introduces nonlinearity and temperature dependency. The semiconductor strain gauges are also considerably more expensive than the conventional metallic gauges. Figure 10 illustrates a typical semiconductor gauge.

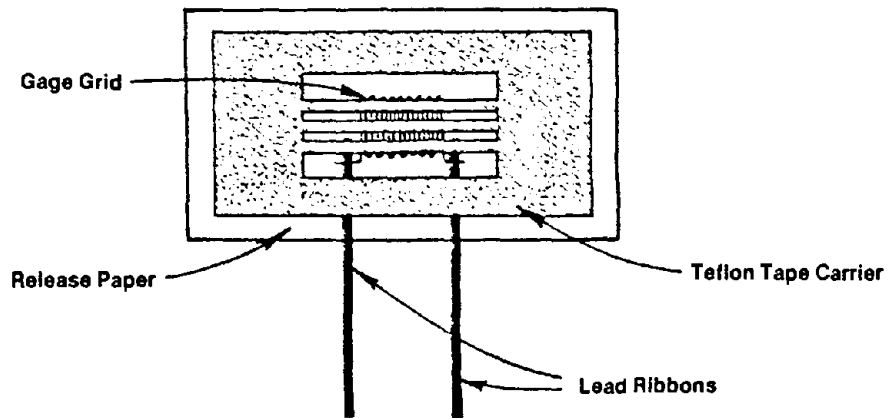


Figure 8. A typical wire strain gauge.

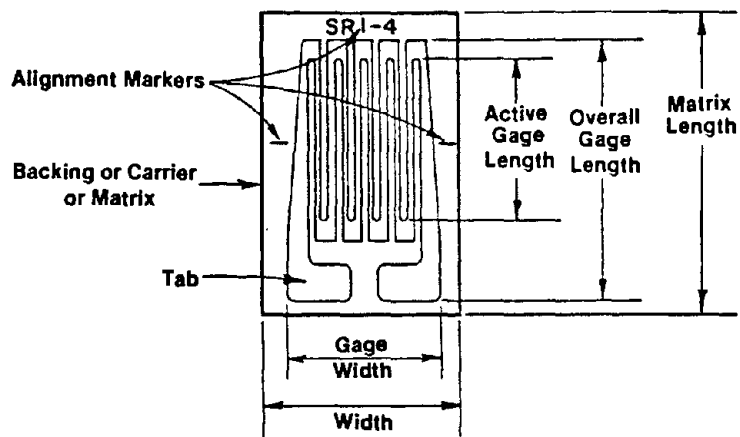


Figure 9. A typical foil strain gauge.^[17]

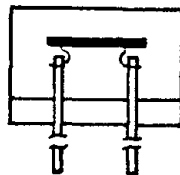


Figure 10. A typical semiconductor gauge.^[17]

STRAIN MEASUREMENT IN FLEXIBLE PAVEMENTS

The magnitude and directions of the critical strains in pavement structures under dynamic loadings are of great concern to researchers in the areas of analysis and design of flexible pavements. Fatigue failure of flexible pavements results from high tensile strains at the bottom of the asphalt layer. Rutting and permanent deformations are related to high shear strains in the asphalt layer and high compressive strains throughout the other layers of the system.

Strain measurement in flexible pavements is usually performed by electrical resistance strain gauges. Strain gauges are generally selected on the basis of their gauge length. For pavement applications, this criterion is based on the maximum aggregate size of the paving mixture. The length is usually three to five times the maximum aggregate size.

STRAIN GAUGES FOR BONDED LAYERS

This section reviews the methods that have been used by various investigators to measure the strain in asphalt concrete pavement layers. These methods can be grouped into four categories:

- H-gauges and strip gauges.
- Foil strain gauges cemented to or embedded in carrier blocks prepared in the laboratory.
- Foil strain gauges cemented to a core extracted from the pavement.
- Strain coils.

H-GAUGES

The H-gauge consists of a strip of a given material onto which a strain gauge is connected. The ends of the strip are connected to metal bars with rectangular cross sections which act as anchors. Since the final shape of the strain gauge transducer resembles the letter "H," they are referred to as

H-gauges. These transducers are embedded at the bottom of the asphalt concrete layer. As the pavement experiences strains under the application of the load, the anchor bars move with the pavement, producing elongation in the strip. The strain registered by the strain gauge attached to the strip will be the same as the true strain in the asphalt concrete if the stiffness of the strip is the same or somewhat less than that of the asphalt concrete layer. Otherwise the strip tends to reinforce the pavement; thus the strain gauge will under-register. A large stiffness differential between the two materials results in the debonding of anchor bars from the pavement materials and failure of the instrumentation. Different investigators have used different materials and dimensions for the strip as well as the anchor bars to overcome the aforementioned problems. Various methods for protection of these gauges have been adopted to improve the survivability and durability of H-gauges and are described briefly below.

The Transportation Road Research Laboratory (TRRL) in England designed the earliest type of H-gauge: a 0.5-in (12.5-mm)-wide by 0.010-in (0.25-mm)-thick aluminum strip onto which a 4-in (101 mm)-long, 225-ohm resistive foil strain gauge was cemented.^[9] Two 0.01-in² (6.3-mm²) steel bars were connected to the aluminum strip at right angles. The resistive foil gauge and aluminum strip were waterproofed and wrapped in PVC tape for protection against intrusion of aggregates into the gauge during pavement construction. Figure 11 shows TRRL H-gauges. In some cases two resistive foil gauges were glued to the aluminum strip, one on each side.

The National Institute for Road Research (NIRR) in South Africa designed a different version of the H-gauges. As shown in figure 12, it consisted of a 0.47-in (12-mm)-wide beryllium copper or brass strip with a thickness of 0.010 or 0.012 in (0.25 or 0.30 mm) and a length of 5.71 in (145 mm). The anchors consisted of two 3.15-inch (80-mm)-long brass angles sandwiching the end of the strip. Protection for these strain gauge transducers was provided by molding polyethylene around each transducer before installation.^[18]

In the Nardo Road Test, five research teams used H-gauges with slight variations. Teams from Australia and France adopted H-gauges similar to TRRL

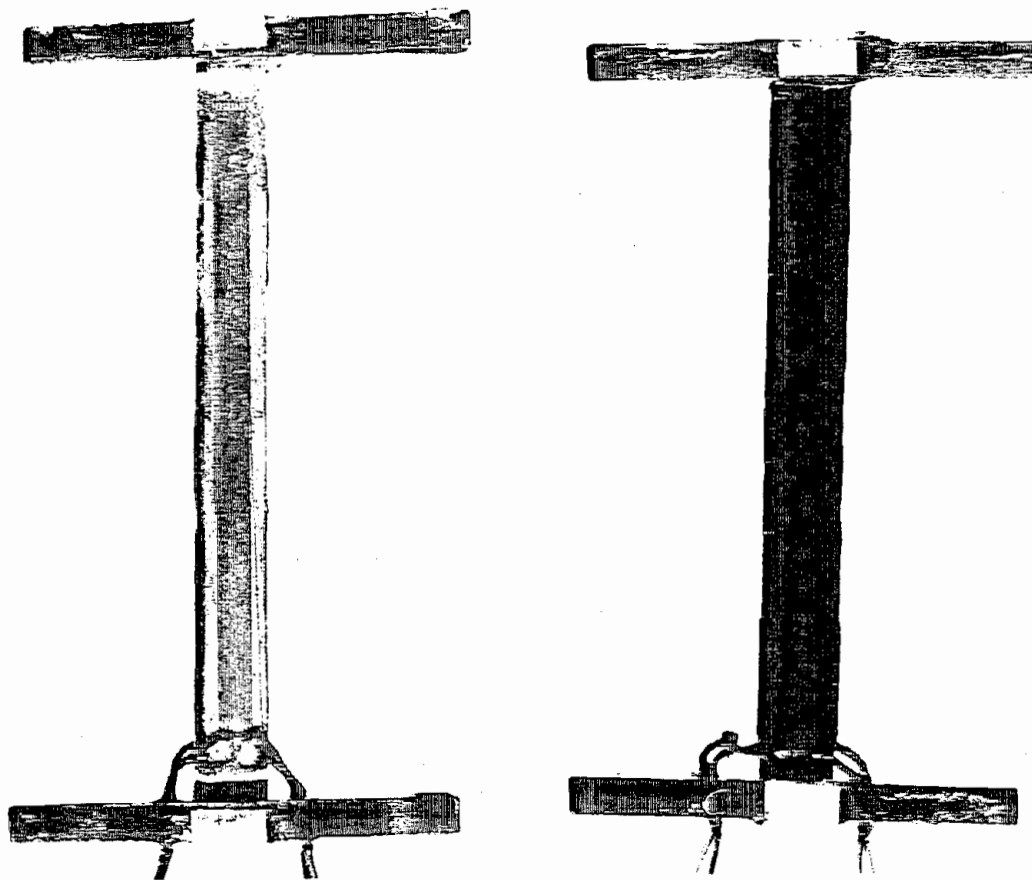


Figure 11. TRRL H-gauges.^[9]

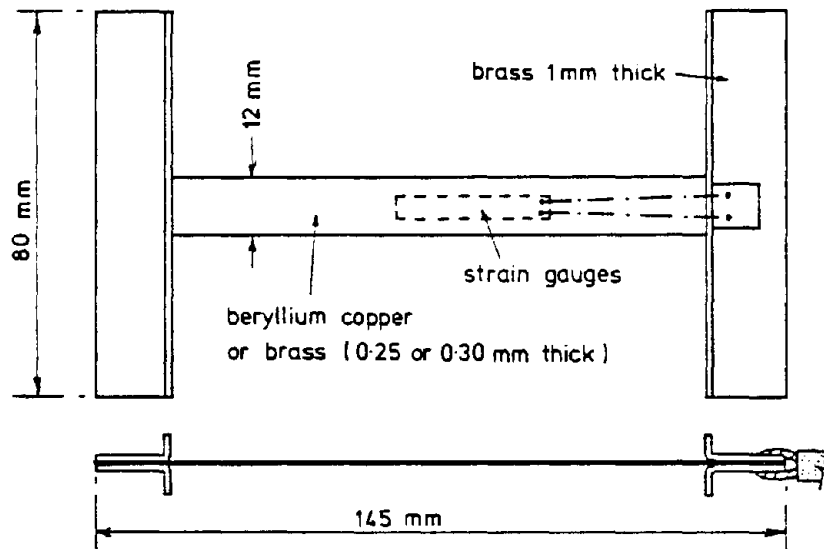


Figure 12. H-gauge designed by NIRR. [18]

gauges. The Australian gauge, shown in figure 13, consisted of a 5.12- by 0.47-by 0.010-in (130- by 12- by 0.25-mm) aluminum strip onto which a 120-ohm, 2.64-in (67-mm) wire gauge was attached.^[7] The anchors were made of 2.95- by 0.39- by 0.28-in (75- by 10- by 7-mm) aluminum bars. Protection against aggregate penetration was provided by an aluminum channel 0.012 in (0.3 mm) thick placed over the strip.

Figure 14 illustrates the strain gauge transducer that was used by the French researchers. The strip was made of aluminum with dimensions of 3.94 in (100 mm) by 0.39 in (10 mm) by 0.031 in (0.8 mm); the sensing element was a 120-ohm foil resistive strain gauge 1.18 in (30 mm) long; and the anchor bars were 2.76- by 0.39- by 0.39-in (70- by 10- by 10-mm) aluminum bars as shown in figure 14. The strain gauge was covered by varnish resin, over which a thin aluminum plate was placed.^[7]

Two Swiss teams and the Danish team also used H-gauges at the Nardo Road Test. These teams used the commercially available Kyowa 120-ohm wire strain gauge embedded in acryl with a modulus of elasticity of 400,000 psi (2800 MPa) as the strip unit and aluminum or steel anchor bars.^[7] The material and geometric characteristics of the anchor bars and the length of the strip varied from one team to another, as indicated in figures 15 and 16. The most important difference among the H-gauges used by these three teams was the method of gauge protection. One team used no additional protection besides the layer of acryl that was over the wire gauge (figure 15). The second Swiss team placed a 0.012-in (0.3-mm) aluminum channel over the acryl strip for additional protection against aggregate intrusion, also shown in figure 15. The team from Denmark covered the strip with a thin coat of silicon grease and then covered it with a 0.039-in (1-mm) aluminum plate wrapped with silicon tape (figure 16).

In recent years, the Technical University of Denmark has modified H-gauges to improve their durability against moisture and fatigue and to better match the stiffnesses of the strip materials and asphalt concrete.^[7, 19] The strain gauge is completely embedded in a strip of fiberglass-reinforced epoxy with low stiffness but high flexibility and strength. Each end of the epoxy strip is attached to a stainless steel anchor bar, and protection against

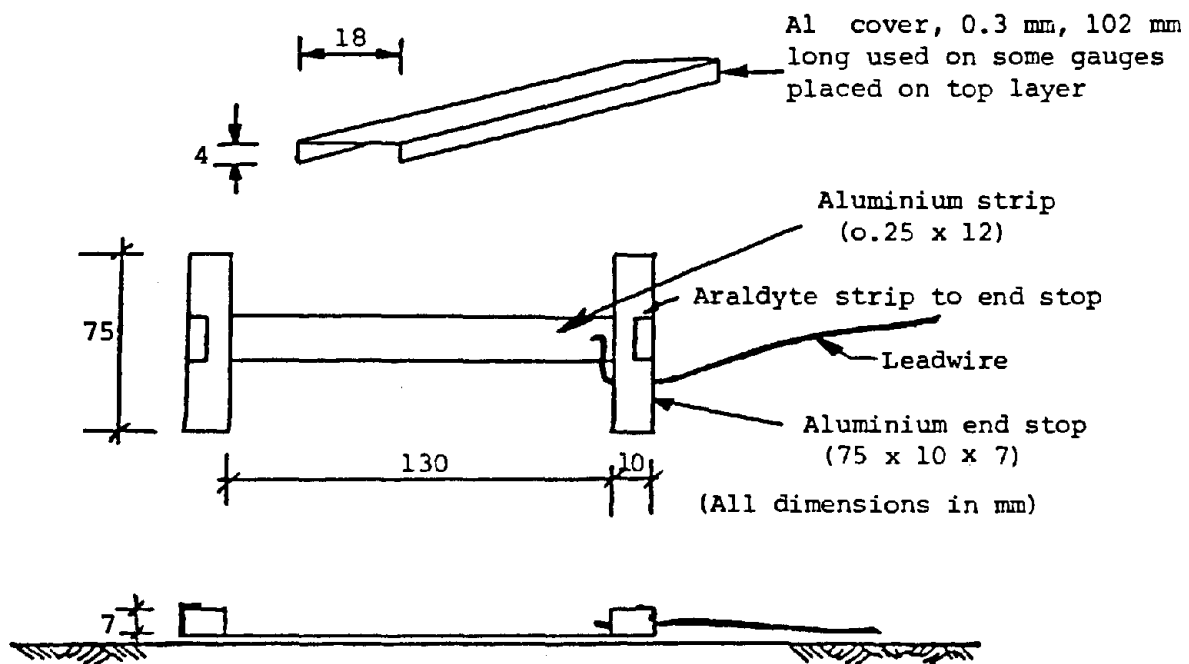


Figure 13. H-gauge used by Australian team at Nardo Road Test.^[7]

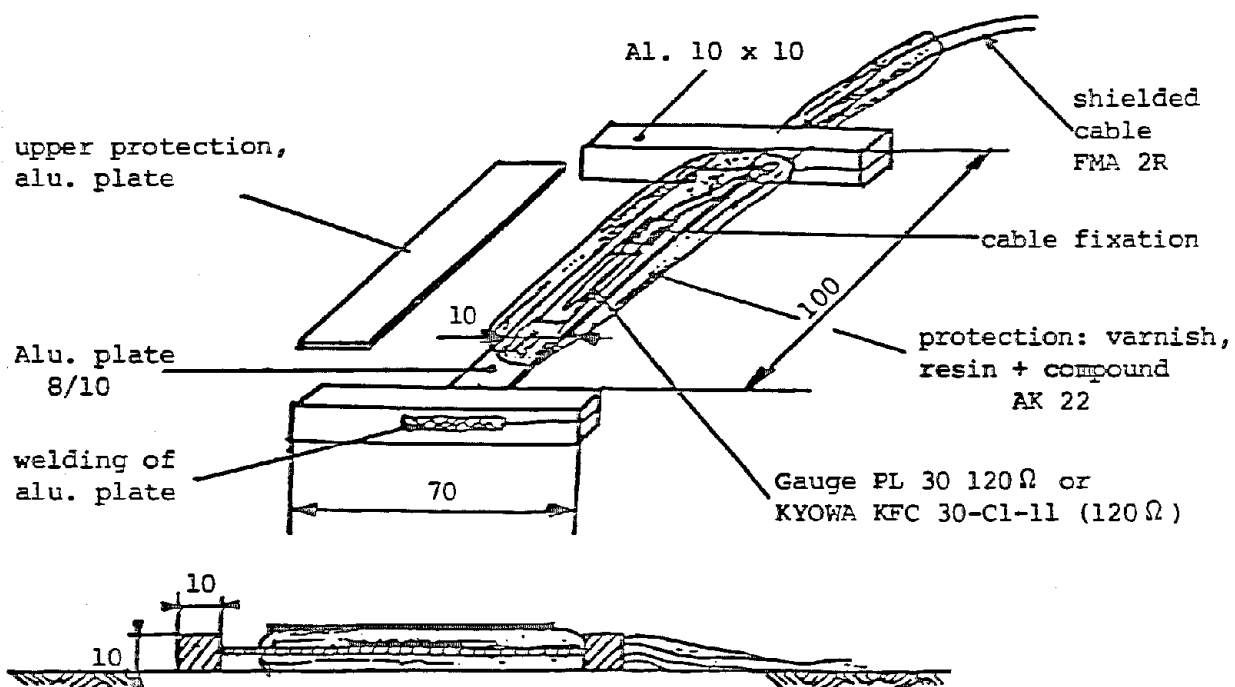
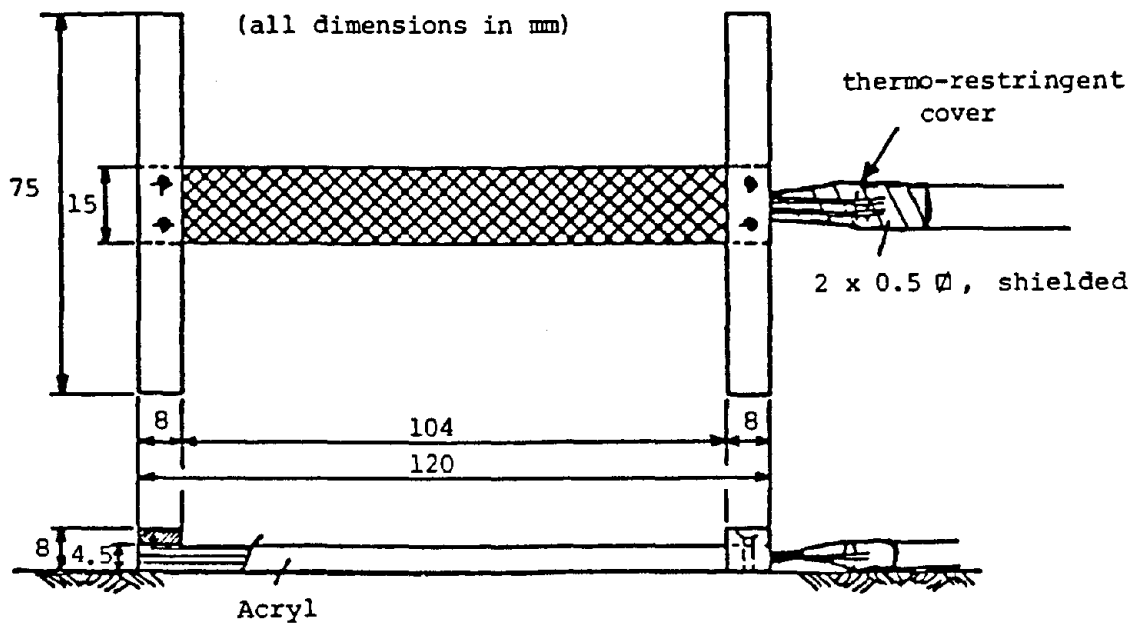
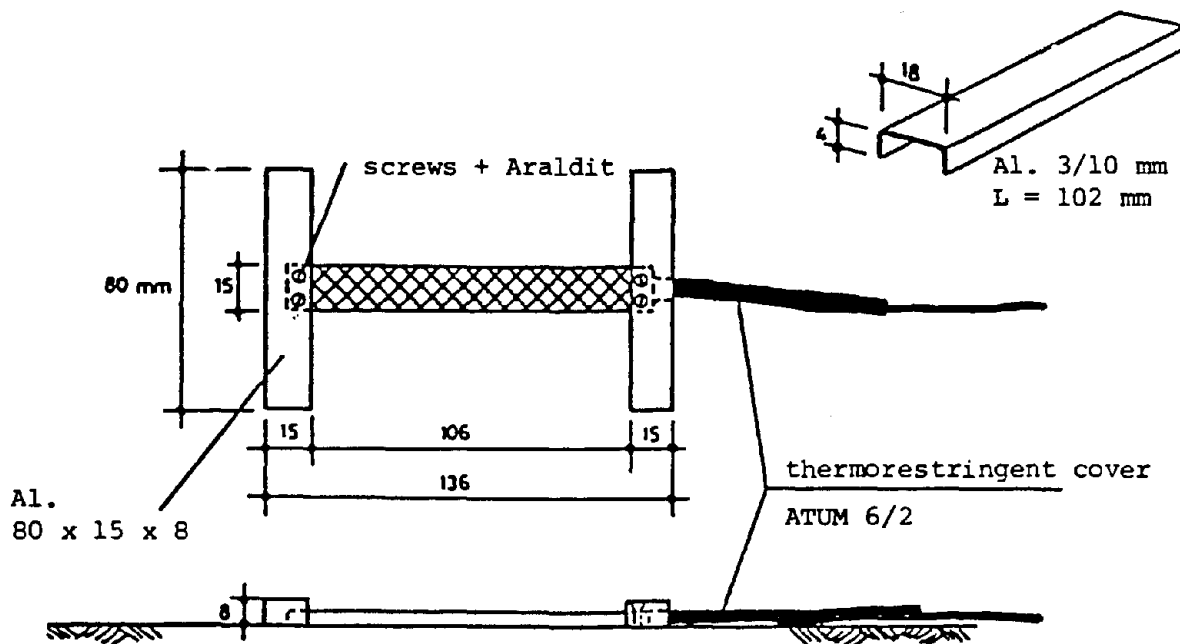


Figure 14. H-gauge used by French team at Nardo Road Test. [7]



A. Gauge with only acryl protective layer



B. Gauge with both acryl and aluminum channel for protection

Figure 15. H-gauge used by Swiss team at Nardo Road Test.^[7]

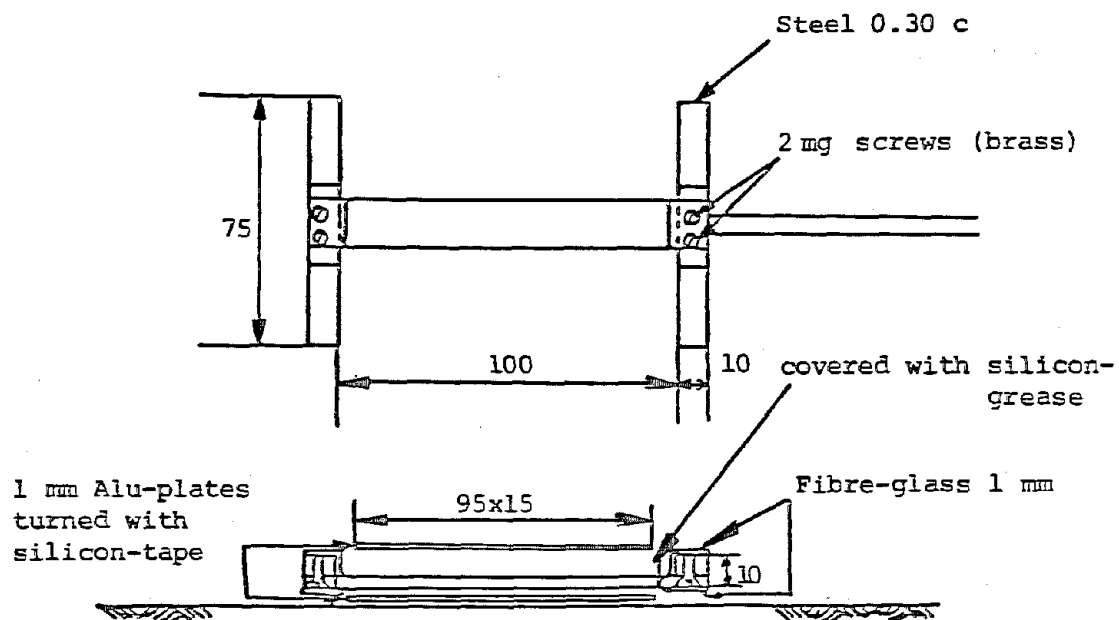


Figure 16. H-gauge used by Danish team at Nardo Road Test.[7]

mechanical and chemical deterioration is provided by several layers of coating, as shown in figure 17. These gauges are commercially available through Dynatest.^[20] Design details and specifications of this transducer are shown in figure 18.

The aluminum or stainless steel plates which are used to protect the gauges are not connected to the end anchors, which means that no strengthening is provided to the gauges in the direction of measured strains.

Another commercially available strip gauge transducer is the Omega encapsulated strain gauge.^[21] These transducers have been designed for use in rough ambient conditions. Various types of these gauges have temperature-dependent characteristics similar to those of asphalt concrete materials. The gauge suitable for direct use in asphalt concrete materials is made of a 350-ohm, 3.5-in (88-mm)-long wire strain gauge embedded between two layers of polycarbonate. The total length of the strip is 10 in (254 mm) and its maximum width is 1 in (25 mm). Figure 19 illustrates an encapsulated strain gauge. The Italian team at the Nardo Road Test used one of these gauges with no special type of protection although, according to the manufacturer of these gauges, their service temperature is from -60 to +160 °F (-50 to 70 °C).^[21]

FOIL STRAIN GAUGES ON CARRIER BLOCK

For several years different researchers have attached strain gauges to the surface of the asphalt concrete layer. The first technique for strain measurement at the bottom of the asphalt concrete layer was developed at Koninklyke Shell Laboratorium in Amsterdam.^[22] These gauges consisted of 1.18-in (30-mm)-long foil strain gauges cemented to a thin sand asphalt carrier block in both longitudinal and transverse directions. The block was then placed at the top of the base and covered by paving mix.

In 1973 researchers at the Alberta Research Council (ARC) in Canada embedded wire resistance strain gauges in thin sheets of asphalt to measure longitudinal strain at the bottom of the asphalt concrete layer.^[10] The asphalt mastic and the strain gauges form a transducer which is approximately 6.5 by 6.5 by .79 in (165 by 165 by 20 mm). In the newer version of these,

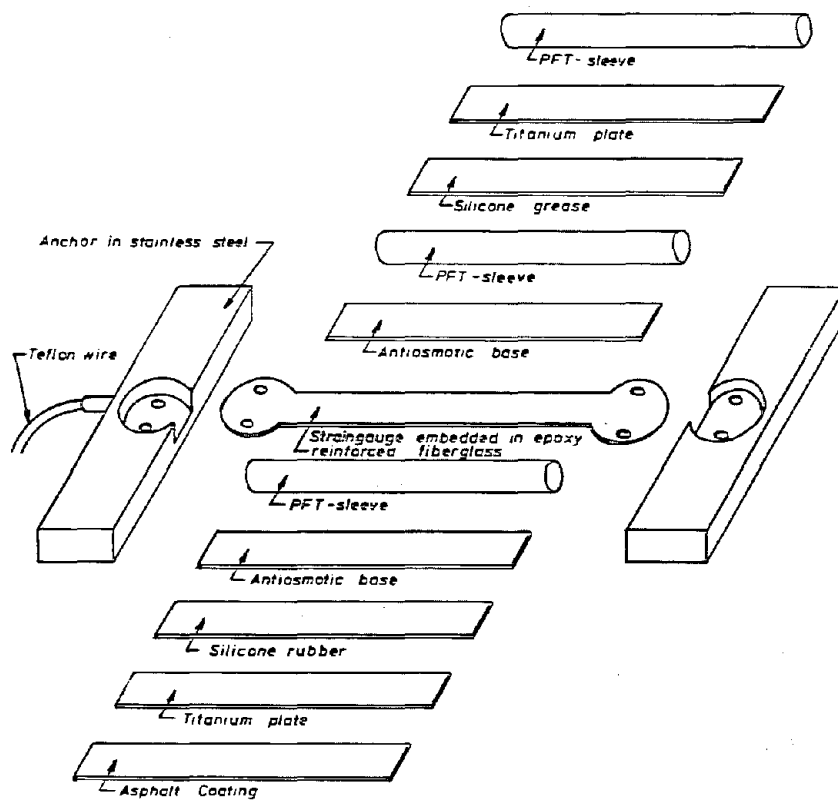
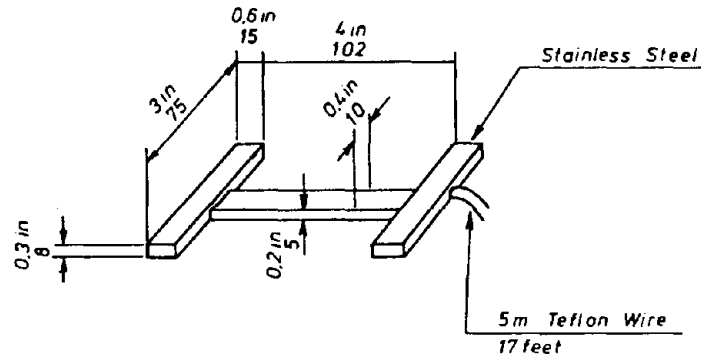


Figure 17. Different layers of modified Danish H-gauges. [19]



Specifications

Type	FTC II A (asphalt)
Range	up to 1500 μ strain
Cell-material	Epoxy - Fibreglass
Coating	Epoxy - Silicone - PFT - Titanium
Temperature	- 30 ~ 150° C - 22 ~ 300° F
Resistance	120 Ω \pm 1,0%; GF=2,0
Voltage	up to 12V (full bridge)
ΣE - modulus	\approx 320 000 psi \approx 2200 MPa
Sq - area	\approx 0,5 cm ² \approx 0.078 sq. inch
Fatigue - life	Theoretical up to 10 ⁸ cycles
Service - life	Typical > 36 months
Strain force	\approx 110 $\frac{N}{1000 \mu m/m}$ \approx $\frac{24 lbs}{1000 \mu strain}$

Figure 18. Design details and specifications of modified Danish H-gauges. [20]

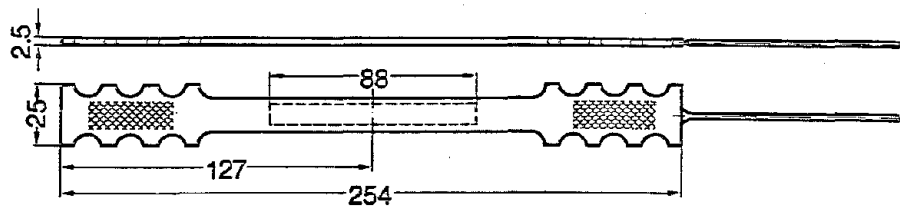


Figure 19. Encapsulated strain gauge or strip gauge.
(all dimensions in millimeters).. [21]

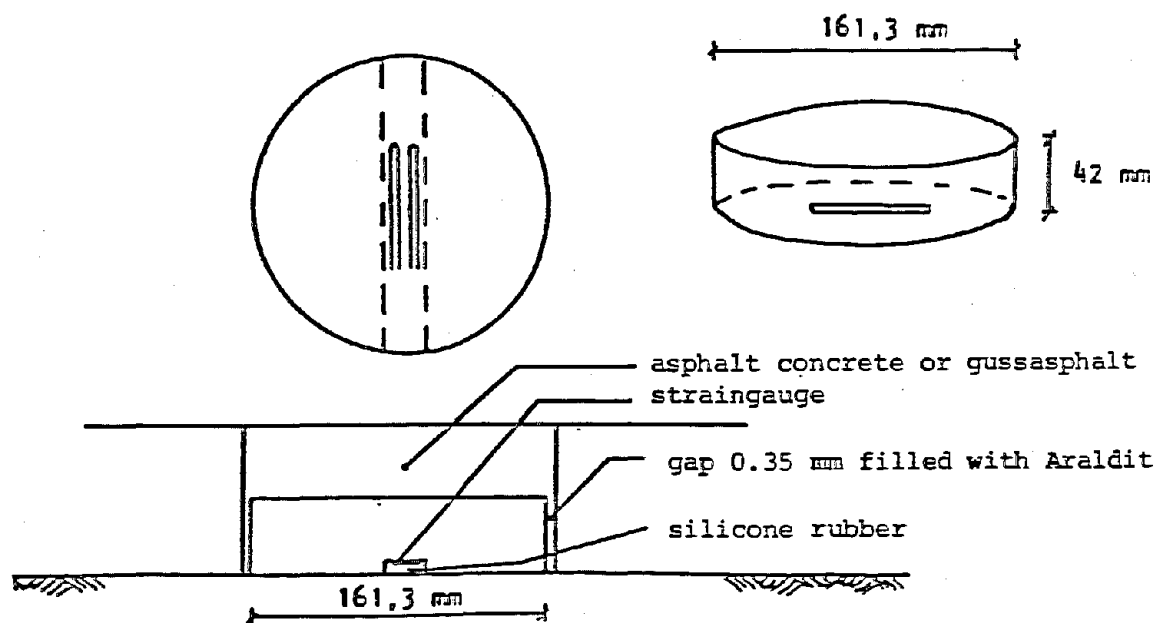


Figure 20. Block-type strain gauge transducer used by
researchers from Finland at Nardo Road Test. [7]

transducer metal foil gauges have been used. These transducers were used in OECD's Nardo Road Test and at FHWA's Accelerated Loading Facilities (ALF). [7, 1]

Researchers at the Road and Traffic Laboratory of the Technical Research Centre of Finland (VTT) used another type of carrier block for embedding strain gauges. They glued a 3-in (75-mm)-long dual foil strain gauge onto a laboratory-compacted cylindrical specimen having a diameter of 6.35 in and a height of 1.65 in (161.3 mm). The foil strain gauge had a resistance of 350 ohms. Then a thin layer of silicon rubber was applied over the strain gauge for protection against penetration of aggregate particles into the sensing element. [7] Figure 20 illustrates this type of block, which was used in the Nardo Road Test.

Researchers from Bundesanstalt für Strassenwesen (BAST) in Germany adopted the Shell method. They cut a laboratory-compacted bituminous mix and mounted a .79-in (20-mm)-long, 600-ohm strain gauge on the cut surface. Then they glued the pieces back together in the laboratory. [7] Figure 21 illustrates this type of transducer, which was used in the Nardo Road Test.

The main idea behind this group of transducers is that the asphalt on the surface of the carrier block will soften when it comes into contact with the hot paving mix. Therefore, the carrier block and the paving mix will bond together and form a monolithic layer of asphalt concrete.

FOIL STRAIN GAUGES CEMENTED TO CORES

This method is similar to the previous approach except that the carrier blocks are cores extracted from the actual pavement rather than laboratory compacted carrier blocks.

The main concern about this approach is the effective bonding between the instrumented core and the surrounding pavement. If the bonding agent, which is usually a type of epoxy, is too stiff relative to the pavement, then stress concentration will be formed around the core. This stress concentration will initiate cracks at the vicinity of the core. If the

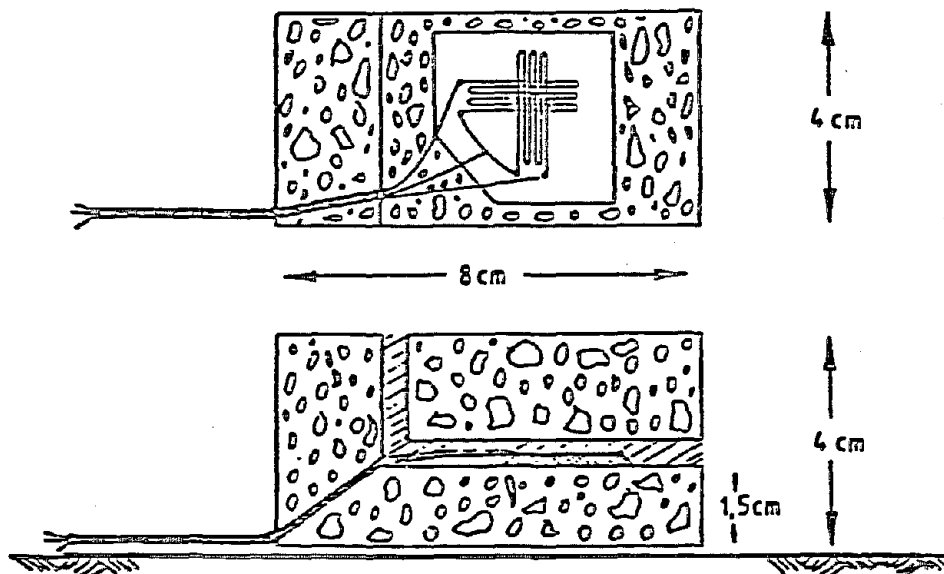


Figure 21. Block-type strain gauge transducer used by researchers from Germany at Nardo Road Test.^[7]

bonding agent is too soft relative to the pavement, as the result of the dynamic loading, the bond between the core and the surrounding pavement will fail. Therefore, the core will act as a rigid body. Based on this discussion, the stiffness of the bonding agent should be very similar to that of the pavement to ensure a monolithic layer behavior.

Researchers at the Technical Research Center of Finland have used this method at the Virttaa test field. They used 6-in (150-mm) core samples retrofitted into a hole in the pavement with a tolerance of less than .04 in (1 mm).^[23] The strain gauges were cemented on the cores, and the cores were glued back to the bituminous pavement. The strain gauges used were 3-in (75-mm)-long dual foil strain gauges with 350-ohm resistance.

Researchers at the Federal Highway Administration have installed this type of transducer at the Pavement Testing Facility (PTF) to be tested with the Accelerated Loading Facility (ALF) machine. The cores, taken with a 4 1/4-in (108-mm) barrel, were instrumented and fitted into 4-in (101-mm) holes in the pavement at the middle of the test section, with a clearance of about 1/32 in (0.8 mm). A commercially available epoxy was used as the bonding agent. No sign of debonding or crack initiation was noticed in the area surrounding the cores for over 6 million repetitions of 18-kip ESALs.

At the Nardo Road Test, teams from Italy and Switzerland used this method. The strain gauges were 2.36 in (60 mm) long with resistance of 120 and 600 ohms, respectively. Then the cores were reinserted into the boreholes and the gap was filled with epoxy resin.^[7]

The main advantage of this method is that the gauge can be retrofitted into an existing pavement and can be used for strain measurement in virtually every direction.

STRAIN COILS

Strain coils (also known as Bison gauges) are inductive coils which produce an electromagnetic output proportional to the distance between two coils. The assembly consists of two coils: One acts as a transmitter and the

other as receiver. The coils can be attached to an intermediate layer by a tack coat or can be cemented to a carrier block.^[18] Due to electromagnetic coupling these coils are affected by moving metals (i.e., wheels) and the energy output from the ignition system of the vehicles.

Methods of Installation

INSTALLATION OF H-GAUGES

The installation of strain gauge transducers in pavements requires a great deal of care and should be performed by skilled technicians. Generally, strain gauge transducers installed at the bottom of the asphalt concrete layer experience the heavy load of the paving machinery plus the high temperature of the paving mix, which is about 280 °F (140 °C), during installation. It is believed that, if the transducers survive the construction phase, they probably will remain functional for some time. Several procedures should be adopted to provide the special care needed to avoid damage to the strain gauge transducers:

- Placement of transducers into position just before the asphalt layer is to be laid, to minimize the risk of damage.
- Removal of sharp and large aggregates under the transducer.
- Placement of paving materials around the transducers to avoid direct impact of paving mix on the transducer and possible relocation of the device.
- Placement of the lead wires in 4-in (10-mm)-deep preformed grooves in the base for protection against heat of paving mix and relocation.
- Allowance for excessive strains in the wires as the pavement develops excessive rutting.
- Securance of the lead wires by plastic connectors to avoid corrosion of the wire.
- Avoidance of direct passage of paver wheels over the transducers.
- Avoidance of the use of vibratory compactors, if possible.

A different method of installation uses cables coiled and laid at the desired location before construction of the base course. After base construction, the cable coils are dug up and brought to the top of the base course.^[24] Before paving, the cable coils are placed in lengths of pipe so that the hot asphalt concrete mix will not damage them. Immediately following the paving process, the buried cables are again dug up, the pipes are removed, and the slots for the gauges are scooped out. While the gauge beds are being prepared, the large aggregate particles are removed from the scooped out asphalt concrete mix. The gauges are then covered with the asphalt concrete mix and the paving mix is hand compacted. This operation should take place immediately behind the paver, while the mix is hot and in a plastic state, and before rolling. This very time-consuming method causes excessive disturbance in both base and surface courses and is inappropriate for block gauges.

The transducer itself must have ample protection against intrusion of moisture and sharp aggregates, and the solder connection between the gauge and lead wire should be hermetically sealed.

The output from the transducers should be monitored before, during, and after pavement construction.

INSTALLATION OF INSTRUMENTED CORES

The installation of an instrumented core begins with the drilling of a hole in the pavement at the desired location using a barrel bit. The diameter of the hole should be such that the instrumented core fits into the hole with a tolerance of about 1/32 in (less than 1 mm). A small trench should be cut from the hole to the edge of the pavement for placement of the cables. The drilling water washes away the finer particles of unbonded base course, a problem remedied by replacing the coarse particles in the hole with a mixture of sand and bitumen and leveling and compacting it with a plate the diameter of the hole.^[23]

Epoxy glue is spread on the side surface of the core and the hole; the instrumented core is placed and the lead wires guided into the trench; and a

surcharge weight of about 20 lb (4.5 N) is then placed on the core until the epoxy glue hardens. Placement of instrumented cores so that their top surface is level with the pavement surface (i.e., so that the depth of the hole matches the height of the core) is difficult. To correct this problem, the core should be extended above the pavement about 1/2 in (13 mm) by placing extra sand and emulsion mix at the bottom of the hole and compacting it. After the glue hardens, the portion of the core which extends above the pavement should be removed by sawing. Any existing void around the hole and the trench should be filled with epoxy before opening the test section to traffic.

DATA ACQUISITION

Strain gauges are considered as passive resistors, so a power source and some circuitry are required for their operation. The lead wires from the strain gauge should be connected to a strain gauge bridge balance unit for signal conditioning. Because of its outstanding sensitivity, the Wheatstone bridge circuit is the most frequently used circuit for static strain gauge measurements. The strain gauge constitutes one arm of the bridge; the other three arms consist of internal precision resistors. The bridge should contain a balancing network to null zero-offset signals from the strain gauge. The Wheatstone bridge is used for converting the change in resistance of the strain gauge to a voltage change. This voltage change should be increased by using an amplifier and processed with a signal conditioner.

Using a microcomputer in conjunction with instrumentation greatly simplifies the use of the bridge circuit, providing multichannel systems for compiling large quantities of data and increasing measurement accuracy. The computer also removes the requirement for balancing the bridge and compensates for nonlinearities in output.^[11]

By using multichannel analog-to-digital interface boards, the acquired analog output from the strain gauges can be converted to digits and then stored on magnetic media for future analysis.

STRAIN MEASUREMENT IN UNBONDED MATERIAL

Soil strain measurement methods are very limited, comprising basically two types of devices:

- Inductive devices (Bison coils).
- Soil strain gauges (TRRL soil strain gauge).

BISON COILS

Bison coils, manufactured by Bison Instruments, Inc., are inductive coils that measure soil strain over a given distance using only electrical inductive coupling.^[25] The essential elements of Bison coils are:

- A pair of rugged disk-shaped sensors embedded in the soil in the nearly parallel and coaxial orientation, relative to each other, separated by a distance over which the strain is to be measured. One pair is a transmitter and the other is a receiver.
- A lightweight portable electronic unit to which the sensors are connected. This device contains all necessary amplification, balancing, recording, and calibration controls and a rechargeable battery pack.

The size of the coils is selected so that the distance between the coils is within the range of 1 to 4 sensor diameters. The sensitivity of a pair of Bison coils varies inversely with the distance between the two coils.^[26] Table 2 lists specifications of these coils.^[25]

An important advantage of Bison coils is that the coils (sensors) are not mechanically connected; therefore, they neither disturb the soil mass excessively, reinforce the soil mass, nor impede its deformation. A disadvantage is that Bison coils operate on the basis of electromagnetic coupling and are thus affected by objects that alter the electromagnetic field of the coils. Moving metal objects, such as moving wheels on a test pavement, interfere with the electromagnetic field of the coils when their distance from the coils is about five times the distance between the coils.^[27] This aspect

Table 2. Specifications of Bison coils.

SPECIFICATIONS:

SENSOR SIZE:

1" (2.5 cm.) Dia., 0.0625 cm. thickness.

2" (5.1 cm.) Dia., 0.125 cm. thickness.

4" (10.2 cm.) Dia., 0.250 cm. thickness.

Sensor bodies are machined linen phenolic base forms with molded plastic coverings for environmental stability. Other dimension sensors available on special order.

EXCITATION CHARACTERISTICS:

Frequency — 20 KHz

Amplitude — 15 Volts peak-to-peak.

Total Harmonic Distortion, 0.3%

Short term frequency stability of $\pm 0.1\%$ (1 hour period under any load.) Provision for external oscillator provided. Input impedance greater than 2 Kohm.

SENSITIVITY: 41 Volt/percent strain (Based on sensor separation of 1 Dia.) Applicable for strains as small as .01% or as large as 50%.

RESOLUTION: Infinite on recorder output. Limited on the meter only by static friction of bearings and readability.

OPERATING TEMPERATURE: 0°C to 70°C ambient.

STORAGE TEMPERATURE: -55°C to +85°C ambient.

SIGNAL TO NOISE RATIO: 50 to 1.

CABLE LENGTHS: 0 to 1000 feet. Longer if desired. Output and strain measurements are independent of changes in cable length and changes in cable characteristics due to temperature, time, pressure and moisture.

POWER SUPPLY: Self-contained rechargeable ± 12 V 1.2 AH battery pack operation. Integral 110/220 V -50/60 hz charger (may be operated continuously with the charger cord plugged into bench supply.) Charging rate of 0.12 Amps.

READOUTS: Panel mounted meter -100 to 0 to +100 scale. Digital readouts 0 to 10,000.

DIMENSIONS: 10" x 6.5" x 12".

OPERATING WEIGHT: 10 lbs.

represents a drawback in the use of the Bison coils for instrumenting inservice pavement sections.

TRRL SOIL STRAIN GAUGE

The TRRL soil strain gauge consists of two aluminum alloy flanges 2.5 in (63 mm) in diameter attached to the ends of a modified variable reluctance transducer (figure 22). The ends anchor into the soil. When the soft iron core moves with regard to the coils, the inductance of the coils is changed. The displacement of the flanges is calculated from the change in inductance measured using an inductance bridge.^[9]

Figure 23 shows a more recent version of the TRRL soil strain gauge. The rubber bellows in this version keep soil particles away from the moving parts of the gauge. The main shortcoming of this device is the mechanical linkage between the disks.^[18] Other researchers have used similar linear variable differential transformers (LVDTs) to measure the differential displacements between flanges.^[19]

The use of dissimilar metals in the design of these gauges should be avoided since they can create a galvanic effect, leading to premature corrosion of the device.^[19]

INSTALLATION

The general precautions and recommendations discussed for strain gauges used in bonded layers apply also to these devices, which can be placed in any desired orientation. During the installation of the TRRL-type soil strain gauges, extra care should be taken to avoid any disturbance of the soil between the flanges.

For the installation of the Bison coils, an electrical technique can be used to place a second coil (a sensor) over the first, already buried one. The coil is moved until a maximum output is recorded. Maximum output is measured when exact coaxiality is achieved.^[27] Lead wires of Bison coils

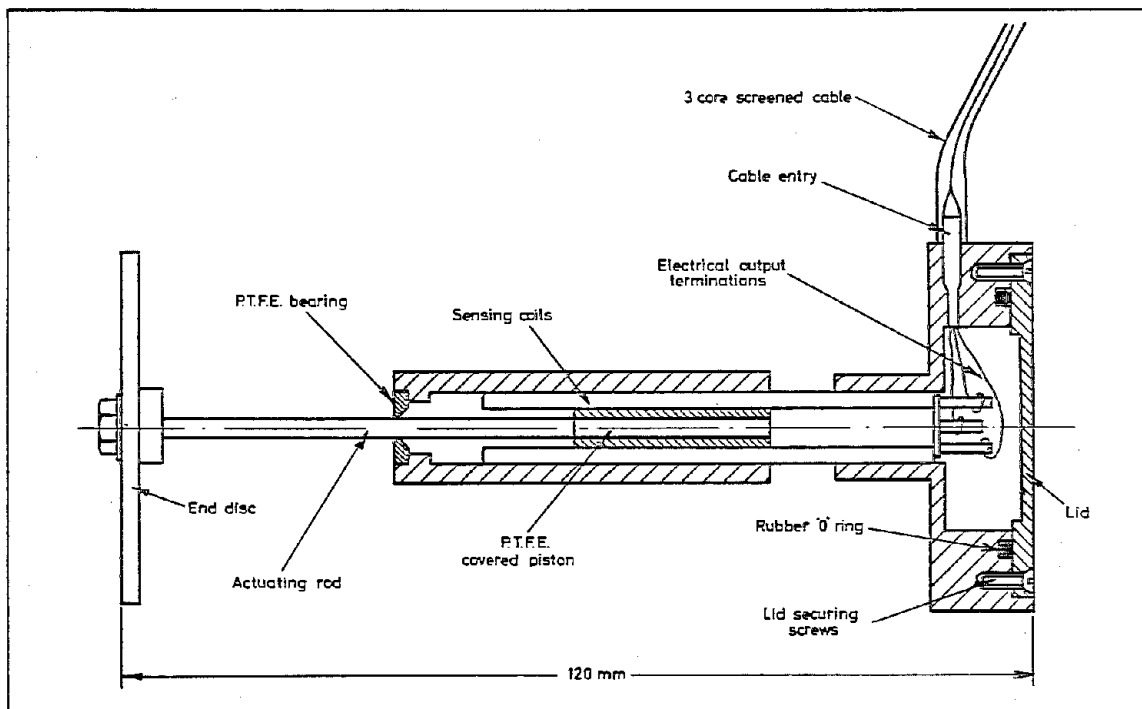


Figure 22. Early TRRL soil strain gauge. [9]

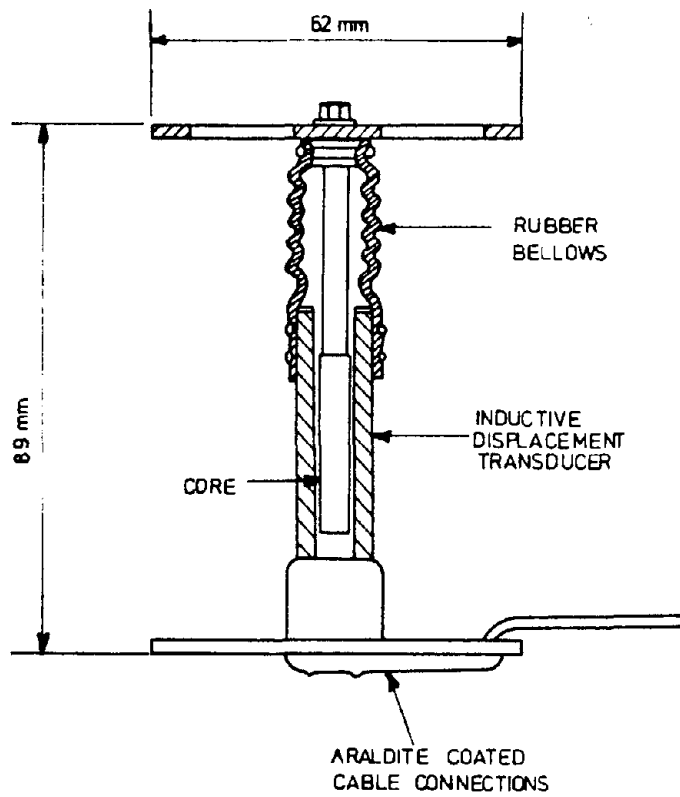


Figure 23. Recent TRRL soil strain gauge. ^[18]

should be placed in a trench separate from the wires of other instruments, and close paralleling with the cables of other instruments should be avoided.

Cost and Availability

Most of the H-gauges that were reviewed in this chapter are not commercially available; some have been developed and manufactured by research institutes. The strip part of the gauges used by research teams from Switzerland and Denmark for the Nardo test were obtained from Kyowa, while their end anchors and moisture protection were supplied by the researchers. Table 3 lists the Kyowa gauge model, lead times, and unit cost. The additional preparation cost is listed which includes the cost of anchors and protection. The H-gauges supplied by Dynatest and TRRL require no additional preparation cost since they are already anchored and protected. The Omega strip gauge, used in the Nardo test by the Italian team, needs no protection or anchoring. For the instrumented core technique, the strain gauges could be obtained from various sources. The BLH gauge, listed in table 3, has been successfully used by the Finnish research team and may be recommended for similar applications. The asphalt block gauges are designed and manufactured by the researchers at the Alberta Research Council and are not commercially available, but are manufactured and installed upon request.

Performance of Strain Gauges

To study the performance of strain gauges in asphalt concrete pavements, one should be concerned with three main factors: the long-term serviceability of the gauge, the accuracy of the measured strains, and the repeatability of results. Unfortunately not enough data exist for every gauge that has been used.

In terms of the protection of gauges from water and aggregate intrusion, the majority of the techniques used fall into the following groups:

- Silicone grease (carrier blocks, instrumented cores).
- Asphalt cement (carrier blocks).

Table 3. Cost and availability of strain gauges.

Type	Manufacturer	Model	Lead Time	Cost	Prep. Cost	Manufacturer's Address
H-gauge	Kyowa	Embedment Gauge KM-120-H2 11L 100-3	2-3 wks	\$26	\$15	Kyowa Dengyo Corp. 10 Reuton Drive Closter, NJ 07624 (201) 784-0500
H-gauge	Dynatest	PAST 1AC PAST 2AC	3-4 mo 6 mo	\$525 \$650	NA	Dynatest Consulting 209 Bald Street PO Box 71 Ojai, CA 93023 (805) 646-2230
48 H-gauge	TRRL	Aluminum Strip	3-4 mo	\$68	NA	R. R. Addis Transport & Road Research Lab Pavement Design & Maintenance Division Old Wokingham Road Crownthorne, Berkshire, UK, RG116AU 0344-770241
Strip	Omega	Encapsulated Gauge DA3	8 wks	\$328	NA	Omega Engineering One Omega Drive PO Box 2669 Stamford, CT 06906

Table 3. Cost and availability of strain gauges. (continued)

Type	Manufacturer	Model	Lead Time	Cost	Prep. Cost	Manufacturer's Address
Block Council	Alberta Research Council (ARC)	Asphaltic Sheet	10 wks	\$300 Canadian	NA	Dr. J. T. Christiso Alberta Research Civil Engineering Department 4445 Calgary Trail Edmonton, Alberta, Canada T6H5R7 (403) 450-5252
64 Core	BLH	FAE2-300-35 PL	8 wks	\$26	\$150	BLH Electronics, Inc. 75 Shawmut Road Canton, MA 02021 (800) 247-2454
Inductive	Bison	4101 A Display unit Coils 1-in Dia. 2-in Dia. 4-in Dia.	8 wks	\$4595 \$74 pair \$78 pair \$74 pair	NA	Bison Instruments 5708 West 36 Street Minneapolis, MN 55416

- Aluminum channel and PVC tape (H-gauges).
- Titanium plate and silicon grease (H-gauges).

The effectiveness of these protection techniques was investigated in the Nardo experiment.^[7] The resistance of the strain gauges was measured after 9 months of embedment. The failure rate of the strain gauges was less than 15 percent in general. High failure rates were reported for the carrier block gauges. The laboratory-prepared asphalt concrete blocks, which were installed by the Finnish team, have experienced the highest failure rate (90 percent), indicating a failure of the bonding between the old and new asphalts. The asphalt cement carrier blocks, installed by the Canadian team, also showed a high failure rate (50 percent).

Researchers at the Technical Research Center in Finland have observed some corrosion problems with the gauges mounted on retrofitted cores. The corrosion appeared in spring 1988, following a very cold winter. Instrumented cores are being installed at the Pennsylvania test track, and their performance will be monitored throughout the year. At the TRRL instrumented pavement sections on the southbound carriageway of the A1 trunk road at Conington, H-gauges and carrier block gauges were installed.^[9] The failure rate of these H-gauges, having an aluminum strip, was 42 percent; the failure rate of the carrier block gauges was 77 percent. These results agree with the observations made at the Nardo experiment.

Asphalt carrier block gauges, supplied by the Alberta Research Council, were installed at the FHWA ALF test sections. All gauges failed during the first few days of loading.^[1] The Kyowa gauges installed at the same site were unprotected, yet the majority of these gauges were still operating after construction, and a few were still operating throughout the test.^[1]

There are no long-term performance data available on the Dynatest H-gauges, but the method of protection looks promising. Some of these gauges were installed at the North Carolina test track and the Minnesota Department of Transportation test sections. Both of these projects are new and no performance data for the gauges are available at this time.

When investigating the accuracy of the measured strains, one should investigate the phenomena by which the gauge measures the strain at the given location throughout the asphalt layer. In the case of the H-gauges, the strip part of the gauge must be strained an amount equal to the strain in the asphalt concrete to which it is attached. If the amount of strain in the strip is known, then the force required to produce such a strain can be calculated using the dimensions and modulus of the elasticity of the strip materials. Under a critical case of high temperature and heavy axle loads, the strain at the bottom of the asphalt concrete layer as calculated from the theory of elasticity solution, can be as high as 800 microstrains.

The total elongation of the 4-in (101-mm)-long strip is calculated by rearranging equation 1 as follows:

$$\delta \ell = \epsilon \times \ell = 4 \times 800 \times 10^{-6} = .003 \text{ in (0.08 mm)}$$

The force required to generate $\delta \ell$ is given by:

$$P = \frac{E \delta \ell t w}{\ell} \quad (4)$$

where

E = modulus of elasticity of strip material

t = thickness of strip

w = width of strip = 0.5 in (12.7 mm)

Table 4 shows the variation of P as a function of t for aluminum and plastic. The calculations are based on a modulus of elasticity of 11×10^6 and 4×10^5 psi (75,800 and 2,750 MPa) for aluminum and plastic, respectively. The expected bearing capacity of the asphaltic concrete materials supports the conclusion that the generation of a force larger than 20 lb (4.5 N) is not feasible.

Under such circumstances, where a larger force is developed there will be a bearing capacity failure at the interface of the anchor bars and the asphalt concrete. Table 4 shows that a maximum thickness of .005 in (0.13 mm)

Table 4. Variation of the required force versus thickness of strip.

Material	Force P (lb)	Thickness (in)
Aluminum	4	.001
	21	.005
	42	.01
	83	.02
	124	.03
Plastic	2	.01
	15	.1
	30	.2
	45	.3

should be used for the aluminum strips. Any strips thicker than that will cause a compressive force, P , in equation 4, that exceeds the bearing capacity of the surrounding asphalt concrete. Repetition of this phenomenon contributes to the looseness of the anchor bars, which might explain the low strain that the TRRL has experienced with its aluminum gauges.^[28] By the same reasoning, it can be seen from table 4 that plastic strips as thick as 0.1 in (2.5 mm) can also be used. For the Dynatest gauges, there are no data on the modulus of the strip material; therefore, no conclusions can be drawn on these gauges. However, the fiber reinforcement should not be placed in the same orientation as the measured strain because that would stiffen the strip. It is also expected, as discussed earlier, that the bending and temperature protections should be placed in such a way that they do not reinforce the gauge.

For the instrumented cores technique, it is recommended that an epoxy with properties similar to that of the asphalt concrete should be used. The clearance between the hole in the pavement and the instrumented core should be as small as possible, approximately 1/32 in (1 mm). Care should be taken not to place a thick layer of epoxy over the gauges, so that the gauges measure the actual strains in the asphalt and not the strains in the epoxy layer. As mentioned earlier, instrumented cores being installed at the Pennsylvania test track will be used to experiment with these problems.

The only approach to studying the accuracy of the measured strains is to compare the measured with the calculated strains as obtained from theoretical solutions. The researchers at the Nardo Road Test have conducted such an experiment in which the moduli of the pavement layers were backcalculated from falling weight deflectometer (FWD) measurements. These modulus values were used in a theoretical analysis to predict the strain values at the bottom of the asphalt concrete layer. The in-situ strain measurements under truck loading were compared with the calculated strains. Figure 24 shows the ratios of measured to calculated strains for the participating teams. For the second day of FWD testing, a range of modulus values was backcalculated for each test site. The corresponding maximum and minimum ratios of measured to calculated strains are represented by the horizontal lines in the second bar of each pair in figure 24. As expected, much variation occurred between the various types

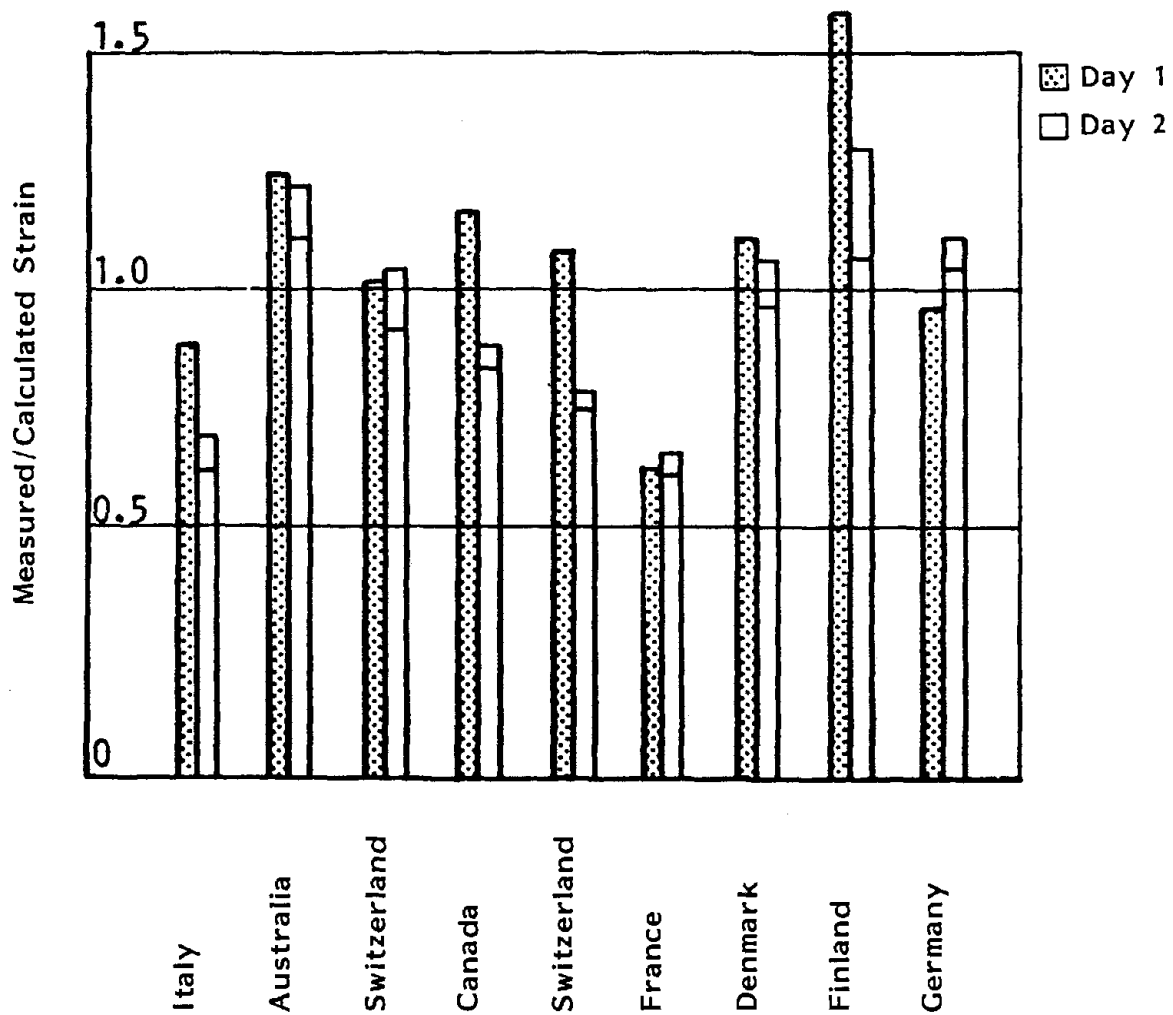


Figure 24. Ratio of measured to calculated strains for the Nardo Road Test.[7]

of gauges, but within the gauge categories, the variations were relatively small. The gauges installed by the French team showed the lowest ratio of measured to calculated strains because the gauge protection against water and aggregate was made of varnish (resin plus compound AK22). This material stiffened the overall gauge, which proves the point discussed earlier. The strain gauges from the Finnish team showed a large ratio for the reasons that were discussed earlier. The accuracy of the rest of the gauges was reasonable, given the variations in material properties of the section.

As mentioned earlier, some H-gauges with the Kyowa plastic strips and the Alberta Research Council (ARC) asphalt cement block gauges were installed at the ALF test sections.^[1] On January 29, 1987, at the beginning of the test period, a load-up experiment was carried out which was used to verify the response of the strain gauges. The wheel load was varied from 9,400 lb to 19,000 lb. Strains were measured on three lateral positions, with the centerline of the test wheels passing over the pavement centerline, as shown in figure 25.^[1] At the time of the load-up test, all of the ARC gauges and one of the H-gauges were inoperable. The strain data for the load-up study are shown graphically in figure 25 for the wheels positioned over the centerline. Also shown in the figures are strains calculated from static and dynamic analyses. The static strains were calculated with the BISAR computer program.^[29] In the dynamic approach to the problem, it is assumed that the wheel load generates a dynamic component as a result of its rolling action. The dynamic strains are calculated with the DYNAMIC1 computer program.^[30] There is relatively good agreement between the measured and calculated strains, especially for the smaller load levels.

To demonstrate the within- and between-gauge variability in the readings, the measured strain values for five load levels and three passes of the test wheels are given in table 5. The average standard deviation within three repeated measurements is approximately 4 microstrains, which compares favorably with the actual readings. Repeatability between gauges can also be observed in table 5 by comparing the readings of the gauges placed to the right and left of the centerline and by comparing gauges at different stations. The repeatability of the gauges is good, considering the nature of the measurements. The long-term repeatability of the gauges that survived is

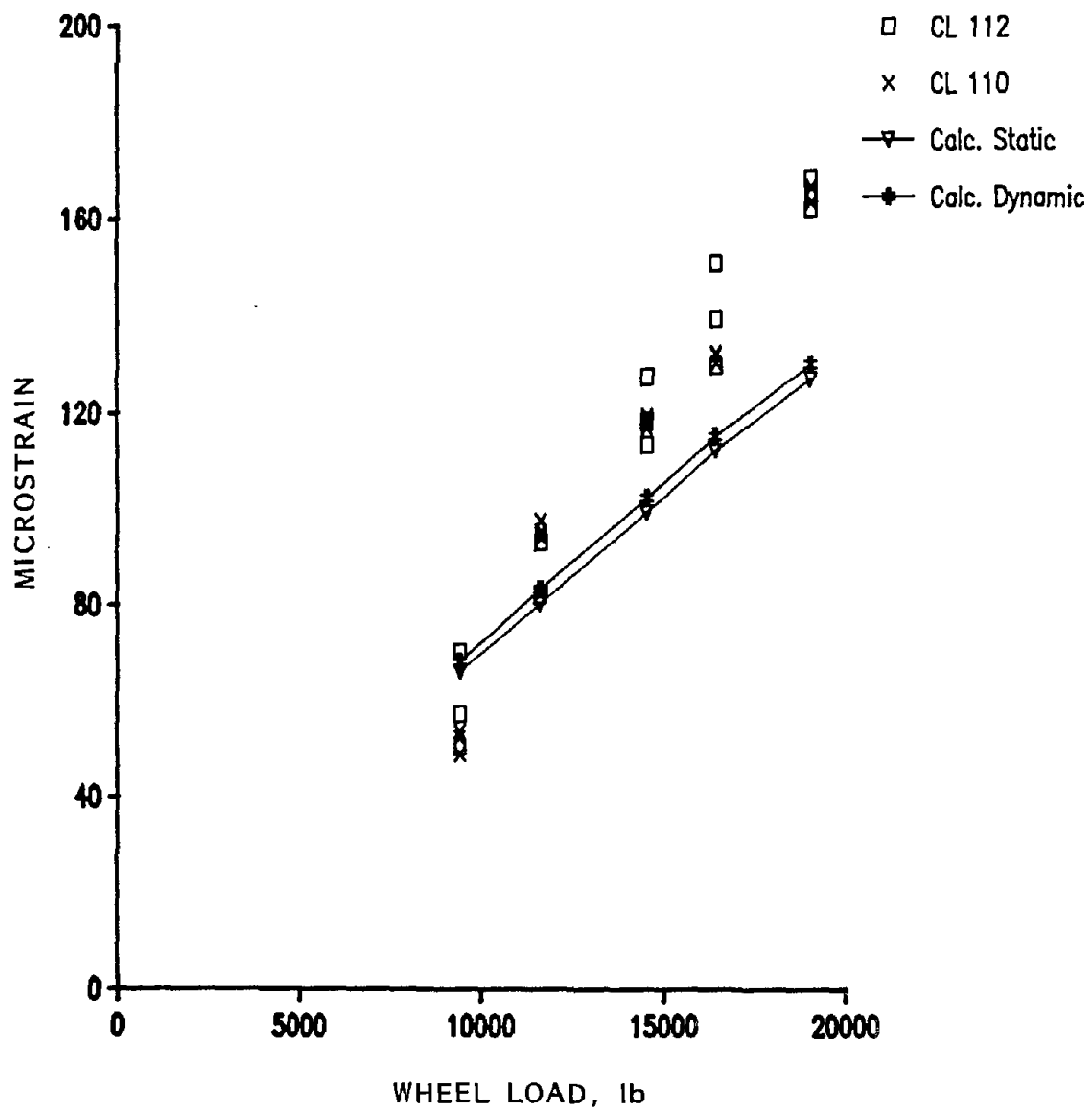


Figure 25. Strain measured during load-up study for testing of section 2.3.⁽¹⁾

Table 5. Strain gauge measurements during testing
under ALF wheel load of 19,000 lb

Wheel Load	Station	Microstrain		
		1 ft Left of Centerline	Centerline	1 ft Right of Centerline
9,400 lb	112	54.2	50.4	55.4
		53.2	70.2	56.4
		<u>58.9</u>	<u>57.3</u>	<u>57.6</u>
	Average	55.4	59.3	56.5
	110	NA	52.3	39.7
		NA	53.5	55.7
		<u>NA</u>	<u>48.8</u>	<u>NA</u>
	Average	NA	51.5	47.7
11,600 lb	112	72.4	81.9	74.0
		76.9	81.9	74.3
		<u>76.2</u>	<u>92.9</u>	<u>75.9</u>
	Average	75.2	85.6	74.7
	110	NA	95.1	81.9
		NA	93.9	63.9
		<u>NA</u>	<u>97.3</u>	<u>84.4</u>
	Average	NA	95.4	76.7
14,100 lb	112	107.4	127.6	99.8
		101.4	118.4	98.9
		<u>95.4</u>	<u>113.4</u>	<u>94.8</u>
	Average	101.4	119.8	97.8
	110	NA	117.8	103.9
		NA	116.8	92.0
		<u>NA</u>	<u>119.4</u>	<u>94.5</u>
	Average	NA	118.0	96.8
16,400	112	124.1	129.8	113.7
		126.0	150.9	115.0
		<u>126.6</u>	<u>139.5</u>	<u>113.1</u>
	Average	125.6	140.1	113.9
	110	NA	130.4	81.9
		NA	132.0	98.6
		<u>NA</u>	<u>132.3</u>	<u>77.5</u>
	Average	NA	131.6	86.0

Table 5. Strain gauge measurements during testing
under ALF wheel load of 19,000 lb. (continued)

Wheel Load	Station	Microstrain		
		1 ft Left of Centerline	Centerline	1 ft Right of Centerline
19,000	112	142.3	168.5	122.2
		142.0	162.2	120.9
		<u>143.0</u>	<u>164.7</u>	<u>123.1</u>
		Average 142.4	165.1	122.0
	110	NA	166.6	118.1
		NA	166.6	117.2
		<u>NA</u>	<u>163.5</u>	<u>120.0</u>
		Average NA	165.6	118.4

shown in table 6. The data show a good repeatability with the H-gauges even at various intervals throughout the test period.

The Dynatest gauges have been installed at sections tested under the Danish Road Testing Machine (RTM).^[19] The strains measured from these gauges were compared with theoretical strains, as shown in figure 26. The data show all scattered points, but the majority of the measurements are around the equality lines.

Table 6. Long-term repeatability of Kyowa gauges.

Day of Test	Microstrain	
	Centerline	1 ft Left of Centerline
12	58.58	31.49
	64.25	29.29
	65.83	30.23
50	175.74	105.82
	172.90	104.24
	179.20	105.19
	180.42	105.82
	178.88	106.42
122	184.55	132.27
	170.70	132.90
	182.04	129.12
	168.18	129.75
	182.04	132.27
140	19.53	658.86
	19.22	671.45
	19.53	634.29
	19.53	622.33
	19.53	627.99

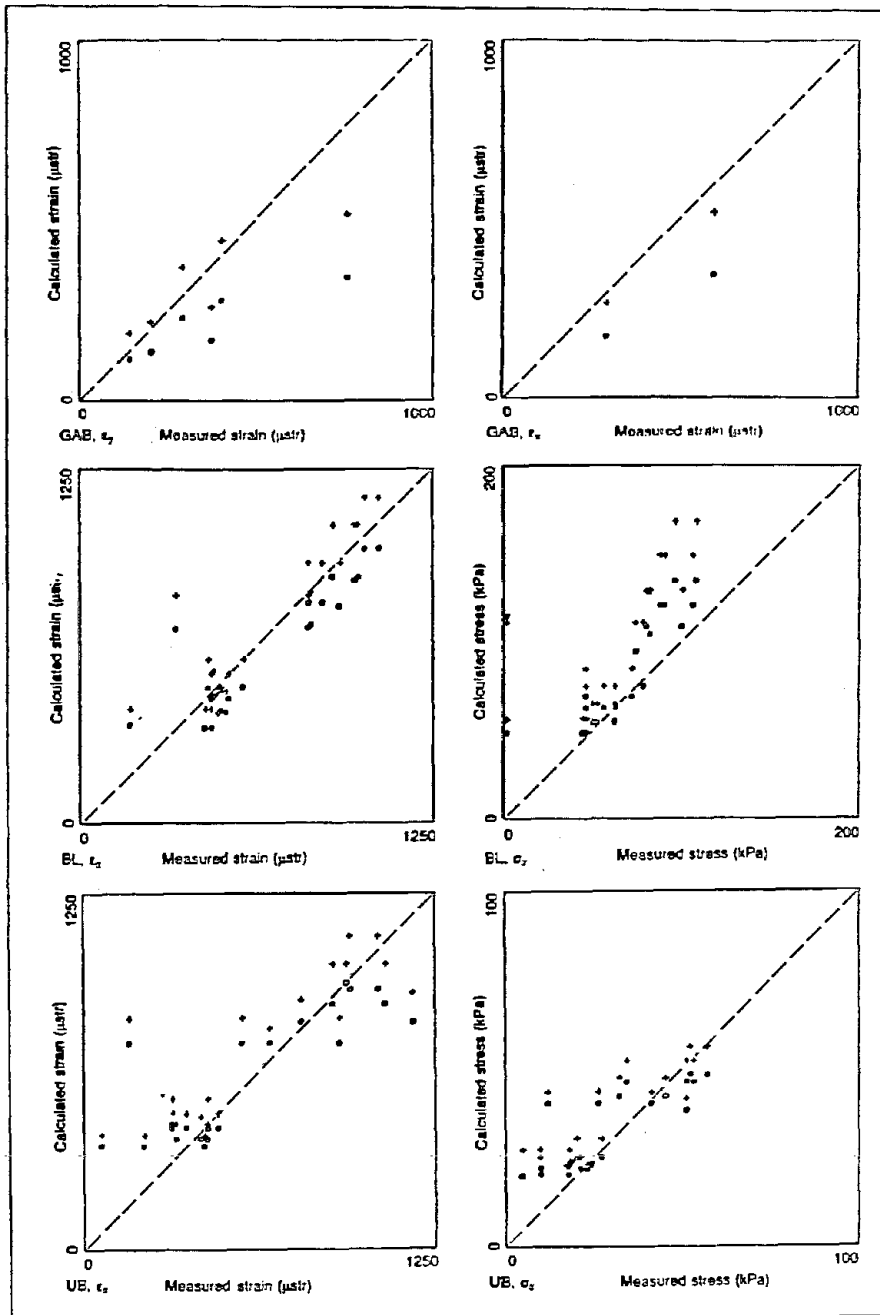


Figure 26. Comparison of measured and calculated peak stress and strain values for different climatic conditions. [19]

4. PRESSURE MEASUREMENT

A knowledge of the stress and deformation field is imperative for the study of many phenomena in solid mechanics. This knowledge can be obtained by a combination of theoretical and experimental investigations. The experimental measurements can be attempted through the placement of pressure cells in the areas of interest. For this task, some design and installation considerations must be taken into account.

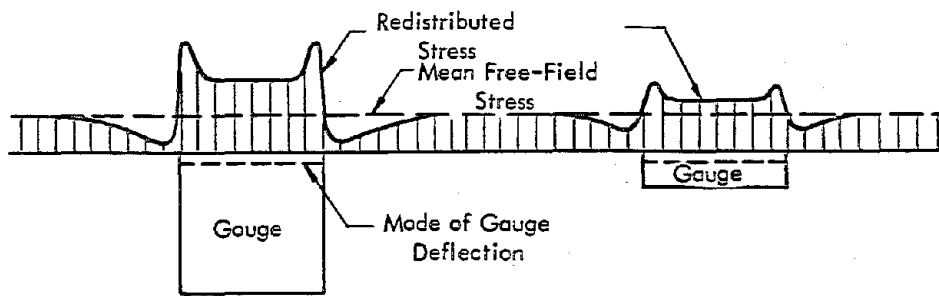
BASIC DESIGN REQUIREMENT

The stress measured by a pressure cell is an electrical output from the instrument that should be related to the measured stress applied to the diaphragm of the cell in a mechanical bench calibration test. For this test, the pressure cell is placed in a pressure chamber and a known pressure is applied to it.^[18]

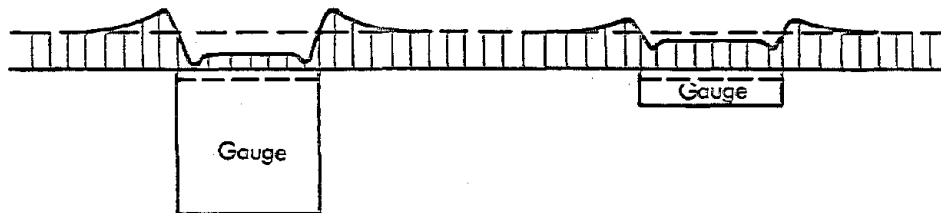
The main requirements in the design of pressure cells are the ability:

- To measure the stress in the free-field condition, that is, without changing the state of stress in the soil mass.
- To place the pressure cell in the soil mass without appreciably disturbing the existing state of stress in the soil mass.

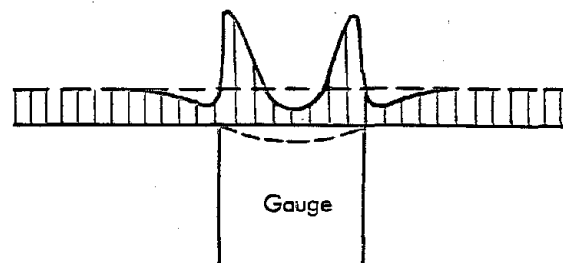
These requirements are interrelated and cannot be fully satisfied because the introduction of a measuring instrument into a soil mass disturbs the stress distribution, as shown in figure 27.^[31] This figure shows that the presence of the instrument will usually cause redistribution of free-field stress. This redistribution depends on the stiffness of the cell diaphragm as well as the ratio of cell thickness to its diameter (also called aspect ratio). Torry and Sparrow performed a theoretical analysis for a pressure



(a) Gauge More Stiff than Soil



(b) Gauge Less Stiff than Soil



(c) Stiff Gauge with Flexible Diaphragm

Figure 27. Stress distribution around embedded pressure cells. [31]

cell in a uniaxial stress field.^[32] They studied the effect of flexibility factor on the pressure cell registration. Flexibility factor was defined by:

$$\text{Flexibility Factor} = \frac{E_s d^3}{E_c t^3} \quad (5)$$

where

E_s = Young's modulus of the soil material

E_c = Young's modulus of the cell material

d = diameter of the cell diaphragm

t = thickness of the cell diaphragm

Figure 28 illustrates the variation of pressure cell registration as a function of flexibility factor for different values of aspect ratio. The cell registration factor (c) represents the ratio of measured to actual stress values. According to this figure, cell registration remains nearly constant for a flexibility factor less than unity. In order to reduce the error in pressure measurements, a cell registration close to 1 is desired. It can be seen that as small an aspect ratio as possible, less than 0.2, with a flexibility factor of less than unity could warrant correct cell registration. Dunnicliff has reported that, in the design of pressure cells, in order to minimize the measurement error, the diaphragm should have high stiffness and an aspect ratio of less than 0.1.^[33]

The ratio of tangential stress to normal stress on the diaphragm is another factor that affects the registration of the cell. Collins et al. studied this factor in their theoretical investigation of pressure cells.^[34] Fossberg also conducted a finite element analysis for a cell with an aspect ratio of 0.17 under different tangential to normal stress ratios.^[35] Figures 29 and 30 compare the results of the separate studies conducted by Collins et al., Fossberg, and Tory and Sparrow. The discrepancy between the results may be due to the effect of lateral tension on the cell.^[18] Fossberg and Tory and Sparrow took the diaphragm deflection into account in their modeling, whereas Collins et al. made no assumptions concerning lateral strain conditions in their calculations. Therefore, the results by Collins et al.

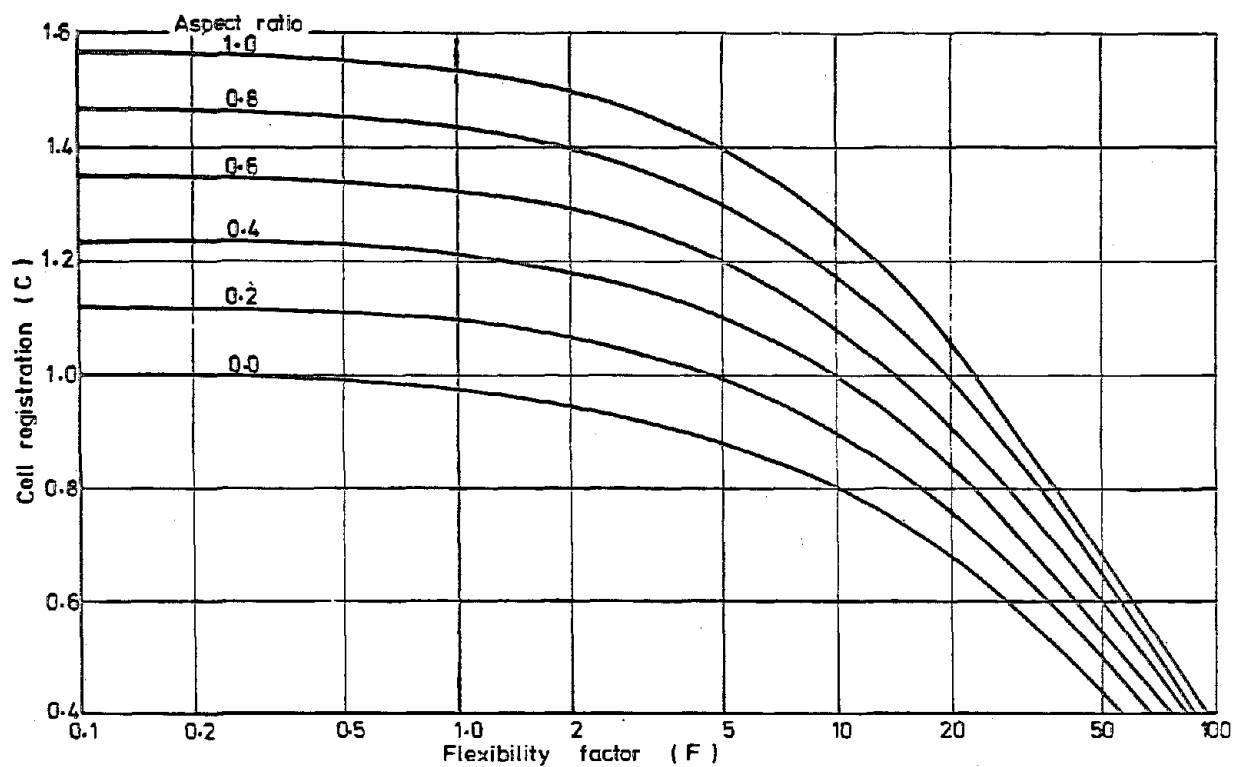


Figure 28. Variation of pressure cell registration with flexibility factor.^[18]

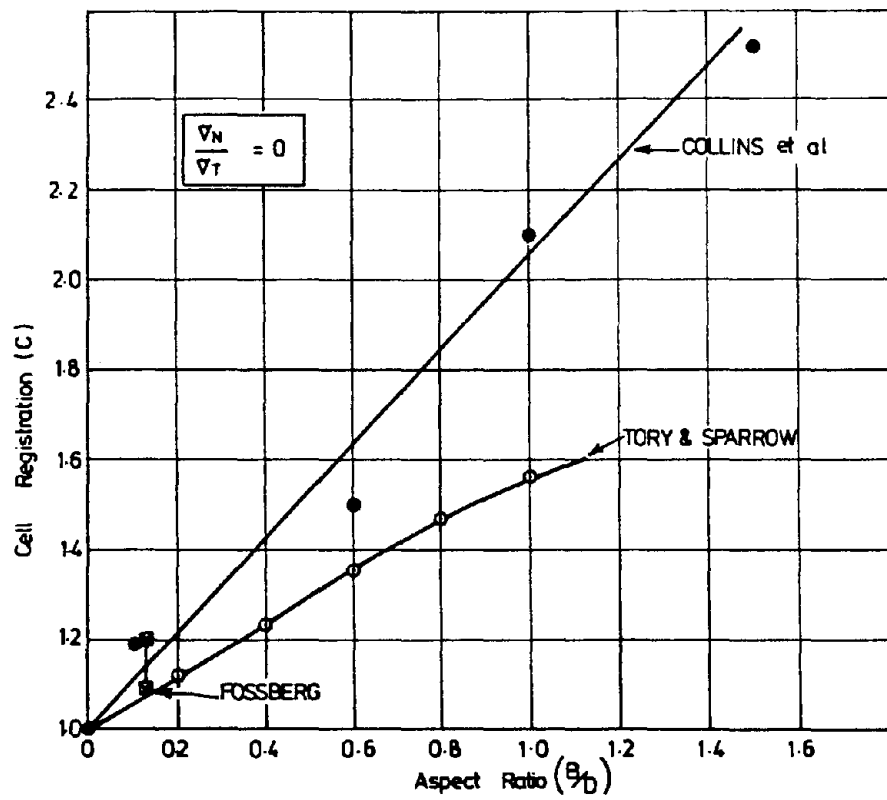


Figure 29. Comparison of theoretical pressure cell registration for zero stress ratio. [18]

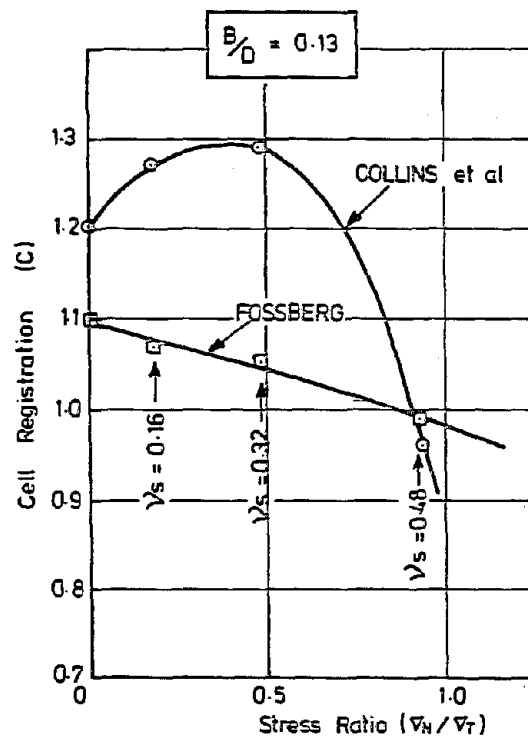


Figure 30. Comparison of theoretical pressure cell registration at various stress ratios. [18]

are applicable to pressure cells with restrained diaphragms, while the other two results are applicable only to free diaphragms.^[18]

Another design consideration concerns the size of the diaphragm. The diameter of the sensing element should be considerably larger than that of the maximum soil particle in the vicinity of the pressure cell. Kallstenius and Bergav have suggested that the cell diaphragm diameter must be at least 50 times that of the largest soil particle.^[36] It is also recommended to keep the unusually large soil particles away from the diaphragm during installation to avoid the possibility of a high stress concentration resulting from point contact with the diaphragm, but the soil gradation should not vary greatly from that in the surroundings.

Peattie and Sparrow have suggested that, for the design of pressure cells with diameters of about 3 in (75 mm), the area of the diaphragm should be less than 45 percent of the overall facial area.^[37] This criterion is based on the general trends of their experiments which showed that high pressures develop near the edges of the cell face. Therefore, to reduce the measurement error, the sensitive area of the cell should not be extended very close to the edges. Also a stiff annular ring is required to reduce the effect of mechanical cross sensitivity from the presence of the horizontal component of soil pressure, especially for the case of free-diaphragm pressure cells.

In case of dynamic measurements, density of the pressure cell should be comparable with that of the soil. If the density of the cell is appreciably greater than that of the soil, then it will not follow the motion of the soil. Therefore, the cell inertia will produce a dynamic stress on the interface which can cause either over-registration or under-registration.^[31] Frequency response of the pressure cell should also be considered in the case of dynamic measurements with a high frequency.^[31]

Another important consideration is the long-term durability of the pressure cells. The cell should be waterproof, and the lead wires should be strong so that they can withstand the stresses imposed during and after

installation. Table 7 summarizes major factors affecting measurements with pressure cells.

Because of the many difficulties with designing and installing soil pressure cells, accuracies better than 20 percent cannot be expected.^[18]

TYPES OF PRESSURE CELLS

In the previous section, general design requirements for pressure cells were reviewed. In this section the particular characteristics of some of the existing cells will be discussed. There are two basic types of embedded pressure cells: diaphragm cells and hydraulic cells.

The diaphragm cells consist of a stiff circular diaphragm supported by an integral stiff annular ring. This diaphragm is deflected by the applied external soil pressure. Electrical resistance strain gauges or some other type of strain measurement sensors are bonded onto the interior face of the diaphragm.^[33] Figure 31 shows two typical diaphragm-type pressure cells. A diaphragm cell may have one or two independent active faces.

The hydraulic-type pressure cells consist of two circular (or in some cases, rectangular) steel plates welded together around their periphery to form a chamber or cavity. This chamber is filled with some type of de-aired liquid such as mercury. Total stress acting on the faceplates is balanced by an equal pressure induced in the internal liquid. This type of cell provides average soil pressure.

The two versions of hydraulic cells are shown in figure 32. The first version has thick active faces (0.1 to 0.25 in (2.5 to 6.5 mm)) with a thin cavity (0.02 to 0.08 in (0.5 to 2 mm)), such that the stiffness of the cell is similar to that of the surrounding soil. Since the amount of liquid in the cell is very small, the cell experiences minimal effects of thermal expansion and contraction of the liquid.^[33] In the second version of the hydraulic cell, both faces are made of thin metal sheet, usually with a rolled edge. The liquid chamber in this case is much thicker (0.1 to 0.4 in

Table 7. Major factors affecting pressure cell registration.^[33]

Factor	Description of Error	Correction Method ^a
Aspect ratio (ratio of cell thickness to diameter)	Cell thickness alters stress field around cell	Use relatively thin cells ($T/D < 1/10$)
Soil/cell stiffness ratio (ratio of soil stiffness to cell stiffness)	May cause cell to under- or overregister Error will change if soil stiffness changes	Design cell for high stiffness and use correction factor
Size of cell	Very small cells subject to scale effects and placement errors Very large cells difficult to install and subject to nonuniform bedding	Use intermediate size of cell: typically 9–12 in (230–300 mm) diameter ^b
Stress-strain behavior of soil	Measurements influenced by confining conditions	Calibrate cell under near-usage conditions ^b
Placement effects	Physical placement and backfilling causes alteration of material properties and stress field around cell	Use placement technique that causes minimum alteration of material properties and stress field ^b
Eccentric, non-uniform, and point loads	Soil grain size too large for cell size used Nonuniform bedding causes nonuniform loading	Increase active diameter of cell ^b Use hydraulic cells with grooved thick active faces in preference to other types ^b Take great care to maximize uniformity of bedding ^b
Proximity of structures and other embedded instruments	Interaction of stress fields near instruments and structure causes errors	Use adequate spacing
Orientation of cell	Changing orientation while placing fill over cell causes reading change	Use placement methods that minimize orientation changes Attach tiltmeters to cell
Concentrations of normal stress at edges of cell	Causes cell to under- or overregister, depending on stiffness of cell relative to soil	For diaphragm cell, use inactive stiff edge ring to reduce sensitive area ($d/D \approx 0.6$) ^b For hydraulic cell, use grooved thick active face and thin layer of liquid
Deflection of active face	Excessive deflection of active face changes stress distribution around cell by arching	Design cell for low deflection: for diaphragm cell, diaphragm diameter/diaphragm deflection at center > 2000 – 5000 ; for hydraulic cell, use thin layer of liquid ^b
Placement stresses	Overstressing during soil compaction may permanently damage cell	Check cell and transducer design for yield strength (hydraulic cells with pneumatic transducers have high overload capacity) ^b
Corrosion and moisture	May cause failure of cell by attacking cell materials	Use appropriate materials and high-quality waterproofing ^b
Temperature	Temperature change causes change of cell reading	Design cell for minimum sensitivity to temperature; if significant temperature change is likely, measure temperature and apply correction factor determined during calibration ^b
Dynamic stress measurements	Response time, natural frequency, and inertia of cell cause errors	Use appropriate type of cell and transducer, together with dynamic calibration ^b

^a D = cell diameter; T = cell thickness; d = diaphragm diameter.

^bApplies also to contact earth pressure cells.

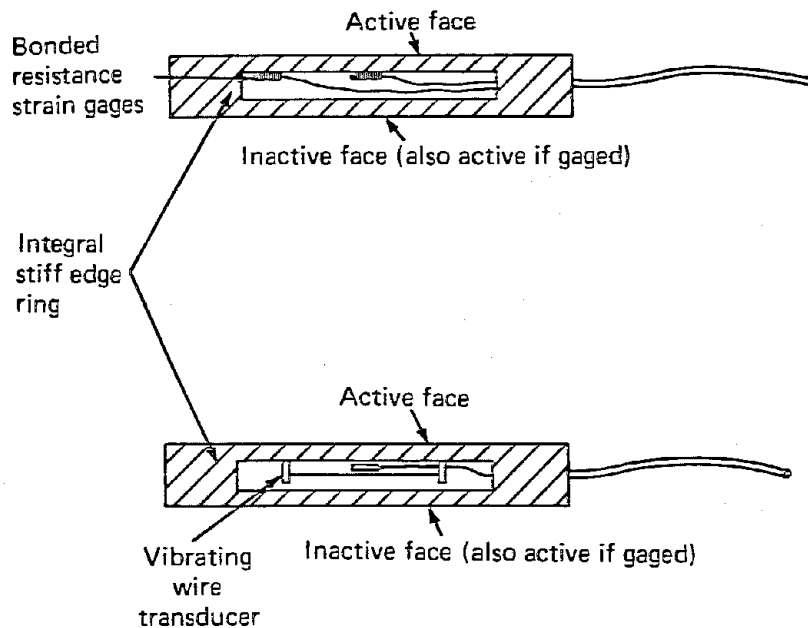


Figure 31. Typical diaphragm type pressure cells. [33]

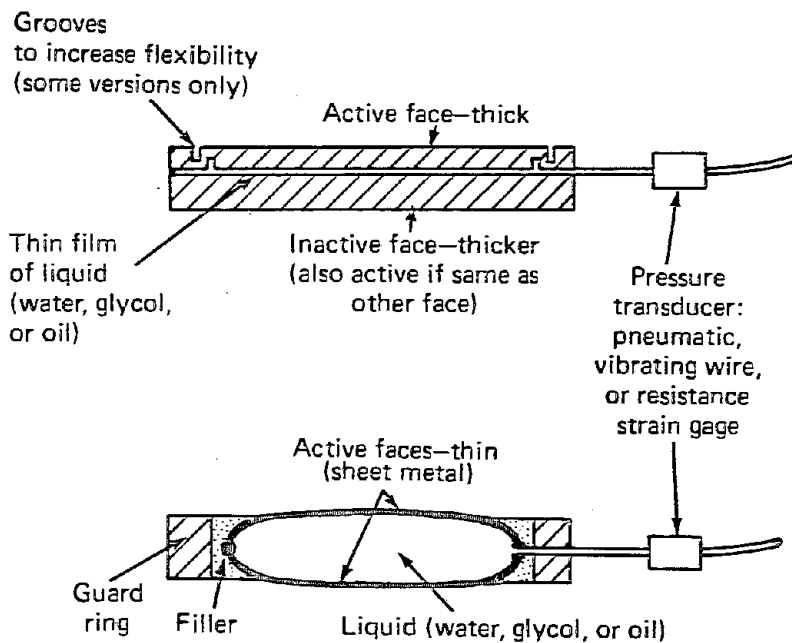


Figure 32. Two versions of hydraulic pressure cells. [33]

(2.5 to 10 mm)); thus the stiffness of the cell is less than that of the surrounding soil. A guard ring can be provided to protect the cell from radial edge loads. The active faces of this version of hydraulic cells are usually domed outward, making their installation harder.^[33]

As mentioned earlier, the applied soil pressure is reacted by an internal liquid pressure. This pressure is measured using pneumatic transducers, vibrating wire, or bonded or unbonded strain gauges.^[33]

TRRL/LVDT PRESSURE CELL

The TRRL/LVDT pressure cell is a diaphragm-type pressure cell that uses an LVDT to measure deflection of the diaphragm under soil pressure (figure 33). The LVDT core fitted to one diaphragm can be screwed to its null position in the LVDT body attached to the other diaphragm. The cell is then sealed and maintained at this position under zero pressure.^[18] A thick annular ring, as shown in the figure, reduces the effect of lateral stress on the cell registration. This cell can be used for short-term static and dynamic loading conditions.

TRRL PIEZOELECTRIC PRESSURE CELL

The TRRL piezoelectric pressure cells are diaphragm-type pressure cells that utilize piezoelectric quartz crystals as the sensing elements. The MK.I cell is used only for measurement of vertical stresses.^[38] The MK.II cell is a modified version with a much stiffer construction, designed to reduce mechanical cross sensitivity. This cell can be used to measure the horizontal component of stress in the soil (figure 34).^[9]

These cells operate on the principle that, when external pressure is applied to the diaphragm, the x-cut quartz crystals undergo a minute distortion and an electronic charge is produced on the faces of each crystal. The quartz crystals are disks with a diameter of 1 in (25 mm) and a thickness of 0.12 in (3.1 mm). Copper foils are used to collect the charge generated across the surfaces during dynamic loading.^[18]

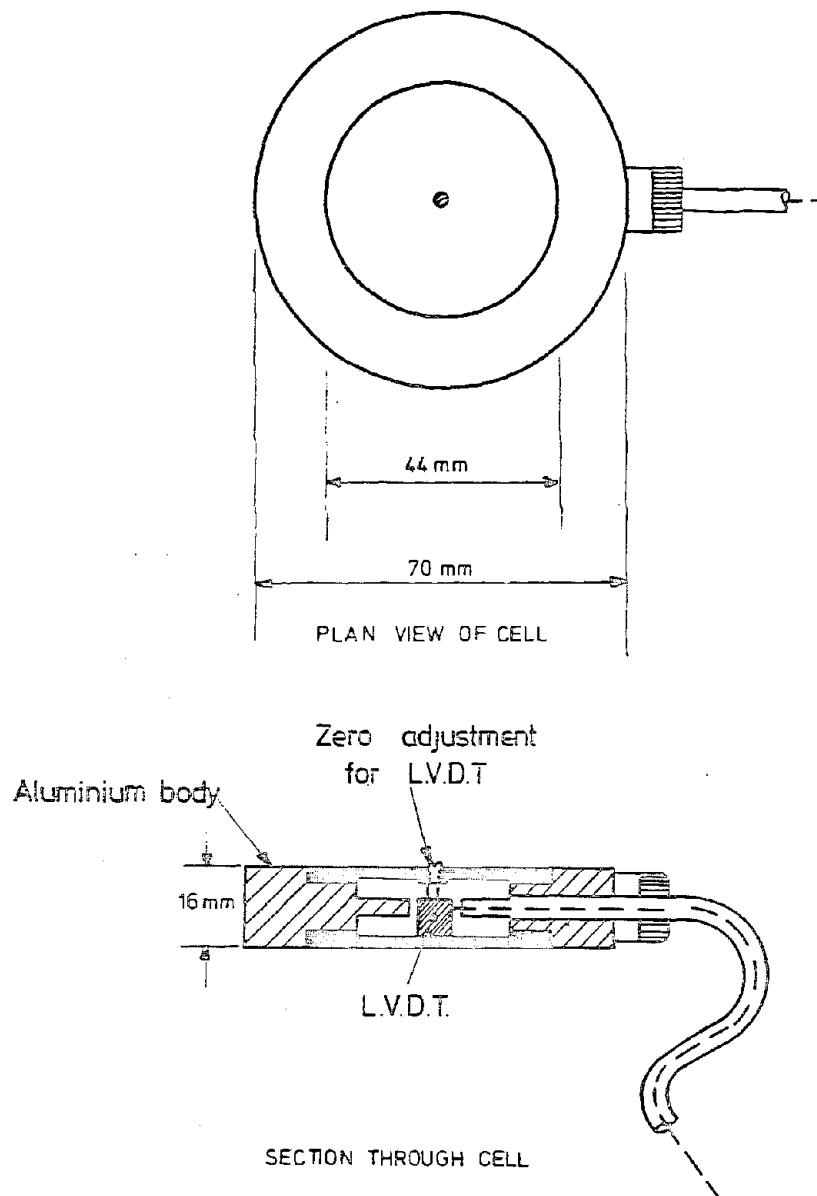
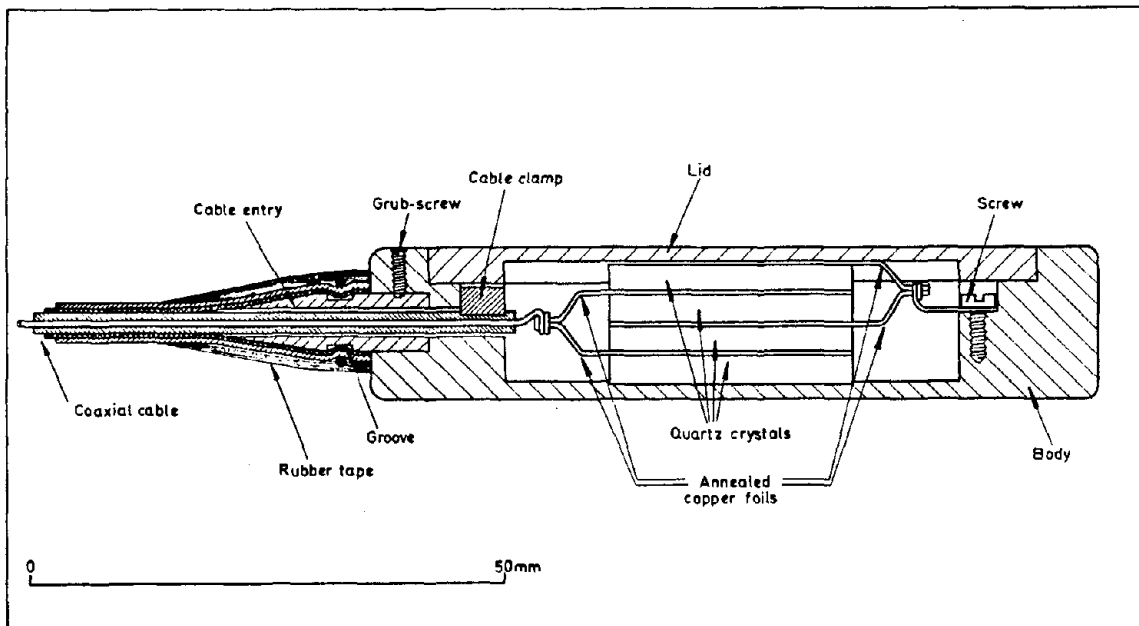
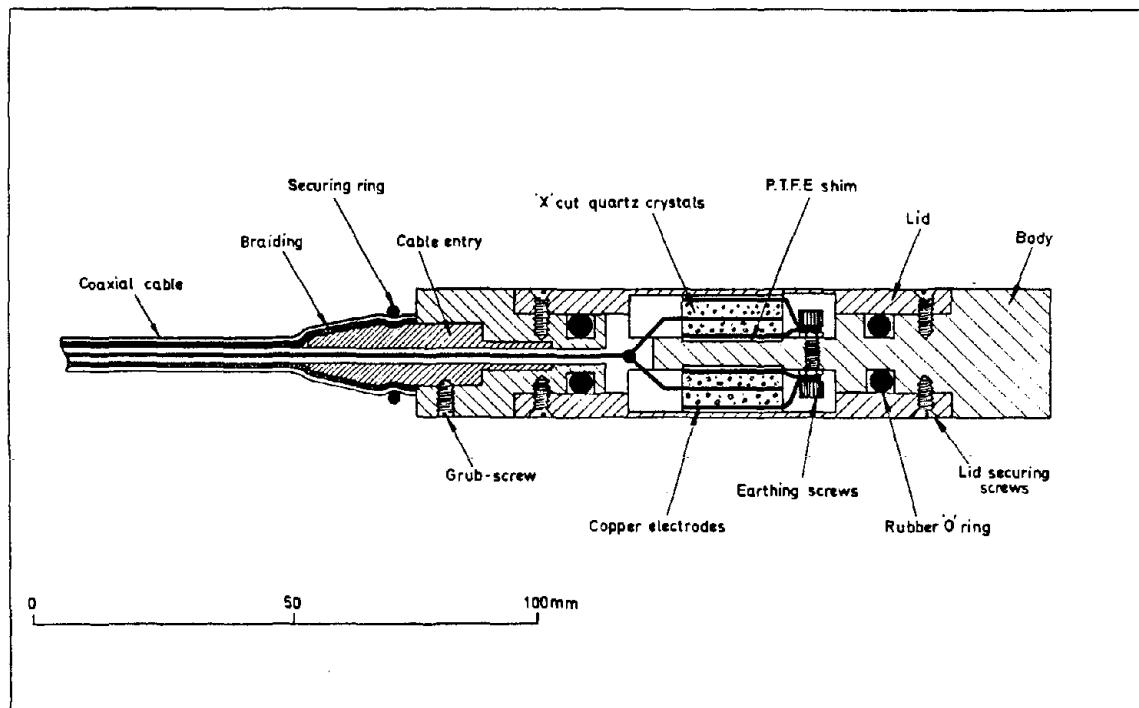


Figure 33. TRRL plan view and cross-sectional views of a TRRL/LVDT pressure cell. [18]



MK. I



MK. II

Figure 34. Cross sections of MK.I and MK.II piezoelectric pressure cells. [9]

These pressure cells are manufactured from aluminum alloy. The dimensions of Mk.I and Mk.II cells are a 3-in (76-mm) diameter with a 0.67-in (17-mm) thickness and a 4-in (101-mm) diameter with 0.78-in (19.8-mm) thickness, respectively. The aluminum body is anodized and the lids are sealed for protection against corrosion and moisture.^[9]

NOTTINGHAM PRESSURE CELLS

The Nottingham pressure cell is a diaphragm-type pressure cell made of titanium. The sensing element is a four-arm active strain gauge bridge (full Wheatstone bridge) bonded to the inner side of the diaphragm. The strain gauges have a resistance of 350 ohms. The bridge is supplied with 10 V of direct current (DC). Potentiometric balance is provided across chosen arms of the Wheatstone bridge, and a 500-K calibration resistor can be switched across one arm to simulate a fixed stress input.^[18, 39]

The diaphragm has a diameter of 1.5 in (38 mm) and a thickness of 0.08 in (2 mm). The cell has an overall diameter of 2.5 in (64 mm) and a thickness of 0.43 in (11 mm).^[39] Figure 35 shows the plan view and cross section of this pressure cell, which is appropriate for both short-term static and dynamic loading conditions.

SE PRESSURE CELL

This diaphragm-type pressure cell was developed by the U.S. Army Corps of Engineers at the Waterways Experiment Station (WES) for the measurement of blast stresses in soil. It has a frequency response range of several kilohertz and can be used for measuring the fastest stress change during dynamic tests. The SE soil pressure cell consists of a semiconductor gauged diaphragm made of stainless steel. This pressure cell has a high rate of response; therefore, it is more susceptible to localized stress variations.^[40] Figure 36 shows some of the physical characteristics of this cell. A modified version of these cells is manufactured by Kulite Semiconductor Products, Inc. (figure 37).^[41]

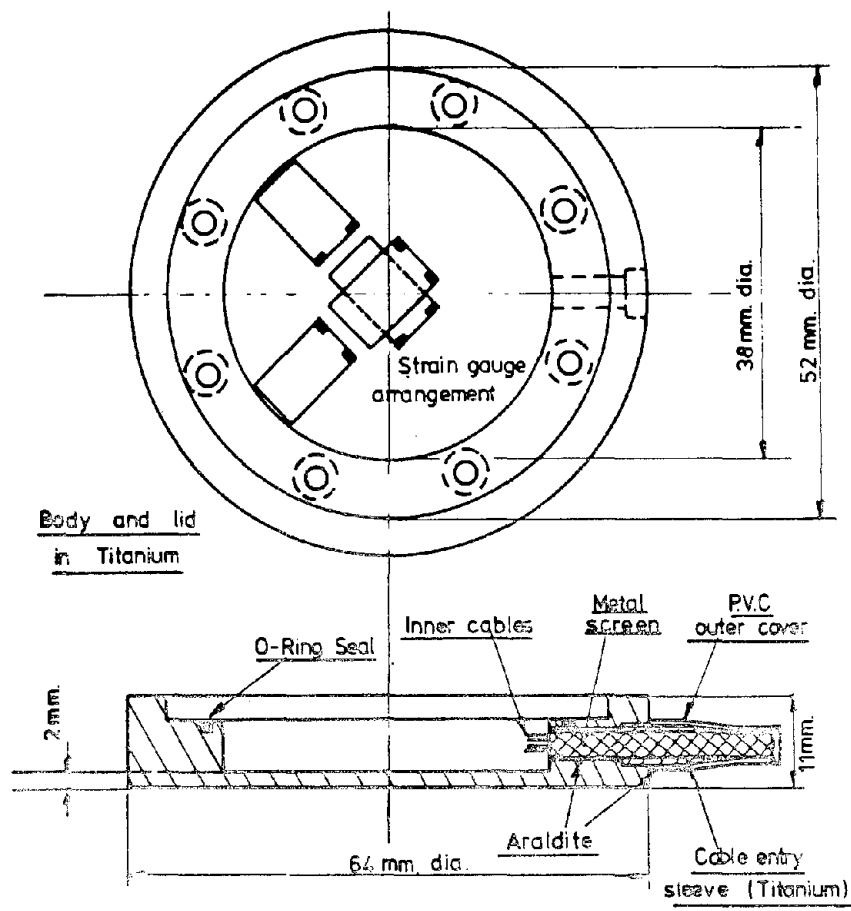


Figure 35. Plan and cross-sectional views of the Nottingham pressure cell. [39]

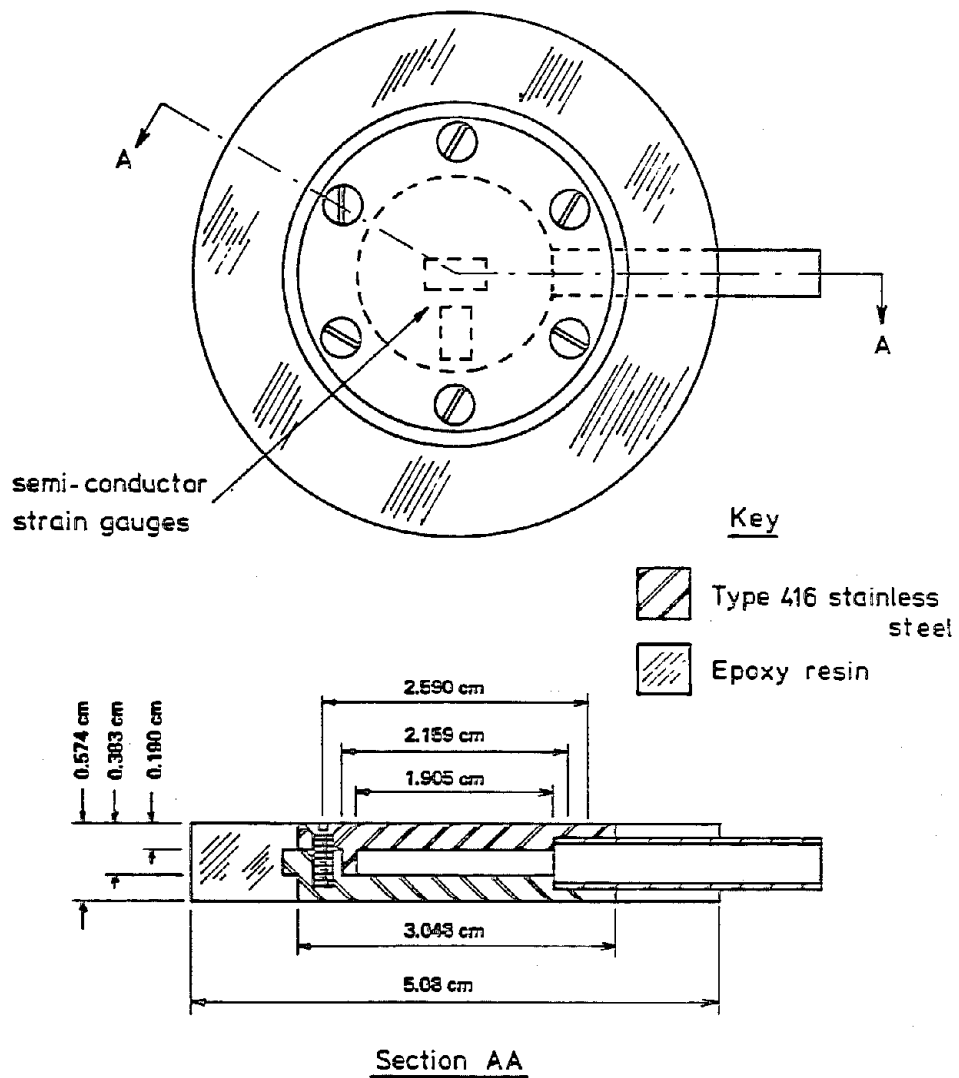


Figure 36. Plan and cross-sectional views of an SE pressure cell. ^[18]

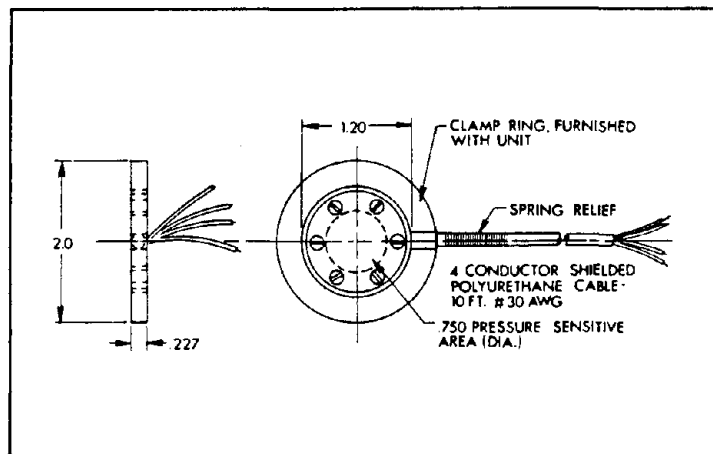


Figure 37. Kulite LQ-080U soil pressure cell. [41]

WES SOIL PRESSURE CELLS

This hydraulic pressure cell was developed by the U. S. Army Corps of Engineers at the Waterways Experiment Station. It has a diameter of 6 in (152 mm) and an overall thickness of 1 in (25 mm). It is fabricated from stainless steel and consists of a circular faceplate which reacts on an internal mercury-filled chamber. Pressure on the faceplate is averaged and transmitted by the mercury to an internal membrane. Four SR-4 strain gauges forming a full Wheatstone bridge are attached to the rear of the internal membrane.^[25] These strain gauges are hermetically sealed within the cell. They undergo resistance change proportionally to strains in the membrane which are induced by the pressure applied on the faceplate and transmitted through the mercury. Other properties of this cell include:^[40]

- Aspect ratio = $\frac{\text{Thickness}}{\text{Diameter}} = 0.167.$
- Flexibility factor (F) = $9.147 \times 10^{-5} \times E_s$
(where E_s is Young's modulus for the soil).
- Working frequency response = 100 Hz.

Figure 38 illustrates the cross section of a WES pressure cell. This cell can be used for pressure measurement under short-term static and dynamic loading conditions.^[18]

KULITE PRESSURE CELL

This pressure cell is a hydraulic-type cell manufactured by Kulite Semiconductor Products, Inc.^[41] Figure 39 illustrates the dimensions of this cell, and table 8 lists some of the properties of this commercially available soil pressure cell.^[41]

SOPT PRESSURE CELLS

SOPT pressure cells were developed at the Technical University of Denmark. They are of hydraulic type with an oil-filled cavity. The cells are made of pure titanium and their geometry has been improved by tapering the

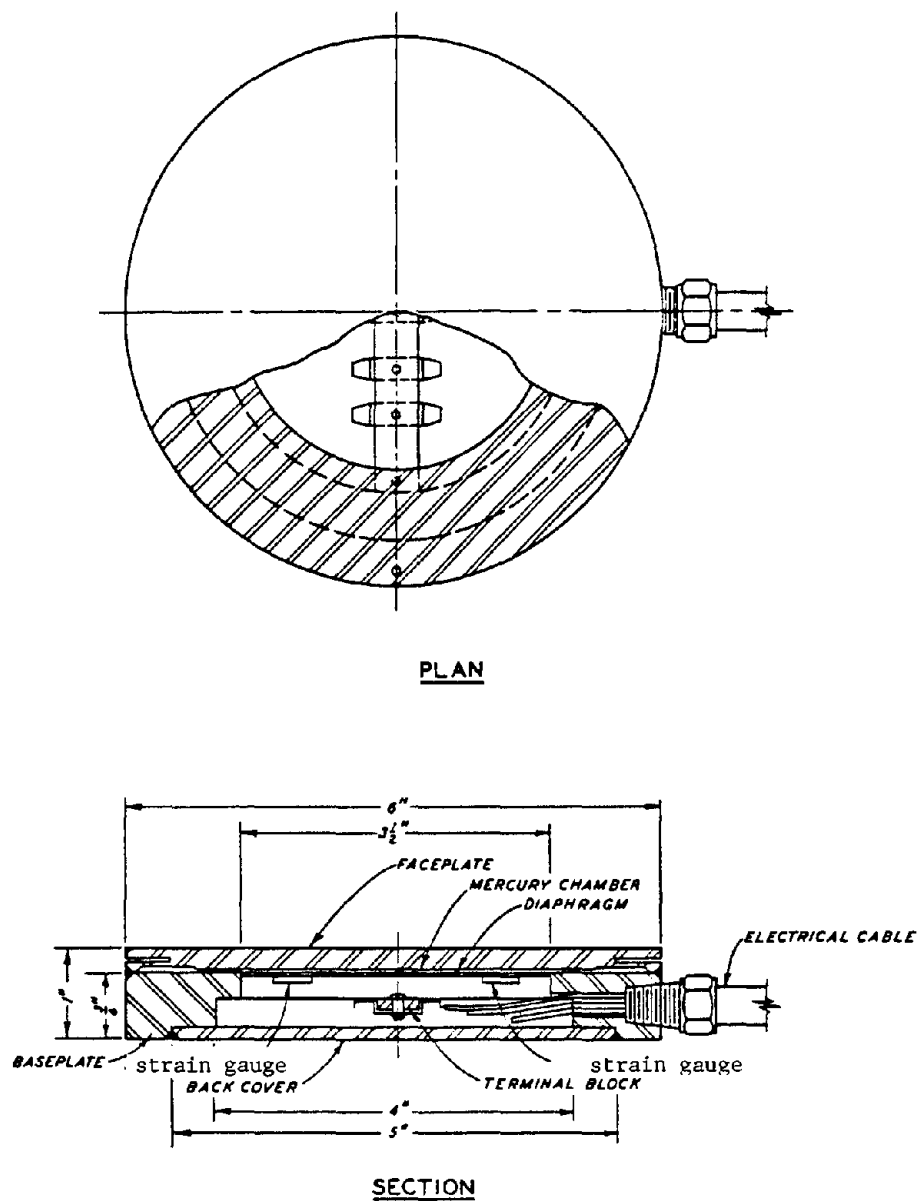


Figure 38. Plan and cross-sectional views of a WES soil pressure cell. [40]

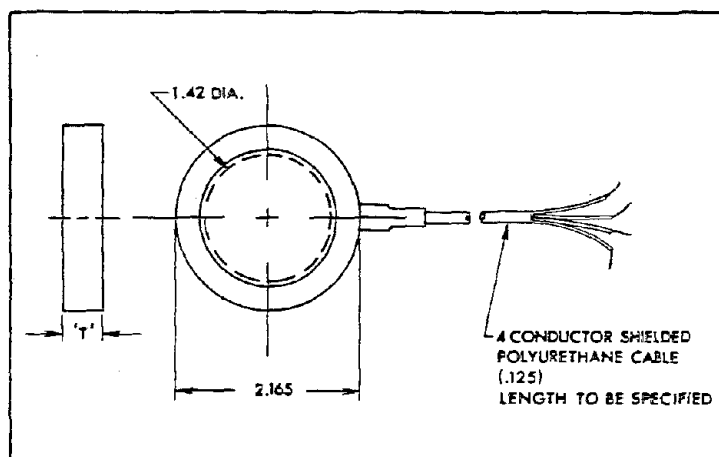


Figure 39. Soil pressure cell type 0234.^[41]

Table 8. Design specifications of type-0234 soil pressure cells.^[41]

	Range PSI	Overpressure
	0-15	2 Times Rated Pressure Range
	0-50	
	0-100	
Deflection	.0001" (0.0025mm) at Rated Pressure	
Natural Frequency (KHz)	2	
Operational Mode	Compression	
Pressure Media	Any Liquid, Solid or Gas Compatible With 17-4 SS (H 900 Condition)	
Rated Electrical Excitation	7.5VDC (Nom.)	
Maximum Electrical Excitation	10VDC (Max.)	
Input Impedance	750 Ohms (Nom.)	
Output Impedance	350 Ohms (Nom.)	
Full Scale Output	100mV (Nom.)	
Residual Unbalance	±5mV (Max.)	
Combined Non-Linearity, Hysteresis and Repeatability	Less Than ±1%	
Resolution	Infinite	
Operating Temperature Range	0°F to 100°F (-15°C to +40°C)	
Compensated Temperature Range	32°F to 84°F (0°C to 30°C)	
Thermal Zero Shift	±0.01% FRO/°F	
Thermal Sensitivity Shift	±0.01% FRO/°F	
Acceleration Sensitivity	NA	
Humidity	100% Relative Humidity	
Response Time (To Step Input)	NA	
Active/Total Area Ratio	43%	
Electrical Connection	Sealed Cable Assembly in Lengths Up to 33' (10 Meters)	
Insulation Resistance	100 Megohms @ 50VDC	
Case Material	17-4 PH (H 900) Stainless Steel	
Weight	250 Grams	
Sensing Principle	4 Arm Strain Gage Bridge	

edges at 45 degrees.^[19] Figure 40 shows different components of the cell. These cells have a thickness of 0.5 in (13 mm) and are available in diameters of 2.68 and 3.86 in (68 and 98 mm). The smaller cell is appropriate for use in clays and sands with fine aggregates, whereas the larger one is used in soils with large aggregates. The induced liquid pressure is measured with a full strain-gauge bridge. Table 9 lists the specifications of these cells. These pressure cells are commercially available and according to the manufacturer, have a service life of more than 36 months and a fatigue life of more than 3×10^6 cycles.^[20]

INSTALLATION

Reliable placement and installation technique is a key factor for obtaining valid data. As it was noted earlier, installation should be such that the minimum amount of disturbance takes place in the stress regime of the soil.

Prior to installation, each cell should be calibrated under fluid pressure to be sure that it is functioning correctly. Most commercial pressure cells are provided with laboratory calibration charts. However, these calibrations are not adequate. To ensure the validity of the pressure measurement, each cell should be calibrated in a triaxial chamber, using the same type of material in which it is to be embedded. Calibration of pressure cells in large chambers is a time-consuming and expensive procedure. Detailed procedures for the calibration in triaxial chambers have been given by both Hadala and Selig.^[42, 43]

To increase the service life of a pressure cell, grease should be smeared or silicon sealant sprayed over the screws holding the diaphragm in place and around the cable entry on the side of the pressure cell.

Procedures for installing pressure cells at different layers of pavement are discussed in the following section.

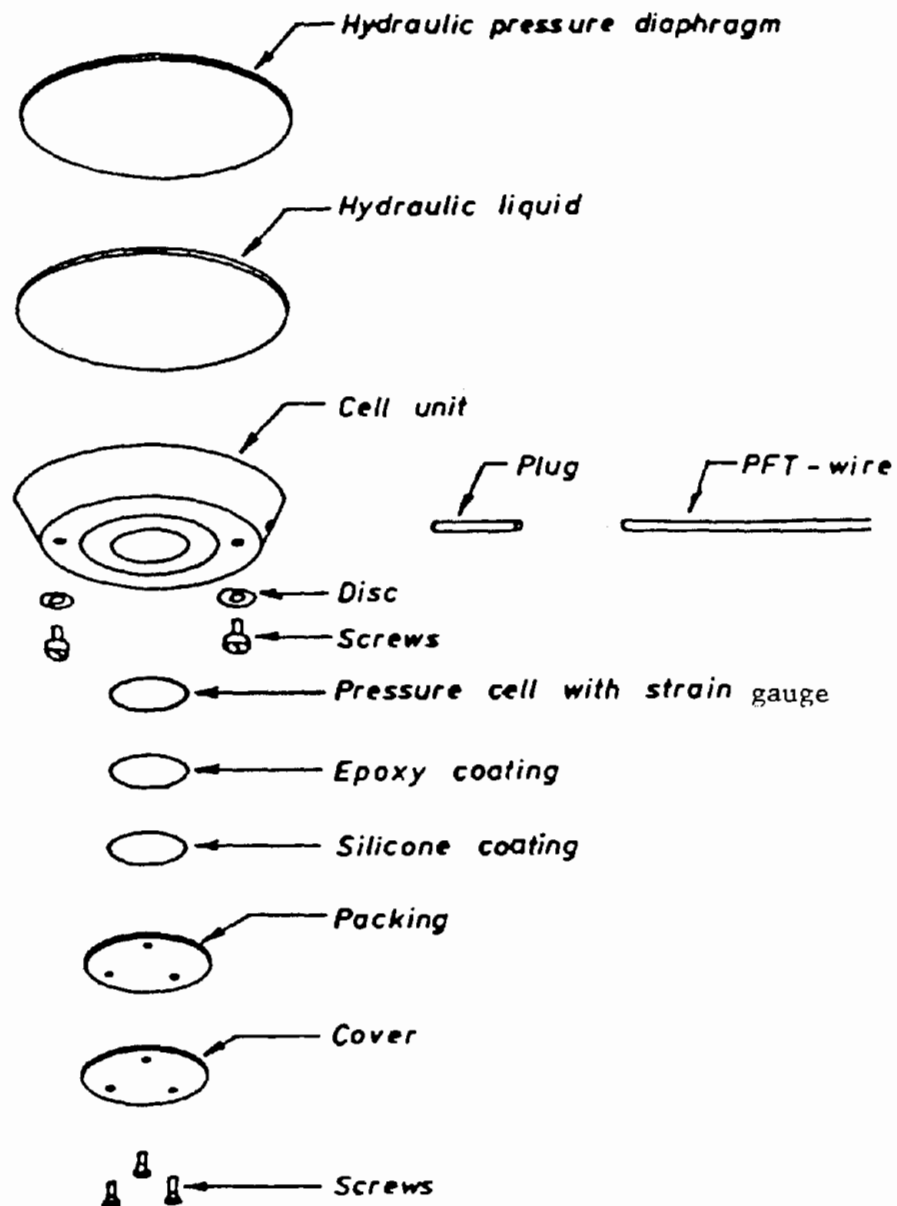


Figure 40. SOPT soil pressure cell.^[20]

Table 9. Specifications of SOPT pressure cells. [20]

Specification

<i>Type</i>	<i>FTC - I</i>	<i>FTC - II</i>
<i>Range</i>	<i>10 - 200kPa, 15-30 psi</i>	<i>100-800kPa, 15-120 psi</i>
<i>Cell-material</i>	<i>Pure Titanium</i>	
<i>Coating</i>	<i>Epoxy and Sand</i>	
<i>Temperature</i>	<i>-30 - 150° C</i>	<i>-22~300°F</i>
<i>Resistance</i>	<i>4×350Ω in full Weston Bridge</i>	
<i>Function</i>	<i>Linear for E-modulus</i> <i>< 500 000 kPa</i> <i>< 70 000 psi</i>	
<i>Output</i>	<i>Reff. Calibration chart</i>	
<i>Voltage</i>	<i>up to 12V</i>	
<i>Fatigue-life</i>	<i>More than 3×10⁶ cycles</i>	
<i>Service-life</i>	<i>> 36 months</i>	

PRESSURE CELLS IN THE SUBGRADE

For pressure cells that are to be installed at some depth in the subgrade, the following points should be followed:^[24]

1. Accurately survey the cell locations and establish the level reference for each cell.
2. Excavate the subgrade to the desired depth; level and smooth the bottom of the hole; and cover it with a very thin layer of fine sand.
3. Place the pressure cell on the layer with the faceplate up.
4. Place the excavated subgrade material around and about 6 in (150 mm) over the cell and compact it by hand.
5. Fill the excavation with the remainder of the subgrade material and compact it with a hand tamper.

Subgrade buildup should then be continued until an elevation of about 1 ft above the next cell installation level is reached. Then the above procedure can be repeated.

PRESSURE CELLS IN THE SUBBASE LAYER

To install pressure cells in the subbase layer (including the top of subgrade), these steps should be followed:^[24, 40]

1. Build the subbase 1 to 1 1/2 ft (0.3 to 0.5 m) above the subgrade.
2. Accurately survey the cell location and establish the load reference for each cell.
3. Excavate the subbase to reach the desired depth; level and smooth the bottom of the excavation; and cover it with a very thin layer of fine sand.
4. Place the pressure cell on the layer with the faceplate up and place fine sand around and about 1 in (25 mm) over it.

5. Place the subbase material, with the large aggregates removed from it, about 4 to 6 in (10 to 15 mm) over the cell and compact it by hand.
6. Fill the remainder of the excavation with regular subbase material and compact it with a hand tamper.

Subbase buildup and compaction can be continued by the contractor at this point.

PRESSURE CELLS IN THE BASE LAYER

The procedure that was described for a subbase layer can be applied for installation of a pressure cell at the top of the subbase or within the base layer.

The procedure for placement of pressure cells at the top of the base layer and directly underneath the asphalt concrete layer is as follows:^[24, 40]

1. Remove a shallow portion of the base course very carefully. Remove just enough material to place the pressure cell in the depression.
2. Place fine sand at the bottom of the excavation and smooth it by hand.
3. Place the pressure cell on the sand, faceplate up and flush with the top surface of base course.
4. Cover the pressure cell with approximately 2 in (5 mm) of fines from a cold-mix asphaltic concrete.

At this point the construction of the asphalt concrete layer can be started. To avoid possible shifting of pressure cells, some hot-mix asphalt can be placed over the cells by using a shovel before the paver approaches.

It should be added that the cables for the pressure cells at each level should be placed in a common trench at that level and covered with fine sand. Also, if large soil movements are anticipated, a gentle loop in the cable near the cable entry is recommended. If possible, the output from the pressure cells should be monitored and recorded using a data acquisition system during the installation. Therefore, if the cell is damaged during the construction,

the damage can be detected and the cell possibly replaced before the construction is complete. If monitoring of the pressure cell response is not possible, electrical checks should be done frequently during the installation.

COST AND AVAILABILITY

As mentioned earlier, pressure cells should be calibrated in a triaxial chamber using the same type of soil in which it is to be embedded. The calibration process is a very time-consuming and, therefore, expensive task. The cost of calibration and preparation is an important factor that should be kept in mind when considering pressure cells for instrumentation. Cost and availability of different types of pressure cells are listed in table 10.

PERFORMANCE OF PRESSURE CELLS

As discussed in previous sections, installation of a pressure cell in a soil mass alters the state of stress in the vicinity of the cell. Theoretically, for a pressure with a small aspect ratio and a flexibility factor less than 1, the distortion of the stress regime becomes very small. The concentration of the stress by a pressure cell would be expected to depend greatly on its compressibility. Thus, if the cell compressibility is less than that of the soil, registered pressure will probably be higher than true pressures.

Some of the factors affecting the accuracy of all pressure cells under field conditions are error parameters of effects such as eccentric loading, compressibilities that do not match, and techniques of cell installation.^[24] The modulus of the soil in which the pressure cell is embedded may be either larger or smaller than the modulus of the cell, thus causing a distortion in the stress regime in the vicinity of the cells, which could be a source of error. Another limitation of pressure cells concerns their stability with time, which depends on the cell design and craftsmanship.

Analysis of data from experiments with WES soil pressure cells has shown that the variability of individual readings, expressed as a percentage of the

Table 10. Cost and availability of pressure cells.

Type	Manufacturer	Model	Lead Time	Cost	Comments	Manufacturer's Address
Hydraulic	Kulite	0234 w/o reinf. plate w reinf. plate	8 wks	\$450 \$470		Kulite Semiconductor, Inc. 1039 Hoyt Avenue Ridfield, NJ 07657 (201) 945-3000
Hydraulic	Dynatest	SOPT098 SOPT298 SOPT068 SOPT268	6 mo 6 mo	\$2650 \$2400		Dynatest Consulting, Inc. 209 Bald Street PO Box 71 Ojai, CA 93023 (805) 646-2230
Hydraulic	WES		3 mo	\$600	Only for loan	Albert J. Bush III USAE Waterways Experimental Station PO Box 631 Vicksburg, MS 39180 (601) 634-3545
Hydraulic	University of Nottingham		2 mo	\$525		Stephen Brown Department of Civil Engineering University of Nottingham University Park Nottingham, UK, NG72RD 0602-56101
Diaphragm	Kulite	LQ-080U				Kulite Semiconductor, Inc. 1039 Hoyt Avenue Ridfield, NJ 07657 (201) 461-0900

Table 10. Cost and availability of pressure cells. (continued)

Type	Manufacturer	Model	Lead Time	Cost	Comments	Manufacturer's Address
Diaphragm	TRRL	LVDT	3-4 mo	\$505		R. R. Addis
Diaphragm	TRRL	Mk.I Mk.II			No Longer available	Transport & Road Research Laboratory Pavement Design and Maintenance Division Old Wokingham Road Crownthorne, Berkshire, UK RG116AU 0344-770241

measured reading, was 1.5 percent when 50 percent of all data was analyzed and 5.6 percent when 99 percent of all data was analyzed.^[24] An analysis of registered pressure on different cells under identical loading conditions showed that the variability of the readings was 3.1 percent for 50 percent of all data and 11.9 percent for 99 percent of all data.^[24] Generally, the accuracy of WES pressure cells was found to be within 10 percent. The residual stress measurements made regularly throughout 9 months were accurate to within 0.5 psi.^[24]

During 9 months of operation, of 17 pressure cells, 2 stopped working and only 1 gave unreliable responses but was still operational.^[24]

The accuracy of the SOPT pressure cells was evaluated under the Danish Road Testing Machine.^[19] The measured vertical stresses were compared with stresses calculated from Chevron and two finite element programs. The results are shown in figure 41. The measured strains at various radical distances agree with the theoretical ones.

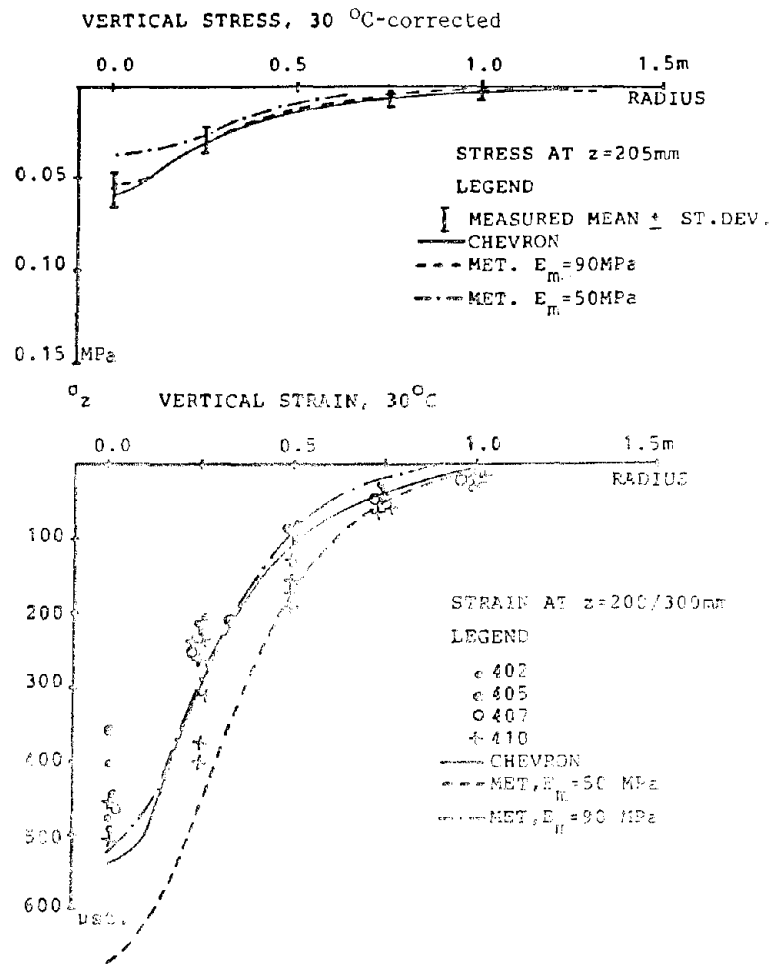


Figure 41. Comparison between measured and calculated vertical stresses and strains.[19]

5. DEFLECTION MEASUREMENT

Deflection response of flexible pavements under dynamic loading has been used by various investigators and researchers as an indicator of the in situ stiffness of the various pavement layers. When the load is applied at the pavement surface, the system will deflect in a bowl shape, which is referred to as the deflection basin. In the early stages of pavement research, only the maximum deflection under the center of the load was measured. This measurement included surface deflection at various radial distances from the center. Recently, the deflections at various depths into the pavement layers have been measured, which is expected to improve the prediction of in-situ pavement parameters.

Different types of instrumentation are available to measure vertical deflections in the pavement system. They can be grouped into the following categories:

- Acceleration-measuring devices.
- Velocity-measuring devices.
- Deflection-measuring devices.

The following is a description of each category and their measuring elements.

ACCELERATION-MEASURING DEVICES

These devices are based on the principle that the acceleration of an object is related to its displacement. In other words, the displacement of a point on the pavement surface can be evaluated by double-integrating the acceleration signal of that point. The devices used to measure the acceleration of a point are referred to as "accelerometers." The output signal of an accelerometer can be integrated by electrical hardware or through the software after digitization. Accelerometers can only measure dynamic instantaneous deflections since the point of measurement should experience a certain level of excitation. Accelerometers are used in pavement

instrumentation because they are very sensitive to small changes, measuring accelerations as small as a fraction of the acceleration of gravity (g). Accelerometers do not need any reference points; their reference is enclosed within the actual unit. Therefore, they can be used as a stand-alone unit on the surface or embedded into the pavement layers at any depth. Figure 42 shows physical characteristics of a servoaccelerometer appropriate for pavement instrumentation.

VELOCITY-MEASURING DEVICES

The velocity signal of the pavement surface under a given dynamic load can be integrated once to generate the deflection time response. The devices that are usually used to measure velocity signals are referred to as "geophones." Figure 43 shows a schematic of a geophone. A mass is attached to a spring with support to the pavement surface. A wire (or coil) attached to the mass becomes part of the total mass. When the pavement surface moves, the magnet and support also move. The mass tends to remain stationary and lags behind the motion of the pavement surface; hence, there is relative motion between the coil and the magnetic field. The resultant voltage output is proportional to the velocity (or speed) of this motion. The geophone frequency is defined as the frequency of oscillation in the theoretical case of no damping. This frequency is controlled by the ratio of total mass-to-spring constant. When the measurement frequency becomes smaller, the mass-to-spring constant should be increased. Therefore, a larger mass should be used for low-frequency measurements. The use of a larger mass would also increase the overall dimensions and unit price of the geophone.

Geophones are very rugged and can withstand high temperatures. In a test of a geophone under high temperature, the unit was placed in an oven set at 275 °F for a period of 12 hours. When it was tested, it showed normal operation. Geophones can measure only dynamic transient deflections, and as discussed earlier, their actual size depends on the frequency of movement. They do not require any reference point and can be placed anywhere in the pavement layers.

SB Series

BENDIX CONNECTOR
TYPE PTIH-10-6P
MATING CONNECTOR PT06A-10-6SR
WHEN SEATED ADDS 1.76 TO HEIGHT

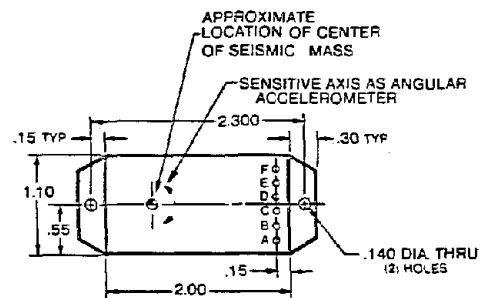
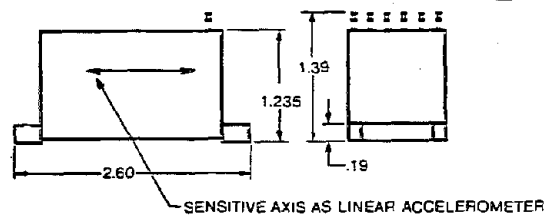
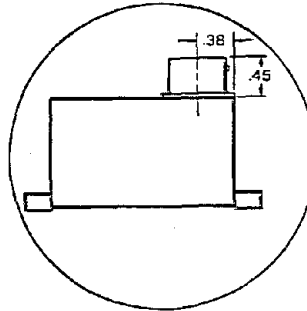


Figure 42. A typical accelerometer used for pavement instrumentation. [44]

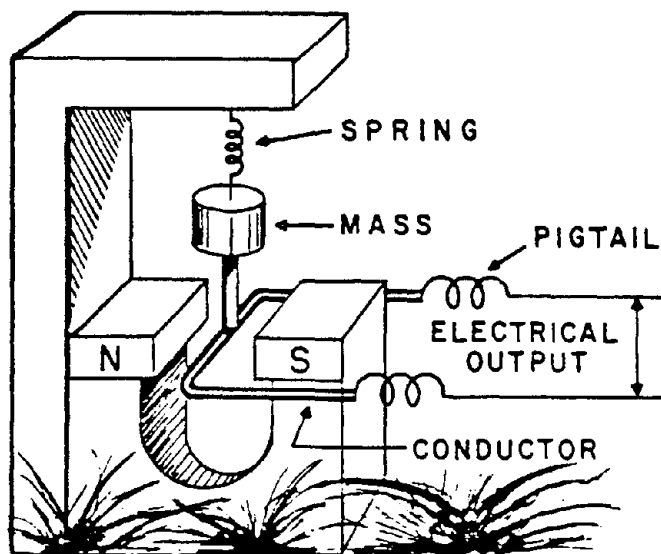


Figure 43. Schematic of a geophone.^[45]

The Army Corps of Engineers has used velocity transducers to instrument airport pavements at the National Aviation Facilities Experimental Center Airport, Atlantic City, NJ.^[40] The pavements were tested under cold and warm weather conditions. It was found that 94 percent of the geophones survived the construction operations and the changes in the environment.

DEFLECTION-MEASURING DEVICES

These devices measure the actual deflection where the signal does not need to be integrated. The majority of these devices use a linear variable differential transformer (LVDT) to measure both the static and transient dynamic deflections. Some deflection devices measure the deflection of a given layer of the pavement system; they are called single-layer deflectometers (SLDs). The most recent type of deflection-measuring device can measure the deflection at various points throughout the pavement depth. This type is a multidepth deflectometer (MDD).

SINGLE-LAYER DEFLECTOMETER

The single-layer deflectometer consists of an LVDT or a strain gauge fixture that is connected to the surface of any layer of the pavement at one end and attached to a reference rod at the other end. Reference rods as long as 8 to 10 ft (2.5 to 3 m) have been used. The basic assumption is that the reference rod is anchored at a point deep enough so that the deflection at that point due to surface loading is at a minimum. When the upper part of the SLD deflects with the pavement, the reference rod will not move. Therefore, the relative movement of the upper part with regard to the reference rod is equal to the actual pavement movement. Figures 44 and 45 show two versions of LVDT single-layer deflectometers. One advantage of the SLD is that it can measure both static and dynamic deflections and also resilient and permanent deformations.

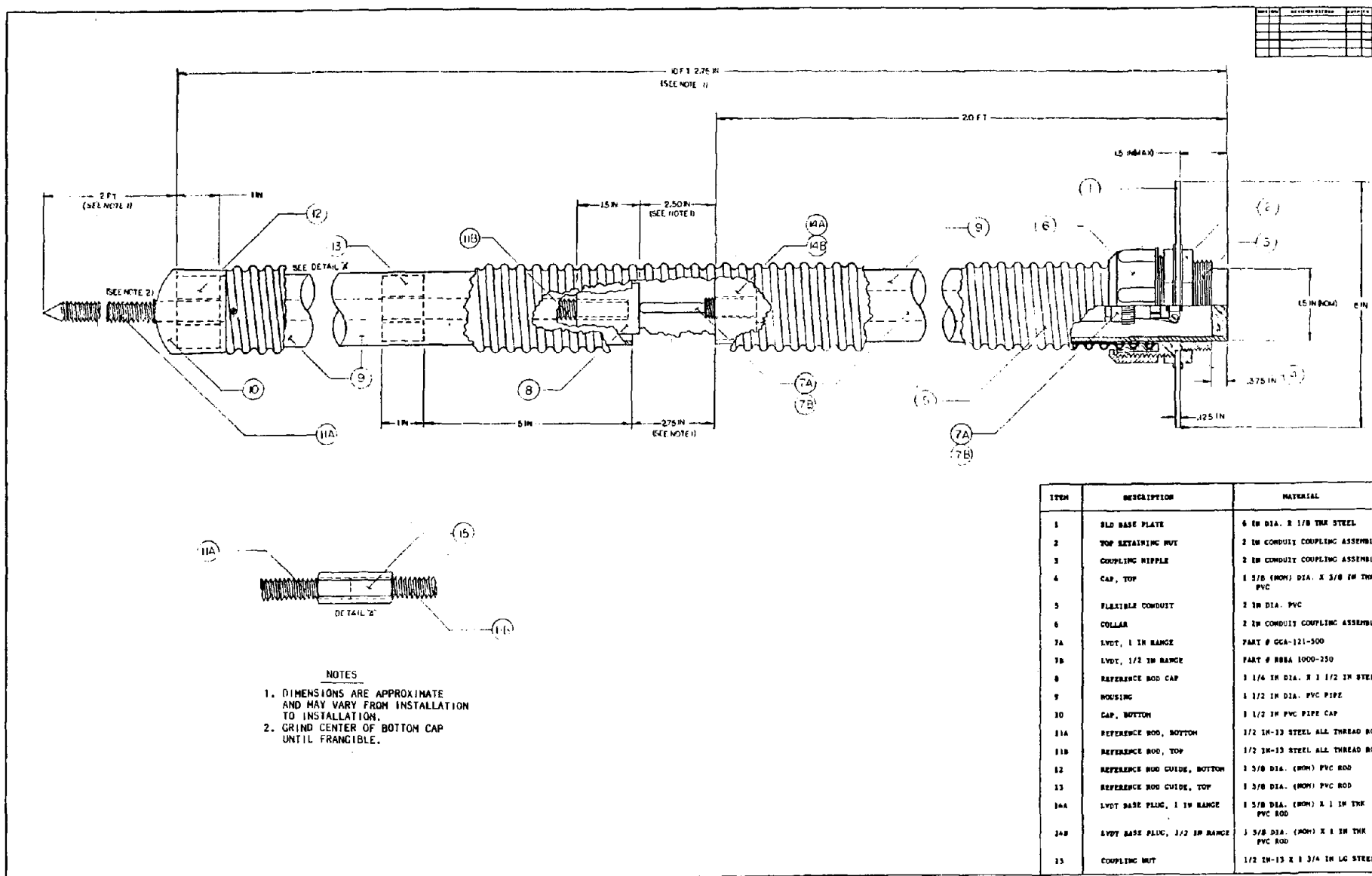


Figure 44. LVDT single layer deflectometer

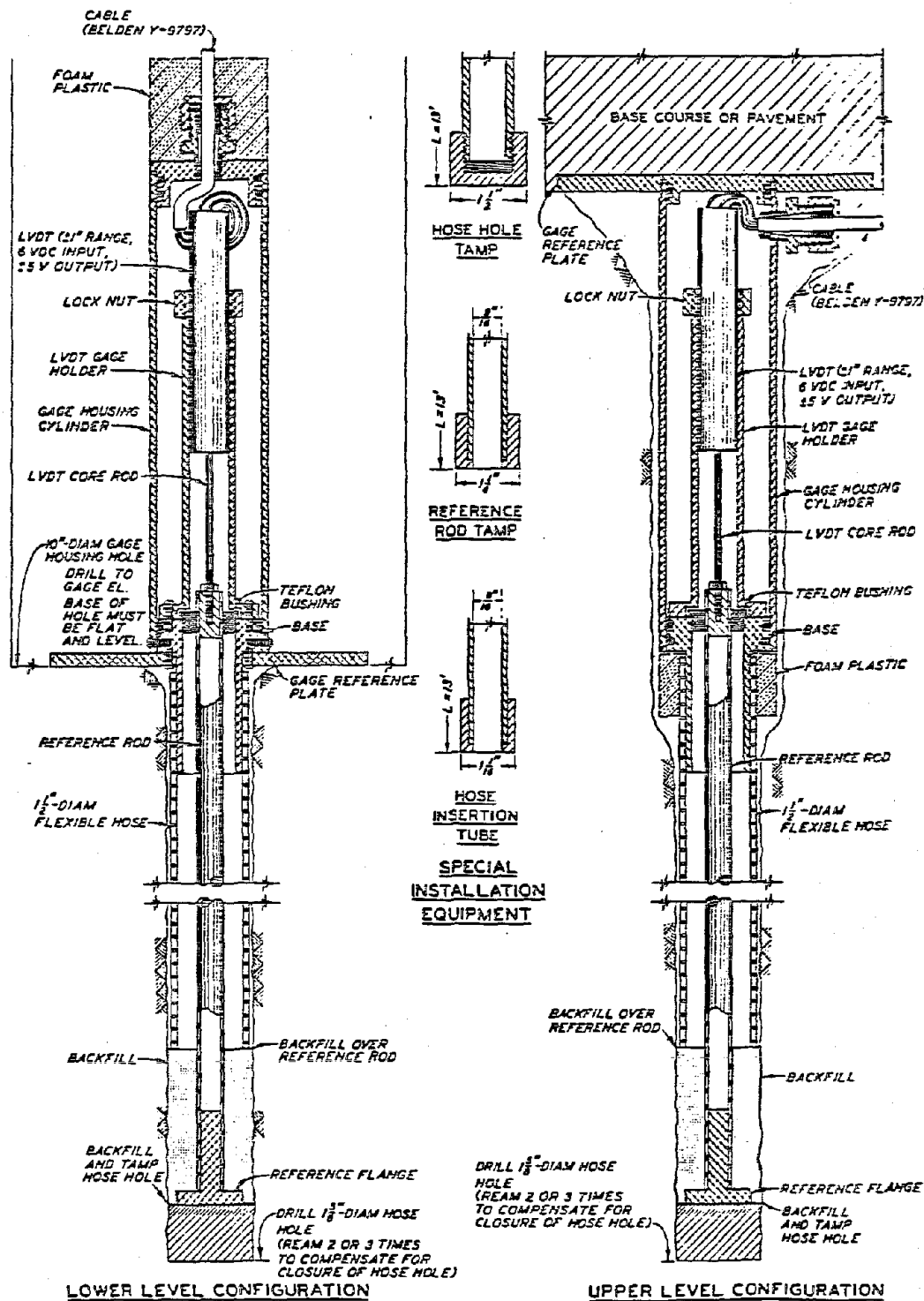


Figure 45. WES-designed soil deflection gauge.

MULTIDEPTH DEFLECTOMETER

The multidepth deflector is an LVDT-based instrument used in pavement research for measuring either the resilient or permanent deformations. In the schematic of an MDD installation shown in figure 46, two MDD modules are installed within the pavement layers. The measuring unit is an LVDT mounted within a module that can expand laterally to clamp onto the sides of the hole. As many as six MDD modules may be placed in any hole. The minimum distance that modules can be placed apart is limited by the length of the module, which is approximately 6 in (15 mm). The anchor for the LVDT cores is placed approximately 8 ft (2.5 m) below the pavement surface. During accelerated pavement testing, module placement frequently is at the layer interfaces. The deformation of each layer can be measured and its contribution to the overall deformation determined.

The Texas Transportation Institute has installed MDD in three research pavements at the Texas A&M Research Annex. The MDD module locations are shown in figure 47. These sites have been tested with the falling weight deflector; the responses under 10.9-kip loading are shown in figure 48. The MDD measures the movement of each pavement layer with regard to the anchor.

INSTALLATION PROCEDURE

ACCELEROMETERS AND GEOPHONES

Geophones should be installed firmly on a mounting surface that is flat and in one plane. If geophones are used in conjunction with other types of deflection devices such as deflectometers, it is usually desirable to place the two as close together as possible. The installation techniques for unbonded and bonded layers are outlined as follows:

1. Mount the geophone on a metal plate having a diameter of 4 to 6 in (10 to 15 mm) and a thickness of 1/10 or 1/8 in (2.5 or 3 mm).
2. Build and compact the unbonded material about 1 ft (0.3 m) over the level at which the geophone is to be installed.

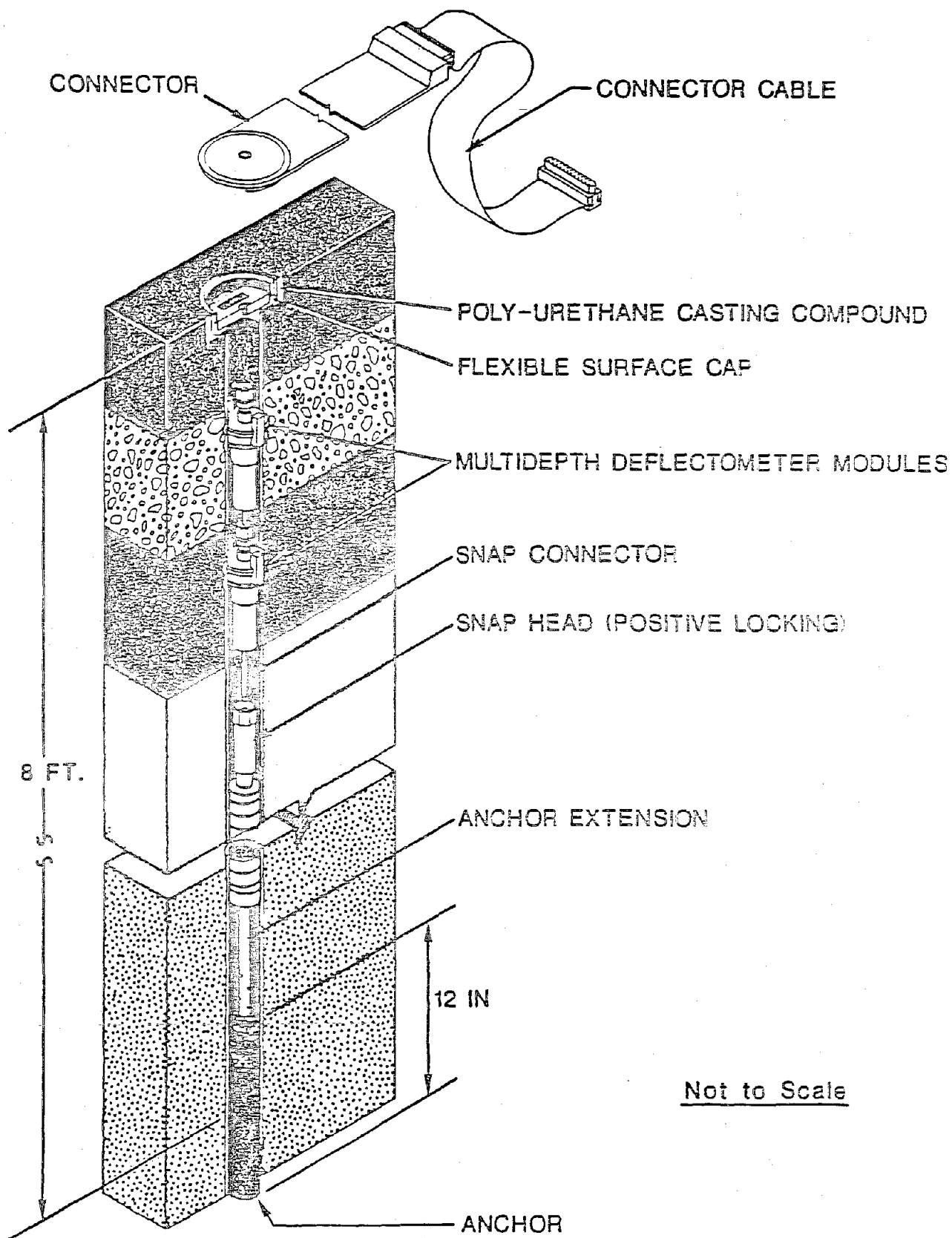
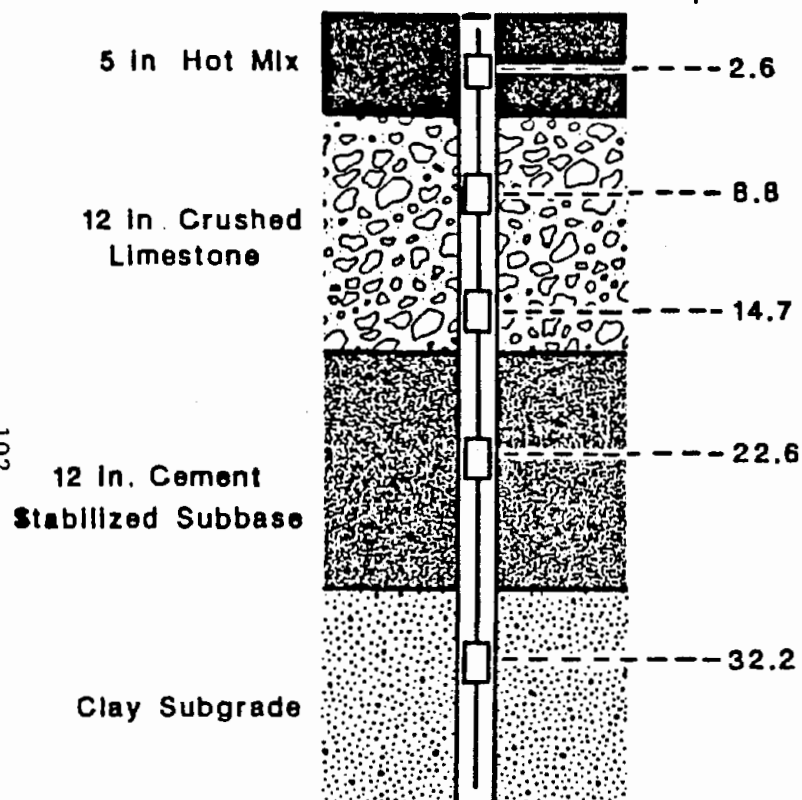


Figure 46. The multidepth deflectometer.

Section 8

MDD Module
Depths (in.)

Section 12

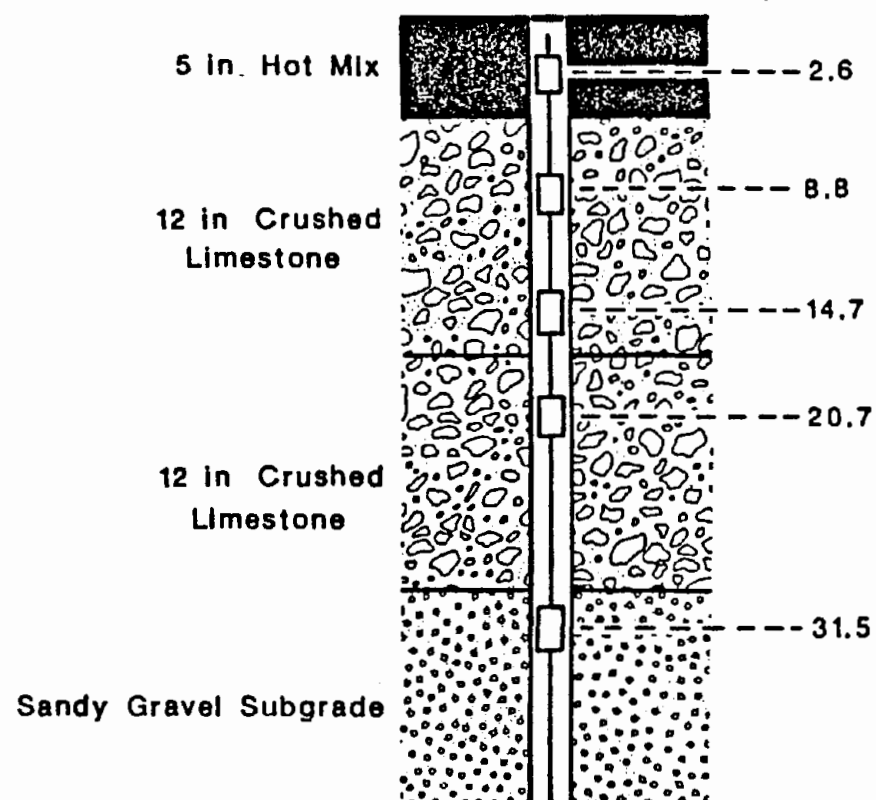
MDD Module
Depths (in.)

Figure 47. Details of MDD installation.

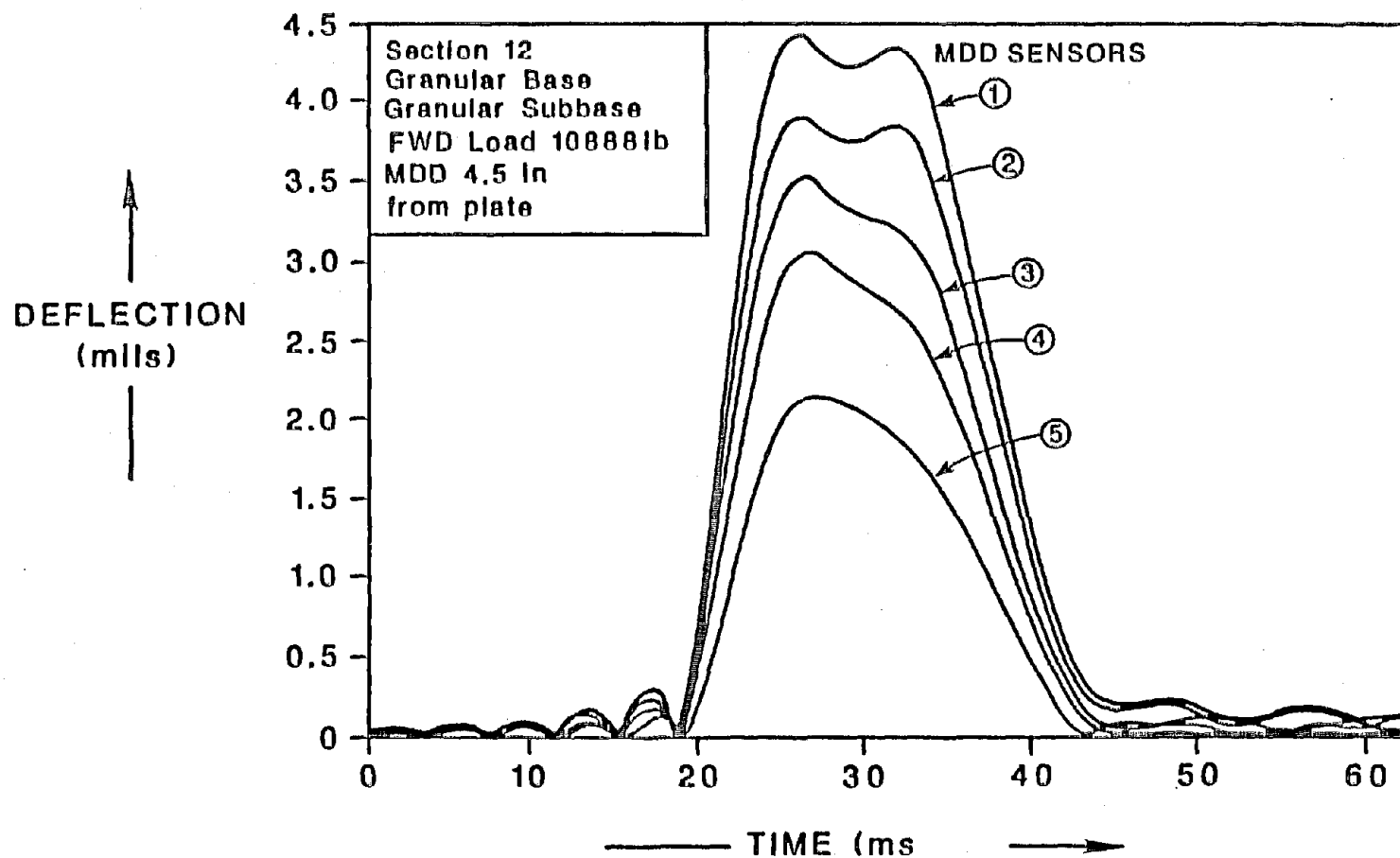


Figure 48. MDD response under FWD loading (section 12).

3. Bore a hole to the desired level with a diameter large enough to be able to pass the base plate attached to the geophone through it.
4. Level and smooth the bottom of the hole and place the geophone assembly into the hole.
5. Fill the hole with the removed unbonded material and compact the material.

BONDED LAYERS

To install geophones in bonded layers, the following steps should be taken:

1. Mount the geophone on a 2-in (5-mm)-diameter metal plate.
2. Make a core in the bond material to the desired depth.
3. Level and smooth the bottom of the hole.
4. Affix the geophone assembly to the bottom of the hole with epoxy.
5. Fill the hole with hot-mix asphaltic concrete.

If geophones are to be installed at the bottom of the asphalt concrete layer in a new pavement, the geophone assembly can be placed on top of the base layer. As the paver is approaching, some paving material should be manually placed on top of the geophone for protection against possible shifting or reorientation. A type of geophone and cable should be selected which can withstand hot-mix temperatures.

As for any other instrument, it is recommended that the output of the gauges be monitored during and after the installation to ensure that they have not sustained any damage. If the geophone unit is not hermetically sealed, it should be encased in a rugged metal casing and waterproofed as well as possible. The lead wires should be placed in a trench and properly protected against mechanical and environmental damage.

SINGLE-LAYER DEFLECTOMETER (SLD)

Detailed installation procedures for single-layer deflectometers vary from one device to another depending on their design specifications. The installation procedure for the single-layer deflectometer shown in figure 44 follows:

1. Drill a 2-in (5-mm)-diameter hole to a depth of 10 ft (3 m).
2. Pour approximately 1/2 gal (2 l) of liquid sealant into the hole.
3. Insert the SLD housing, base plate, and the guide tube into the hole until the base plate is flush with the surface. The amount of liquid sealant in the hole should be sufficient so that some of it is extruded around the housing onto the surface.
4. Place a weight on the base plate.
5. Allow the sealant to cure for at least 12 hours, depending on the ambient temperature.
6. Drive the reference rod through the frangible bottom cap for 2 ft (0.6 m).
7. Remove the guide tube and insert the LVDT housing assembly.
8. Adjust the height of the LVDT housing to zero the LVDT output.
9. Fasten the LVDT housing to the collar nut.
10. Cut the LVDT housing flush with the collar nut.
11. Route the wires and glue the top cap in place.

If another layer is to be built over the top of the SLD, it should be covered manually with some of the material used for the top layer and tamped to avoid damage from the paving machinery.

If the SLD is to measure the surface deflection, some modifications in the above-mentioned procedure will be needed to countersink the base plate and the collar nut.

MULTIDEPTH DEFLECTOMETER

The following procedure is recommended for installing multidepth deflectometers:

1. A 1.5-in (40-mm)-diameter hole is drilled to a depth of 86 in (2.2 m). The use of a high-speed percussion drill and a specially designed drill rig will ensure that no major disturbances occur in the pavement layers and that the hole remains straight.
2. A thin rubber lining installed in the hole prevents moisture and loose material from damaging the transducers.
3. An anchor is placed at the bottom of the hole and fixed in place by cement grout.
4. An interconnecting rod is lowered and fixed into the snap connector. The MDD modules are slid over the interconnecting rod to the desired depth and locked in place.
5. The interconnecting rod is then replaced with a rod that contains the LVDT cores. The locations of the cores can be adjusted to facilitate zeroing of the LVDTs prior to the completion of installation.
6. The final step is down-hole calibration, achieved via a specially designed calibration unit.

MDD installation takes 2 days for two technicians. On day 1 the hole is drilled and lined and the anchor is grouted into place. On day 2 the MDDs are installed and calibrated and testing can begin.

DATA ACQUISITION

ACCELEROMETER

The following equipment are needed for the operation of accelerometers and the acquisition of their response:

<u>Item</u>	<u>Estimated Cost</u>
DC power supply	\$1000
DC gain amplifier	\$1000
Low-pass filter	\$2000
Analog-to-digital board	\$1000
Portable microcomputer	\$2000
Appropriate data acquisition software	\$1000 to 2000

GEOPHONES

The following equipment are needed to operate geophones and to acquire their response:

<u>Item</u>	<u>Estimated Cost</u>
Signal conditioning circuit	\$25
Analog-to-digital board	\$1000
Microcomputer	\$2000
Appropriate data acquisition software	\$1000 to 2000

These cost estimates for the data acquisition system may be used for more than one geophone or accelerometer at a time. The number of units that can be monitored depends on the available input channels on the data acquisition board.

SINGLE-LAYER DEFLECTOMETER

The following equipment are needed to operate single-layer deflectometers and to acquire their response:

<u>Item</u>	<u>Estimated Cost</u>
LVDT signal conditioner	\$500
Analog-to-digital board	\$1500
Portable microcomputer	\$2500
Appropriate data acquisition software	\$1000 to 2000

MULTIDEPTH DEFLECTOMETER

<u>Item</u>	<u>Estimated Cost</u>
6-channel conditioner box	\$5000
Analog-to-digital board	\$1200
Portable microcomputer	\$2500

COST AND AVAILABILITY

ACCELEROMETERS AND GEOPHONES

The cost of appropriate accelerometers and geophones for pavement response measurement is given in table 11.

SINGLE-LAYER DEFLECTOMETER (SLD)

The itemized cost of the SLD system shown in figure 44 is listed below:

<u>Item</u>	<u>Estimated Cost</u>
LVDT	\$381
Other parts, machining time, labor for assembling, sealant	<u>\$435</u>
SLD	\$816

MULTIDEPTH DEFLECTOMETER

Two sizes of LVDT may be used, depending upon the application. The long-stroke LVDT (± 0.3 in (± 7.5 mm)) is appropriate for long-term monitoring where pavement deformations may occur. The short-stroke (± 0.1 in (± 2.5 mm)) LVDT is ideal for evaluating nondestructive testing (NDT) equipment. When

Table 11. Cost and availability of accelerometers and geophones.

Instrument	Manufacturer	Model	Range	Dimensions ¹ (in)	Lead Time	Cost	Comments	Manufacturer's Address
Accelerometer	Schaevitz	LSB	0.5 g 1.0 g		8 wks	\$994		Schaevitz Engineering U.S. Route 130 & Union Avenue Pennsauken, NJ 08110 (609) 662-8000
Geophone	Mark Products	L10A	10-30 H _z	d=1.25 h=1.4	2 wks	\$15.50		Mark Products, U.S. Inc. 10507 Kinghurst Drive Houston, TX 77099 (713) 498-0600
		L15	4.5-40 H _z	d=1.25 h=1.4	6-8 wks	\$300	High temp	
		L10B	4.5-10 H _z	d=1.25 h=1.4			No longer available	
		LAC	1.0 H _z	d=3.0	8 wks	\$650	without calibration coil	
				h=5.125		\$710	with calibration coil	
		LAA	2.0 H _z	d=3.0	8 wks	\$650	without calibration coil	
				h=5.125		\$710	with calibration coil	

¹ d = diameter
h = height

long-term applications are planned, it is desirable to use hermetically sealed units to prevent moisture damage. The cost of the LVDT units is:

<u>Stroke (in)</u>	<u>Regular</u>	<u>Hermetically Sealed</u>
$\pm .1$	\$33	\$212
$\pm .3$	\$60	\$240

The cost of the hardware for a complete MDD installation excluding LVDT is estimated to be \$2,000. The cost of installation is estimated to be \$2,300. The cost of each part of the system is shown below, assuming 4 MDDs per hole:

<u>Item</u>	<u>Estimated Cost</u>
Down-hole parts plus LVDT holders	\$2,000
LVDTs (4)	\$135
Installation Cost	\$2,300
Connector Cable	\$500

Two points must be remembered concerning these price estimates:

- Only one connector, conditioner, and computer are needed regardless of the number of holes instrumented.
- The MDD modules and LVDT are recoverable; the only parts which remain at the installation site are the anchor and hole lining.

Repeatability of Multidepth Deflectometer

The following MDD data were collected for a pavement structure consisting of a 1-in (25-mm) surfacing over a 16-in (0.4-m) granular base. The MDDs were placed at 9 in and 23 in (0.23 and 0.58 m) below the surface. The load was applied by a falling weight deflectometer (FWD) with the loading plate placed 3 in (75 mm) from the MDD hole.

<u>FWD</u> (Load, lb)	<u>MDD Readings (mils)</u>		<u>Backcalculated</u> <u>Moduli (ksi)</u>	
	(MDD 1)	(MDD 2)	(E _{Base})	(E _{Sub})
10824	12.74	7.34	40.5	13.5
10824	12.77	7.37	40.4	13.4
10808	12.74	7.34	40.4	13.5
10824	12.79	7.34	40.4	13.5
10744	12.74	7.42	39.9	13.3
16232	16.66	10.13	45.1	15.0
16144	16.39	9.84	45.9	15.3
16160	16.54	9.89	45.7	15.2
16088	16.49	9.91	45.5	15.2
16072	16.51	9.89	45.5	15.1

The modulus backcalculations were performed using the MDD data with the generalized backcalculation procedure developed at the Texas Transportation Institute.^[46]

6. TEMPERATURE MEASUREMENT

The temperature throughout the asphalt concrete layer has a significant influence on the magnitude of deflections and strains. The temperature affects the stiffness of the asphalt concrete layers, which in turn affects the pavement response.

Measurement of pavement surface temperature does not provide reliable information regarding the average pavement temperature or the temperature gradient. Pavement surface temperature can change rapidly as a result of a temporary shade by a vehicle or because of rain. Therefore, measurement of temperature at different depths in the pavement is required to provide sufficient information. Depending on the thickness of the pavement layers, the number of measurements can vary, but temperature measurement at four to six points in the pavement appears to be adequate in most cases. Temperature can be easily measured with a thermocouple, resistance temperature detectors (RTDs), thermistors, and integrated circuits. These devices can be installed during or after construction.

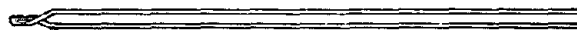
TYPES OF TEMPERATURE GAUGES

THERMOCOUPLES

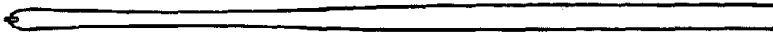
Thermocouples are the most widely used temperature sensor. A thermocouple operates on the basis that, when two dissimilar metals are put in contact with each other, a small voltage is induced at their junction. This phenomenon, discovered by Thomas J. Seebeck in 1881, occurs because each metal has a different number of free electrons at different temperatures.^[47]

Figure 49 illustrates typical thermocouple element assemblies.

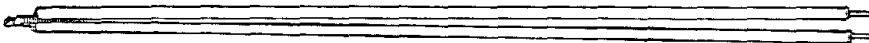
Each thermocouple unit consists of two dissimilar metals, homogeneously joined at one end to form the measuring junction, also called the exposed junction. The measuring junction is very susceptible to the environment (oxidizing and reducing atmosphere), and therefore must be protected.^[49]



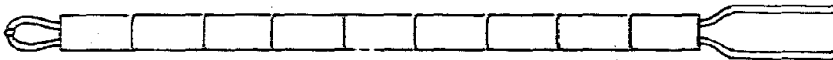
A. Bare thermocouple element, twisted and welded.



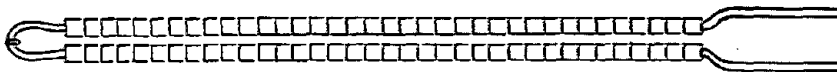
B. Butt-welded thermocouple element.



C. Thermocouple element, twisted and welded with asbestos insulation.



D. Butt-welded thermocouple element with double-bore insulators.



E. Butt-welded thermocouple element with fish-spine insulators.



F. Two butt-welded thermocouple elements with 4-hole insulators.

Figure 49. Typical thermocouple element assemblies. [48]

Standard diameters for thermocouple wires are 1/16, 1/8, 3/16, and 1/4 in (1.6, 3.2, 4.8, and 6.4 mm), and the usual immersion length is 12 in (300 mm).^[50]

Thermocouples are suitable for point sensing only. To measure the temperature at several points relatively close to each other, a thermocouple tree should be formed. Thermocouples are rugged and can withstand shock and vibration.^[51] They have a very fast response time and are considered active gauges, which means there is no need to introduce a source of power into the circuit. An important point concerning the connection of a thermocouple is that all lead wires from the thermocouple junction to the readout device should be of the same alloy.^[48] Thermocouples have nonlinear output with temperature and should thus be calibrated prior to installation.

Various types of thermocouples are available. The selection of a specific type is based on the environmental conditions under which it will be used. Type-T thermocouples, made of copper and constantan, are usually used in pavements, since they can be used from subzero temperatures to about 700 °F (370 °C). This type of thermocouple has an accuracy of about ± 1.8 °F (± 1 °C).

METAL FILM RTDs

Resistance temperature detectors (RTDs) are temperature-sensitive resistors. The fundamental principle underlying these sensors was discovered in the same year that Thomas Seebeck made his famous discovery about thermoelectricity, when Sir Humphrey Davy announced that the resistivity of metals showed a marked temperature dependence.

The modern construction technique for RTDs involves depositing or screening a platinum or metal glass slurry film onto a small flat ceramic substrate, etching with a laser trimming system, and sealing. The most common RTDs are made of either platinum nickel or aluminum alloys.^[52] Figure 50 shows a typical platinum RTD. As the surrounding temperature increases, the resistance of the metal is increased. The operating temperature for RTDs is from -328 to 1202 °F (-200 to 650 °C), and their measurements are very accurate and repeatable.^[51] An RTD element can be spread over a large area,

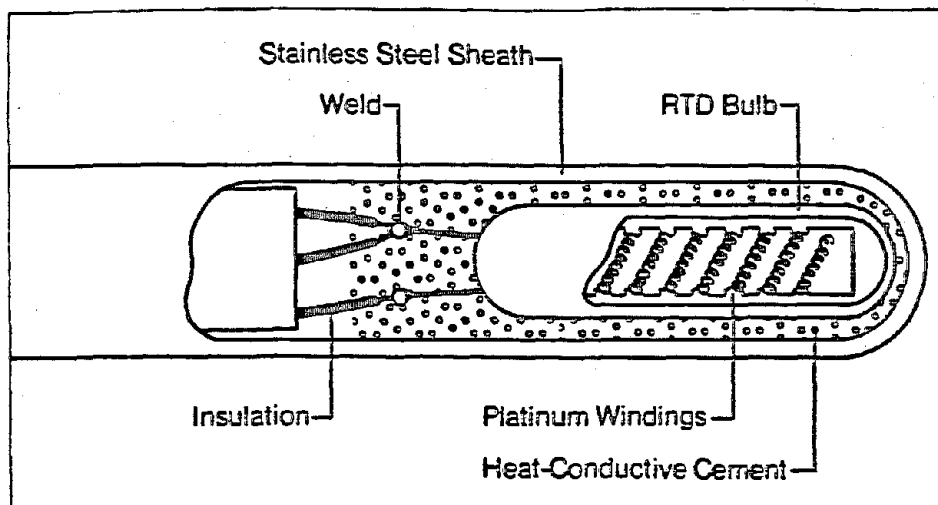


Figure 50. A platinum RTD. [49]

providing a representative temperature of a member by averaging the temperature over the area.

Unlike the thermocouple, RTDs are not self-powered; a current must be passed through the RTD to provide a measurable voltage. RTDs are not as rugged as thermocouples in their construction; special attention must be paid during their installation.

THERMISTOR PROBES

Thermistors are temperature-sensitive resistors, generally made of semiconductor materials. Different metal oxides, such as nickel, manganese, iron, cobalt, copper, magnesium, and titanium, are used in their construction.^[50] Thermistors exhibit a very large change in resistance with temperature, which makes them very accurate devices, to ± 0.18 °F (± 0.1 °C). However, this increased sensitivity has caused it to be extremely nonlinear. Manufacturers have not standardized thermistor curves to the extent of RTD and thermocouple curves, so the performance and cost of these devices vary widely among manufacturers.

Thermistors are very susceptible to permanent decalibration at high temperatures. Their use is generally limited to temperatures from -58 to 572 °F (-50 to 300 °C). Extended exposure of thermistors to high temperatures will cause them to drift out of their specified tolerance.^[52]

Thermistors have diameters as small as 0.05 in (1.2 mm); therefore, they respond quickly to temperature changes. However, their small mass makes them especially susceptible to self-heating errors.^[52]

Thermistors are wired as one leg of a Wheatstone bridge. Since the lead length between the thermistor and bridge is not normally a limiting factor, this device can be used for temperature measurement at a site remote from a central location. Thermistors are not self-powered and require a current source for operation. Also, they are much more fragile than the RTDs. Overall, thermistors are poor candidates for use in pavements.

MONOLITHIC INTEGRATED CIRCUITS

Monolithic integrated circuits or solid-state transducers are a recent innovation in thermometry. These devices comprise two terminal integrated circuit temperature transducers that produce output currents proportional to absolute temperature.^[53] These devices have a linear output and are highly repeatable; therefore, they need neither linearization circuitry nor calibration.

Due to their high impedance current output these devices are not affected by voltage drops. Thus, the length of the lead wires will not affect the measurement. Any well-insulated twisted pair of wires is sufficient for operation hundreds of feet from the readout device.^[53]

These transducers are available in hermetically sealed packages and can be used within a temperature range of -65 °F to 300 °F (-55 °C to +150 °C).^[54] Figure 51 shows a solid-state temperature sensor. These transducers can be very useful for embedment in the pavements.

INSTALLATION OF TEMPERATURE TRANSDUCERS IN FLEXIBLE PAVEMENTS

Thermocouples can be placed in pavement layers during construction. The measurement junction should be located at the desired depth and the lead wires can be extended to the shoulder and out to the readout device. If the temperatures at several points are to be measured, a tree-shaped assembly of thermocouples may be used.

Thermocouples can also be retrofitted into existing pavements. To do this, a hole should be drilled to the desired depth, the thermocouple or the thermocouple tree put into place, and the hole refilled with quick-seal emulsion or epoxy. A small trench for the lead wires should be covered with quick-seal or epoxy.

In thermocouple connections, the lead wires to the readout device should be continuous, and the largest possible wire that will not shunt heat from the

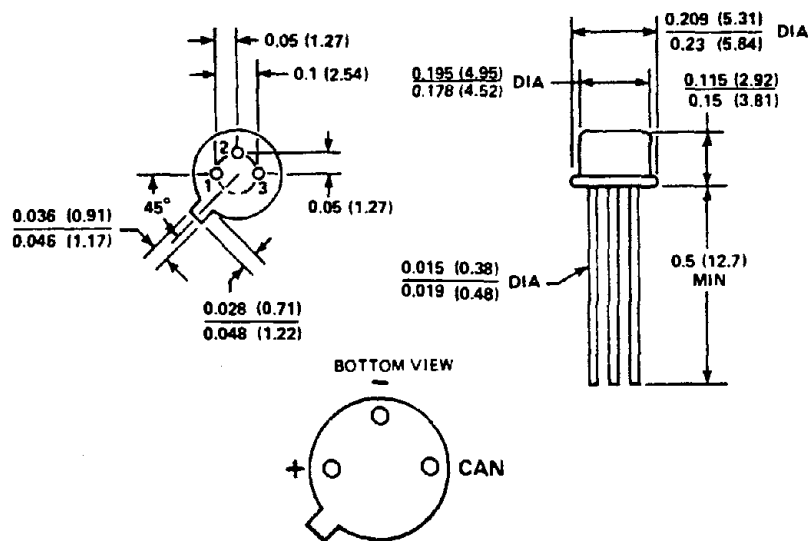


Figure 51. A solid-state temperature sensor. [54]

measurement area should be used. Thermocouple wires should not be strained by rough handling or vibration, or the physical properties of the wires might be changed, resulting in a condition known as decalibration. Decalibration causes erroneous results that cannot be detected easily.

The same installation technique can be used for thermistors, RTDs and solid-state sensors. For retrofit installation, RTDs and solid-state sensors can be attached to a 1/8-in (3-mm)-diameter wooden rod at the desired locations. The rod is then dipped in an epoxy container and placed in the predrilled hole. Additional epoxy is applied to fill the hole, if needed. Lead wires should be placed in a trench and covered with epoxy as well.

COST AND AVAILABILITY

Temperature is the most widely measured process parameter. For this reason, a wide variety of temperature measurement devices in various configurations are commercially available. Similar temperature devices are usually built by many manufacturers; therefore, to choose the best device for the job, one should study the various options. Table 12 shows the cost and availability of typical configurations of different temperature-measuring devices for pavement instrumentation.

PERFORMANCE

Thermocouples have been used by many researchers to monitor pavement temperature. Their long-term performances have been well investigated at the FHWA ALF test site. Figure 52 shows the average pavement temperature measured by thermocouples installed at various depths in the asphalt layer, and the maximum and minimum air temperatures. The average pavement curve fits within the air temperature curves throughout the period, which indicates that the thermocouples' readings are reasonable.

Table 12. Cost and availability of temperature-measuring devices.

Type	Manufacturer	Model	Lead Time	Cost	Comments	Manufacturer's Address
Thermocouple	Omega	Type T				
		Teflon glass insulation	2 wks	\$0.48-0.62/ft	Price varies	Omega Engineering One Omega Drive PO Box 2669 Stamford, CT 06906
		Polymers	2 wks	\$0.14-0.30/ft	with diameter	
		8TX20PP	2 wks	\$1.82/ft		(800) 862-6342
Integrated Circuit	CE	AD590IH	2 wks	\$2.50		Newark Electronics 500 N. Pulaski Rd. Chicago, IL 60624
		AD590JH	2 wks	\$2.93		(312) 784-5100

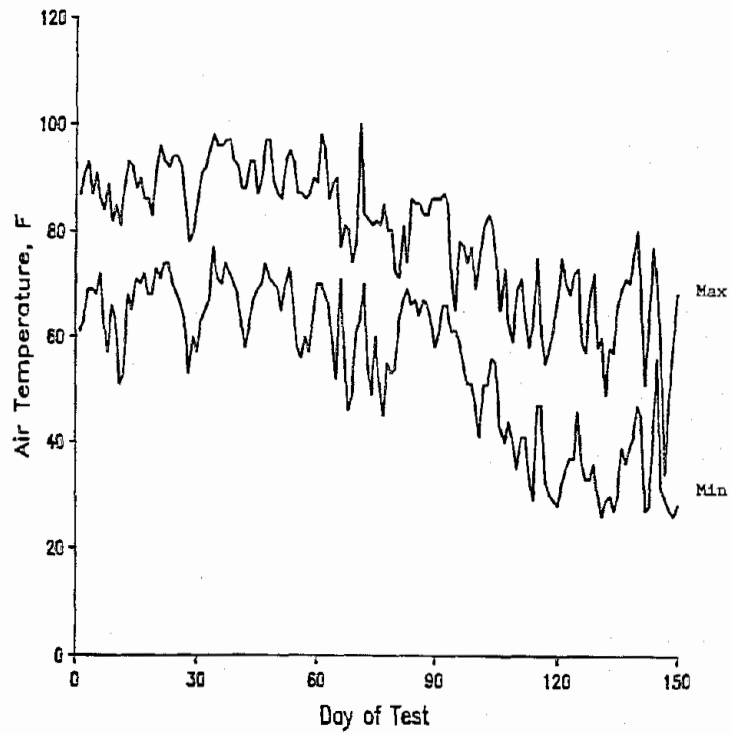


Figure 52. Pavement temperature at the FHWA ALF site.

7. MOISTURE MEASUREMENT

The subsurface moisture condition is an important variable in pavement monitoring. This variable can be measured by determining either the in-situ suction (water potential) or the in-situ moisture contents.

By measuring both water content and suction at different locations vertically or horizontally, it is possible to observe the following:

- Water content and suction.
- Soil permeability, in situ.
- Direction of water movement.
- Points on the water content versus suction curve, called the soil-moisture characteristic curve.
- Soil diffusivity, in situ.

The last two items must be known if it is necessary to predict the change of water content, suction, or layer modulus with programs such as the Climatic-Materials-Structures (CMS) model, the U.S. Army Cold Regions Research Laboratory frost heave model, or the Texas A&M Infiltration and Drainage model.^[55, 56, 57] These three models are presently being integrated in an ongoing FHWA project, Verification and Extension of Previously Developed Pavement Analysis and Drainage Models. Implementation of this combined model will require the use of the soil-moisture characteristic curve, and, because of its importance, the instrumentation of each test site to measure both water content and suction should be considered.

MOISTURE CONTENT SENSOR

The dual-tube nuclear moisture and density apparatus is recommended for measuring moisture profiles. The recommended equipment is manufactured by Troxler at a total cost of about \$10,000, which includes a supply of tubes for installation and a data readout device.^[58]

INSTALLATION

Parallel access tubes (2-in (50-mm) outside diameter) are placed in the material to the required depth and the two probes are lowered to equal depths. One tube contains a 5-millicurie cesium-137 source and the other, a gamma detector. Gamma rays omitted through the source are collected by the detector. A registered operator is required to run the test.

CALIBRATION

The procedures recommended in the June 1986 issued of Soil Science should be used.^[59] The device measures moisture content to within 1 percent of the total amount present in the profile.

SUCTION MEASUREMENT SENSOR

Two devices are recommended for suction measurement: In drier areas, thermocouple psychrometers are recommended; in wetter areas, thermal moisture sensors should be used.

It is anticipated that the thermal moisture sensor, manufactured by Agwatronics, Inc., of Merced, California, will be the best device for the in-situ conditions.^[60] This device has been used extensively by the Texas Transportation Institute to monitor the soil suction in subgrades beneath pavements on expansive clays. Figure 53 shows a cross section of the thermal moisture sensor. Its principle of operation is to measure the thermal conductivity of the ceramic tip, which depends upon the volume of water in the voids in the ceramic. Consequently, the thermal conductivity can be calibrated to the matrix suction of the soil. The device has been proven to be very stable, and some instruments placed by research team members several years ago still function well.

The sensors cost approximately \$250 each, depending on the number of calibration points requested. A drawback to this system is that a fairly expensive data logger "AWGA-SIP" is required to take readings, at a cost of

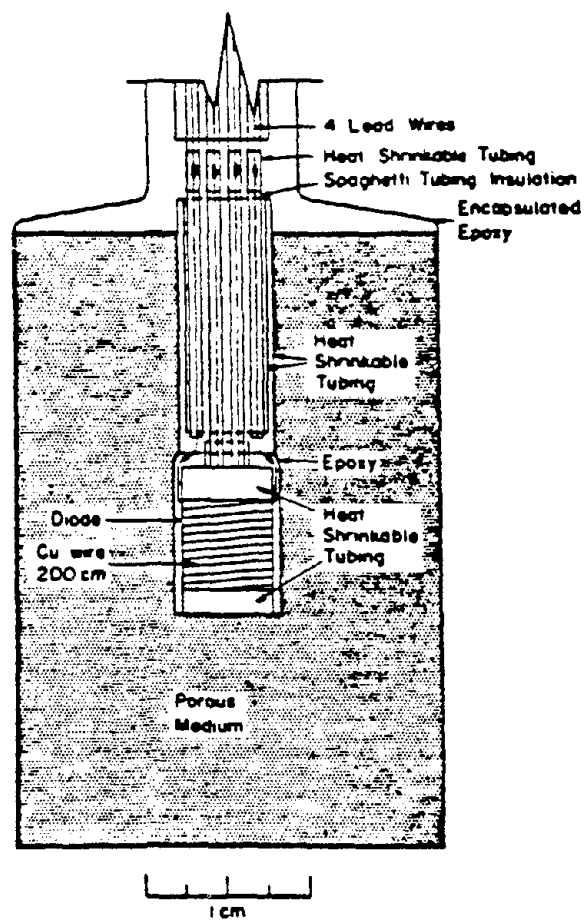


Figure 53. Cross section of the thermal moisture sensor.

\$9,000. Other, less expensive data loggers, although available, have been found to be inaccurate and unreliable.

INSTALLATION

These devices can be retrofitted into existing pavements by auguring a 6-in (152-mm) hole and placing the sensor into the sides of the hole. The hole is then carefully backfilled with saturated in-situ material and sealed. This technique has been used on 22 monitor sections in Texas. In all, 32 sensors were installed; after 1 year's service, 30 still function well.

CALIBRATION

The instruments are calibrated by the manufacturer and are spot checked on these values using a pressure plate apparatus. In general, the manufacturer's calibrations have been acceptable.

RECOMMENDATION

An ideal setup for moisture instrumentation would use a dual-tube nuclear moisture apparatus to measure moisture profiles, with a series of thermal moisture sensors arranged vertically to measure suction, and an array of thermocouples distributed vertically to determine the temperature with depth. In addition, in frost zones, it would be useful to have a frost tube installed so as to determine the depth of frost penetration by its changing color. A data-logging system would be required for reading all instruments automatically in a preset cycle and recording all data in a computer-accessible form. Also, it would be important to situate the test site in the vicinity of a first-order weather station in order to have accurate rainfall, solar radiation, wind speed, and air temperature data. The instrumentation setup described above would provide practically every datum item that is desired for pavement moisture instrumentation.

8. AXLE LOAD MEASUREMENT

The dynamic axle load exerted by vehicle tires on a road surface can be measured on both sides of the interacting system, that is, using sensors installed either in the pavement or on the vehicle. In the former approach, a large number of load cells must be placed in the traveled road surface. The main limitation of this method is that the axle load is known only at the locations of the load cells; the number of load cells is limited by the number of input channels to the data acquisition system. As a result of these limitations, only short sections of roads can be instrumented, and this method is impractical on public highways.

Within the measurement-on-the-pavement-surface category fall the various groups of weigh-in-motion (WIM) devices, including those manufactured by Radian Corporation, Streeter Richardson, International Road Dynamics, Golden River Corporation, Siemens-Allis, and WeighWrite Systems. All of these systems are very expensive and could not be easily moved from one site to another. Therefore, determination of the load profile along the highway is not feasible. Piezoelectric cables represent another WIM technique which is used extensively at the present time. One advantage of the piezoelectric cables is that they are relatively inexpensive, with a unit cost of less than \$10,000. Numerous demonstration projects around the country use low-cost piezoelectric cables. The Iowa and Minnesota departments of transportation are currently conducting these projects in coordination with the FHWA. While the performance of these cables has not been fully examined, an accuracy of about ± 10 percent has been reported from various tests. No standard installation and measuring method has been established for these devices.

The FHWA sponsored the design of a loading plate to measure the total load under dual tires.^[61] The plate is placed flush with the pavement surface, and four load cells are sandwiched between the bottom and top steel plates. The dimensions of the plate have been selected such that the full contact areas of the tires are on the center of the plate at a given time. Figure 54 shows a sketch of the loading plate.

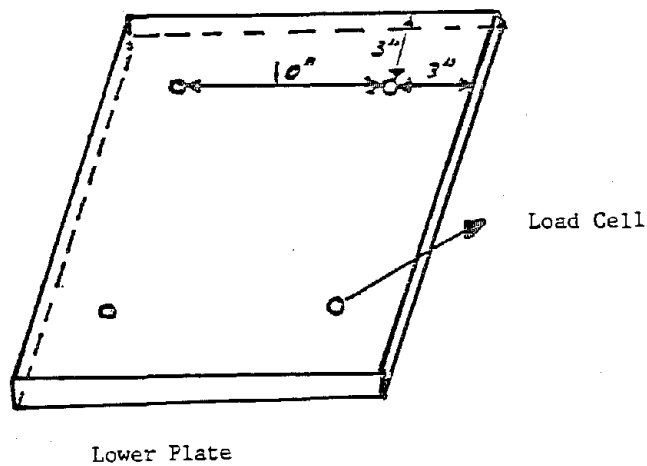
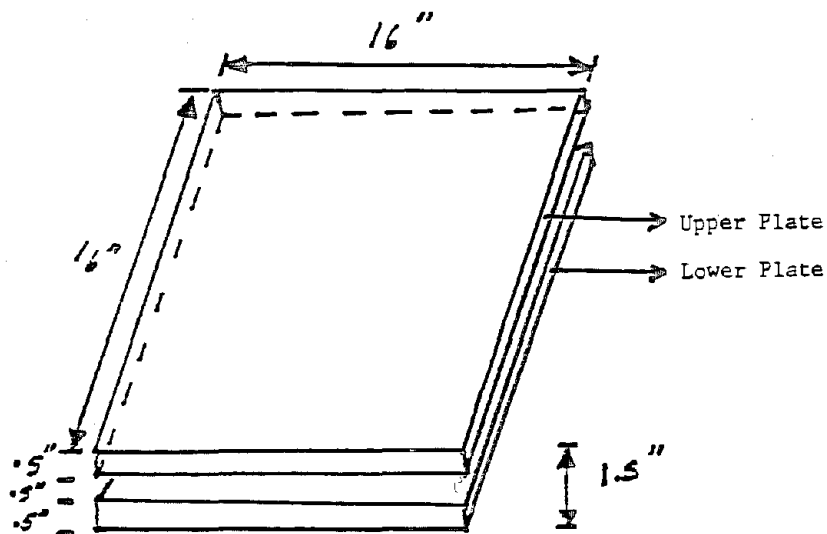


Figure 54. Sketch of the loading plate for measuring the total load under dual tires.

Axle load measuring devices installed on the vehicle are classified into two groups: instrumented axle systems and wheel force transducers.

In the first group, force sensors are installed on the test vehicle axle. In most cases, these are permanent installations which cannot be easily moved from one vehicle to another. The instrumented axle method is therefore used with designated test vehicles or trailers. A flatbed trailer with an instrumented axle has been used successfully in truck tire tests.^[62] A photograph of this truck tire tester is shown in figure 55. The main limitation of this system is in the suspension characteristics: The axle with test tires is suspended on two air cylinders, and no possibilities exist for including actual truck suspensions.

Another system that should also be classified in the instrumented axle category was developed by the Swedish Road and Traffic Research Institute.^[63] A laser sensor is installed on the axle to measure displacement between the axle and the road surface. The axle height signal is multiplied by the tire spring constant to obtain the dynamic axle load. The spring constant of a rotating tire is predetermined on a level truck weighing scale by measuring the wheel load and the axle height under various load conditions. One of the main problems with this system is that the tire inflation pressure must be kept constant to avoid variations of the tire spring constant. The quality of the measurement obtained with this system is reported to be very good.

The second category of axle load measuring devices consists of wheel force transducers. The main advantage of these devices is that they can be mounted on different types of trucks and on different axles although their applicability is usually restricted to a specific type of wheel design. The main drawback associated with wheel force transducers is that they may considerably affect the wheel dynamics by the addition of their mass and by causing a wheel offset. A wheel force transducer developed by Maritime Dynamics is shown in figure 56.^[64] This transducer, which has been used in truck tire testing programs, can be mounted only on spoked (sometimes called Dayton) wheels. The majority of tractor semitrailers and doubles configurations today use dish wheels with a 10-bolt pattern, on which the transducer cannot be installed. The wheel offset caused by this transducer is

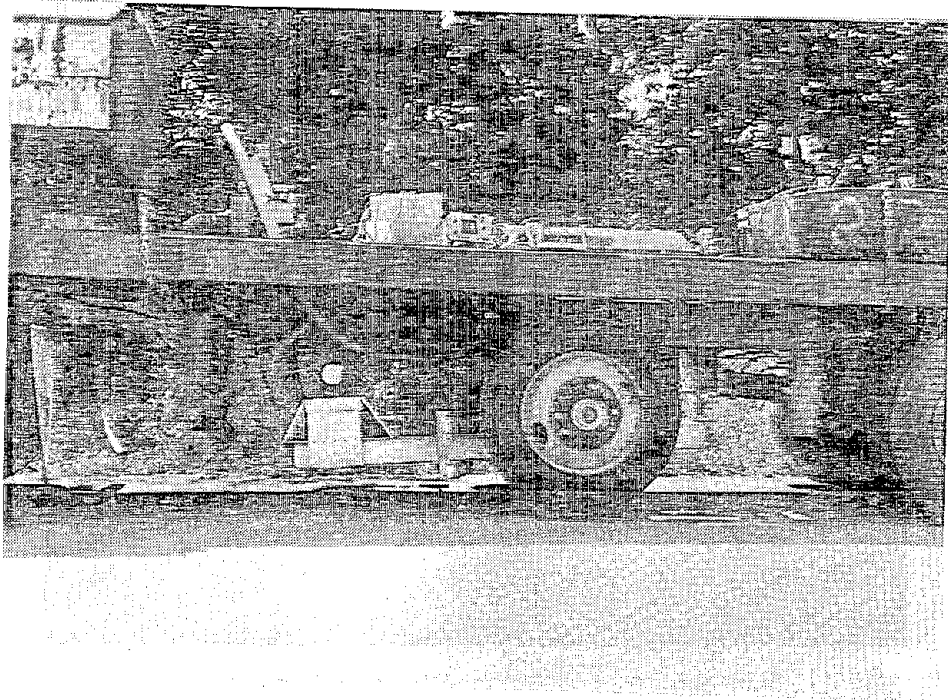


Figure 55. Truck tire tester.^[62]

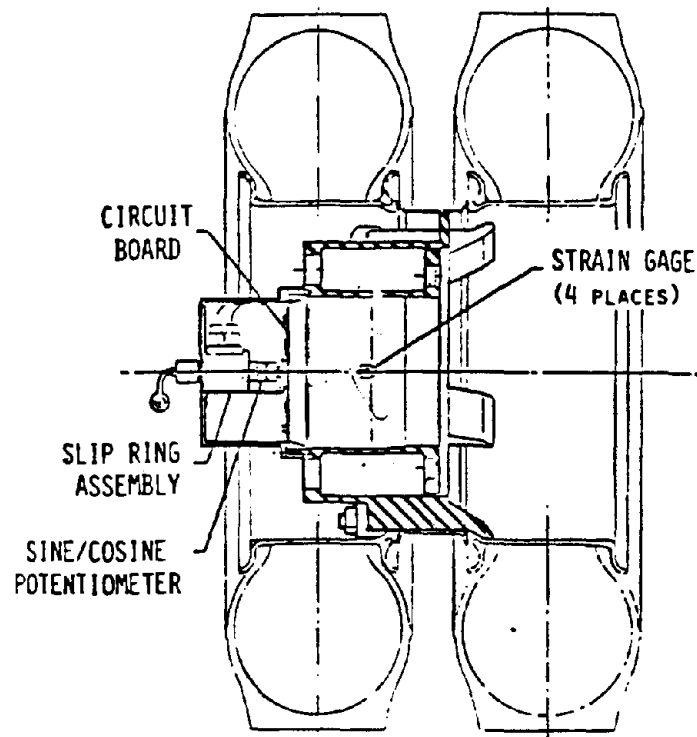


Figure 56. Wheel force transducer. [64]

very small, less than 1/2 in (12 mm), but its weight is substantial, around 300 lb (65 N), which has a strong effect on wheel dynamics.

A different type of wheel force transducer was designed in an FHWA-sponsored study.^[61] The weight of this transducer is only about 50 lb (11 N), and it can be mounted on dish-type wheels with a 10-bolt pattern. The wheel offset caused by this transducer is about 2 in (50 mm). Such an offset may change the wheel performance in cornering maneuvers significantly; however, its effect on the vertical load, which is of primary interest in this study, is marginal. The results of a computer simulation indicates that the 2-in (50-mm) wheel offset may result in a 3-percent change in the vertical force. This result was obtained for a straight truck simulated in combined braking and cornering on a road surface with a sinusoidal bump 4 in high, spread over 6 in (152 mm).

The magnitude of the applied load on the pavement surface is a critical component in the evaluation of the various types of sensors. It is well known that the static load is not a representative figure for the actual applied load due to variations in road roughness and vehicle speed.

9. VEHICLE TRANSVERSE LOCATION SENSORS

In a field testing operation, in order to study the pavement response under the load, it is imperative to know the location of the loaded area relative to the measuring instrument. For a small number of measurements at low vehicle speed, visual observation of painted marks on the pavement may be adequate. However, for a large number of measurements at high speeds, visual observation of painted marks does not provide sufficient measurement accuracy. State-of-the-art vehicle transverse location measurement is discussed in this chapter.

TYPES OF TRANSVERSE LOCATION SENSORS

PHOTOELECTRIC SYSTEM

The photoelectric locator system uses a high-intensity light attached to the test vehicle, which is directed onto an array of photocells or photodiodes mounted in the center of the vehicle travel path. The light activates one or more photo devices as it passes directly overhead, thus indicating a relative vehicle position.

The illumination source is normally constructed of a high-intensity 12-V halogen bulb with a concentrating reflector similar to the type found in a common flashlight. This assembly is mounted under the test vehicle on a gimbal which permits the lamp to be manually adjusted in any direction, as shown in figure 57. Power is supplied from the test vehicle battery.

A photo array consisting of either photoelectric or photodiode cells is fixed to the center of the test lane just before the test section. The decision to use photodiodes or photocells is related to the expected maximum vehicle speed. Photocells are less expensive than photodiodes but are also slower to react, requiring a slower moving vehicle. On the other hand, photodiodes, phototransistors, and photofets, while slightly more expensive than photocells, provide extremely fast rise times. The cost difference between the various cells is relatively low but escalates rapidly considering

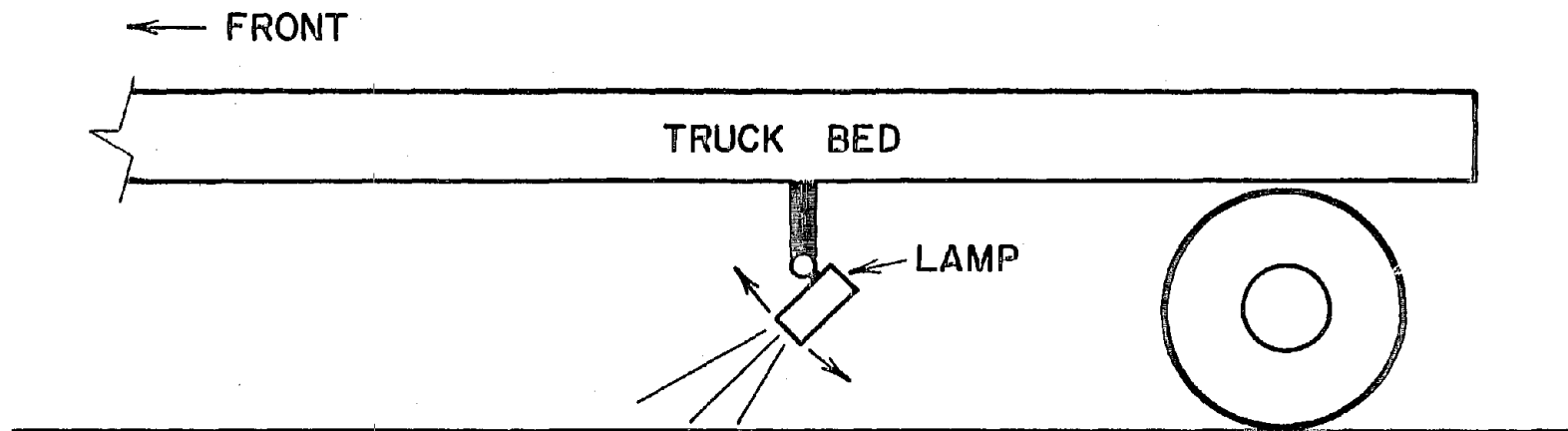


Figure 57. A high-intensity halogen bulb mounted under the test vehicle.

that an array with a 12-in (300-mm) span and an accuracy of 0.25 in (6.3 mm) contains 49 transducers.

The photo array is mounted in an in-line or staggered configuration depending on the selected transducer's physical size and the required resolution (see figure 58). Two louvers shade the array from direct exposure to sunlight, decreasing the background noise level. The optimum exposure acceptance angle for the transducers is adjustable by twisting the assembly to a position which provides minimal ambient light entry. Although the ideal position is perpendicular to the pavement, a maximum angle of 45 degrees in either direction is acceptable.

A flat ribbon cable connects the array to the controller circuit board. A flat cable is selected in order to minimize the vehicle bounce created as the tires roll over it at high speeds. The controlling electronics consists of a digital latch with an accompanying light-emitting diode (LED) display. Each LED represents one sensor in the array and is activated only when the vehicle light beam saturates its respective sensor. Activation of any sensor also generates a trigger pulse which is used to start the data acquisition computer. The data can be either manually read from the display and entered into the data acquisition computer through the keyboard or entered automatically via the digital input port on the acquisition board. A manual reset button clears the display between tests.

LASER-GUIDED SYSTEM

The laser tracking system operates in exactly the same manner as the photoelectric system, except a laser is substituted for the halogen lamp and the sensor array is moved to the side of the road. The active guidance option is the only major difference between the two systems.

A 5- to 10-mW helium neon laser operating in the 632.8-nm range, which emits a visible red beam of randomly polarized light, was selected as a light source for this method. Essentially it consists of a small plasma discharge tube with an internal 12-V power converter mounted on the side of the test vehicle. A single-axis beam expander is attached to the laser head to provide

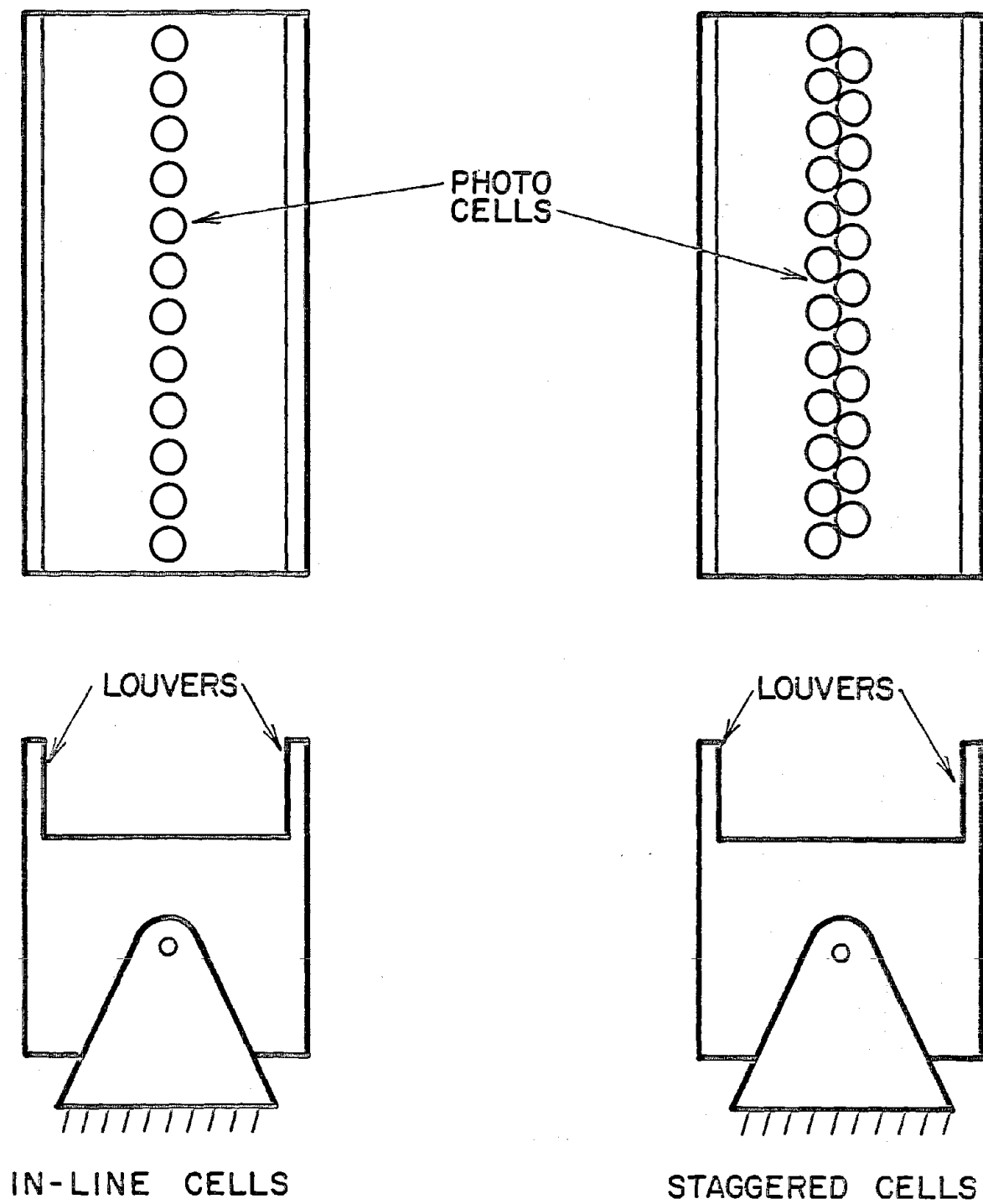


Figure 58. Two configurations for photo cell arrays.

a vertical fan-shaped output beam projected outward in front of the vehicle, as shown in figure 59.

This beam is intercepted by an array of near-infrared photodiodes mounted on the side of the road adjacent to the test section. As the vehicle approaches the section, the highly coherent laser beam illuminates one or more sensors, indicating the relative offset from the target centerline. An illuminated sign board replaces the LED display used above and serves as a visual feedback device, instructing the vehicle driver to move to the right or left in order to properly track the centerline. Each light on the sign board represents one sensor in the array and thus provides an error-magnitude measurement as well as a rate of correction measurement which helps to prevent excessive correction overshoot. The last position read by the sensors is automatically latched in the display for either manual or automatic entry into the data acquisition computer. The latch sequence also generates a pulse which is used to start data acquisition.

The test vehicle must have a reasonably tight and properly aligned suspension system for this tracking system to operate properly, as any fish tailing by the trailer will generate false readings.

ULTRASONIC SYSTEM

This method uses ultrasonic waves to judge distance, the same method used by bats when they fly. In operation, a sound pulse is transmitted from the edge of the test section toward the targeted vehicle and the return echo is detected and timed (figure 60). The elapsed time between the two pulses is proportional to the vehicle distance. A target-to-transmitter distance of 10 ft (3 m) translates into a period of approximately 17.55 ms with a resolution of 0.12 in (3.05 mm) over this range. Measurements can be made as far as 33 ft (10 m) away and still be accurate to within 1 percent.

If the target vehicle is a truck or tractor pulling an enclosed trailer, the physical vehicle can serve as the target. If the vehicle is pulling a flatbed trailer, a target must be mounted on the trailer to obtain accurate

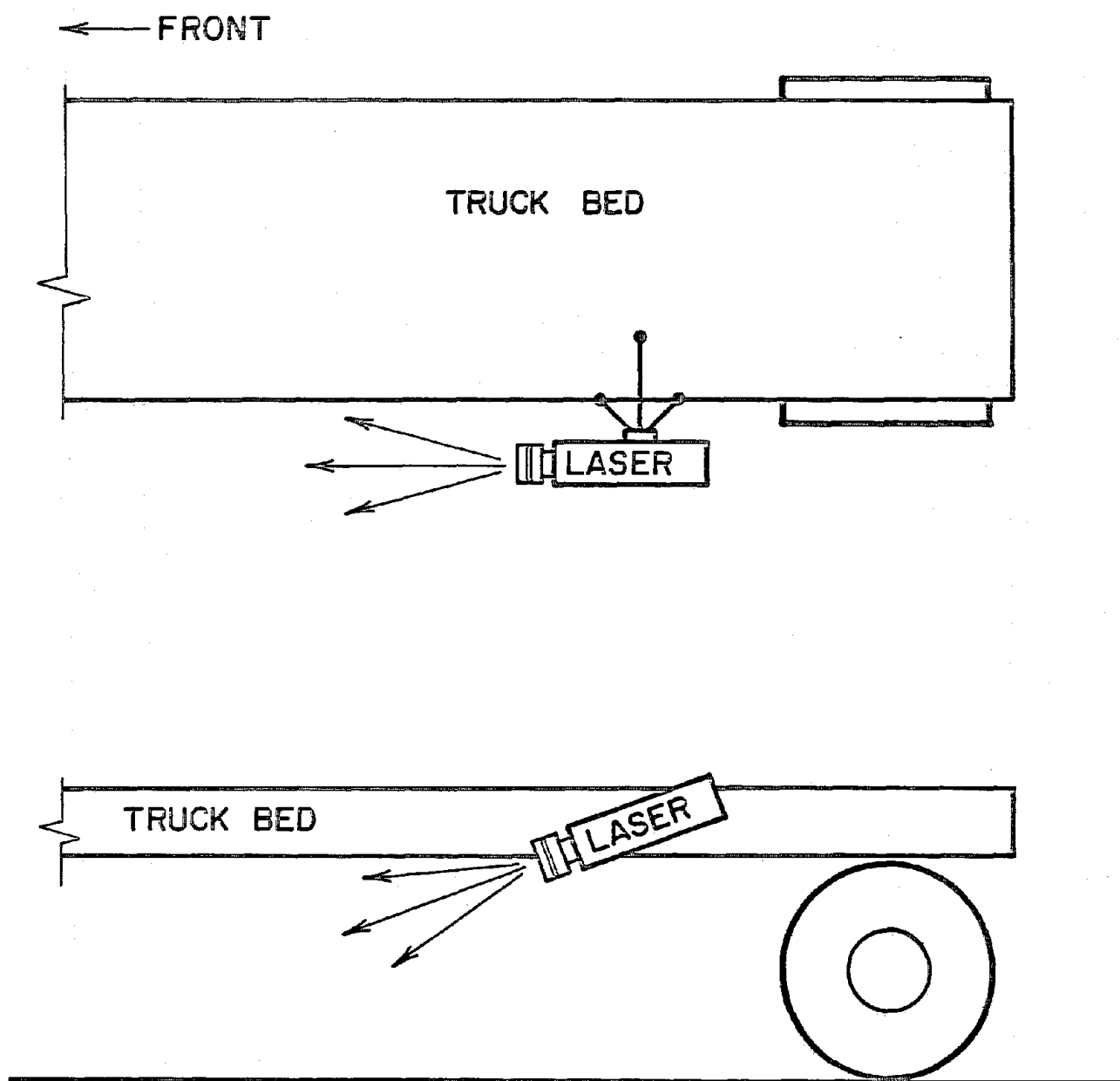


Figure 59. Sketch of a laser beam attached to the side of a test truck.

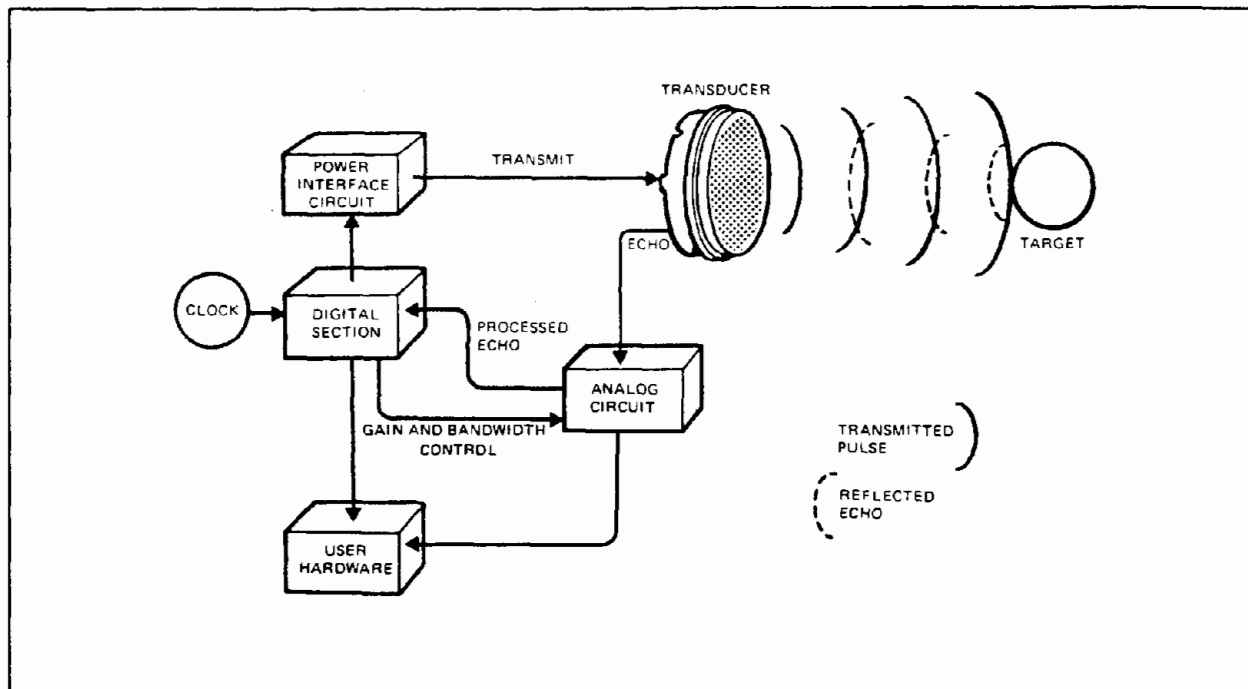


Figure 60. Transmitting and receiving a sound pulse.

measurements. A piece of 4- by 8-ft (1.2- by 2.4-m) plywood mounted perpendicularly to the road surface is an adequate target.

An optical system consisting of a pulsed infrared beam should be set up just before the test section. It is used in conjunction with a delay circuit to trigger the ranging system when the center of pulse is also used to start the data acquisition computer.

One channel of the data acquisition system receives both the transmitted and received pulses while internal system software calculates the period between them and converts them into engineering units for subsequent display and storage.

All three of the above-mentioned systems have both advantages and disadvantages. The photoelectric unit requires the vehicle to travel over a cable, limiting the system reliability because of cable wear. A stronger cable can be substituted, but large cable creates a sizeable bump in the road. The laser system has obvious advantages in the ability to direct the vehicle driver to correct for errors; it is also the most expensive system. Ultrasonic systems require no cables and no photocells or photodiodes on the test section and are the least expensive of the options; however, they require the most computer calculation time of the three. Careful software planning can overcome this potential problem.

10. PAVEMENT PERFORMANCE MODELS

Field testing has shown that the performance of flexible pavements can be related to certain failure mechanisms. From a structural capacity point of view, flexible pavement may experience two kinds of failure: fatigue, which shows as excessive alligator cracking, and rutting, which shows as permanent deformations along the wheel path.

Fatigue distress, the failure most often encountered in flexible pavements, causes the highest portion of rehabilitation cost. Researchers and investigators have proposed and implemented various types of laboratory tests and field measurements in an effort to predict the fatigue failure in actual pavements. Whether laboratory testing or theoretical analysis is used, the idea of relating tensile strain at the bottom of the asphalt layer to the number of load repetitions was adopted by several researchers. Rauhut and Kennedy show 13 different curves that related strains in asphalt concrete to the number of load repetitions of 18-kip axle load.^[65] Eleven relations were obtained through laboratory testing with different loading conditions, and two were produced from multiple regression analysis of the data from the AASHO Road Test. The equations for the 13 different curves follow the general form, shown as:

$$N_f = K_1 \left(\frac{1}{\epsilon} \right)^{K_2} \quad (6)$$

where

N_f = number of load cycles to failure for a loading that results in a tensile strain

ϵ = the critical horizontal strain at the bottom of asphalt concrete layer

K_1, K_2 = coefficients depending on material properties and temperature

Equation 6 indicates that the fatigue life of a flexible pavement may be predicted if the critical horizontal strain at the bottom of the asphalt concrete layer is evaluated.

Concerning rutting, several failure criteria have been recommended. The majority use correlations between strains and load repetitions. Correlations between the vertical strain on the surface of the subgrade and the number of equivalent single-axle load (ESAL) repetitions is widely used.^[66] Other rutting criteria correlate the rate of permanent strain to the elastic vertical strain and the number of load repetitions. The Asphalt Institute rutting criteria are among the most widely used in pavement design.^[67] The criteria provide the allowable number of ESAL repetitions for various levels of compressive strains at the subgrade surface. This type of criterion assumes that no permanent deformation occurs in the layers above the subgrade. Therefore, it is mandatory that material specifications for these layers be closely controlled to ensure minimal deformations.

PDMAP Pavement Performance Models

A recent NCHRP study recommends equations to predict the number of load repetitions to develop 10- and 45-percent-fatigue class 2 cracking in the wheel path.^[68] The study was based on data from the AASHO Road Test and laboratory tests on material from the Road Test sections. The forms of the equations are:

$$\log N_f (10\%) = 15.947 - 3.291 \log (\epsilon/10^{-6}) - 0.854 \log (|E^*|/10^3). \quad (7)$$

and

$$\log N_f (45\%) = 16.086 - 3.291 \log (\epsilon/10^{-6}) - 0.854 \log (|E^*|/10^3). \quad (8)$$

where

- N_f = load applications of constant stress to cause fatigue failure
- ϵ = critical tensile strain at bottom of asphalt concrete layer
- $|E^*|$ = complex modulus of elasticity of asphalt concrete in psi

Equations 7 and 8 indicate that the amount of fatigue cracking is a function of the critical tensile strain and the stiffness of the asphalt layer.

A rutting prediction criterion is also recommended.^[68] A regression analysis procedure was used to correlate the rate of rutting with various

combinations of primary response factors. The study concluded that the most significant correlations were obtained with vertical deflection at the surface of the pavement, followed by vertical compressive stress at the interface with asphaltic concrete. Two rutting prediction models are recommended by this study. For an asphalt concrete layer less than 6 in (152 mm):

$$\log RR = -5.617 + 4.343 \log d - 0.167 \log (N_{18}) - 1.118 \log \sigma_c \quad (9)$$

For an asphalt concrete layer equal to or greater than 6 in (152 mm):

$$\log RR = -1.173 + 0.717 \log d - 0.658 \log (N_{18}) + 0.666 \log \sigma_c \quad (10)$$

where

RR = rate of rutting, microinches per axle load repetition

d = surface deflection $\times 10^3$ in

σ_c = vertical compressive stress at interface with asphaltic concrete, psi

N_{18} = equivalent single-axle loads $\times 10^5$

TEXAS TRANSPORTATION INSTITUTE PAVEMENT PERFORMANCE MODEL

This model is based on a modified version of the ILLI-PAVE program.^[69] The specific types of distress included in the model are fatigue cracking, rutting in the wheel paths, and slope variance on the surface.

The fatigue model follows the phenomenological approach, where the fatigue life of the pavement is related to the tensile strain at the bottom of the surface layer. The relationship is given by:

$$N_f = K_1 \left(\frac{1}{\epsilon} \right)^{K_2} \quad (11)$$

The TTI model assumes that the K_1 and K_2 constants are related to the fracture properties of the mix. Therefore, K_1 and K_2 are expressed as:

$$K_1 = \frac{d^{1-\frac{n}{2}} \left(\frac{C_0}{d} \right)^{1-nq}}{A(1-nq)(Er)^n} \quad (12)$$

and

$$K_2 = n \quad (13)$$

where

$$n = 2 (1 + m)^{1/2}$$

d = depth of the beam

m = slope of the log creep compliance curve

C_0 = initial crack length

E = modulus of the material

r and q = regression constants

The rutting model uses a three-parameter function that relates permanent strain to loading cycles. The equation describing the relationship is represented by the form:

$$\epsilon_a = \epsilon_0 e^{-(\rho/N)^\beta} \quad (14)$$

where

ϵ_a = pavement strains

N = number of load cycles

ϵ_0 , ρ , and β = material parameters

The material parameters ϵ_0 , ρ , and β are variables derived from a permanent deformation test. Various forms of equations which relate these parameters to properties such as stress state, density, moisture, temperature, and other material characteristics were developed.

The model describes the rut depth as dependent on the vertical resilient strain in each layer and on the fractional increase of total strains. The total rut depth under a single-axle load as a function of the number of load applications can be found from the following relationship:

$$\delta_a(N) = \sum_{i=1}^n \left\{ \frac{\epsilon_{oi}}{\epsilon_{ri}} e^{-\left(\frac{\rho_i}{N}\right)^{\beta_i}} \int_{d_{i-1}}^{d_i} \epsilon_c(Z) dZ \right\} \quad (15)$$

where

N = number of load applications

n = number of pavement layers

d_1, \dots, d_n = depths of each layer in the pavement

ϵ_c = compressive strain at depth z under center of tire

$\frac{\epsilon_o}{\epsilon_r}$, ρ , β = material parameters obtained from laboratory tests

Similarly, the rut depth at some specific number of load repetitions by the tandem-axle load can be calculated as:

$$\delta_a(N) = \sum_{i=1}^n \left\{ \frac{\epsilon_{oi}}{\epsilon_{ri}} e^{-\left(\frac{\rho_i}{N}\right)^{\beta_i}} \int_{d_{i-1}}^{d_i} \left(1 + \frac{\Delta\sigma(Z)}{\sigma_{\max}(Z)}\right) \epsilon_c(Z) dz \right\} \quad (16)$$

where

$\Delta\sigma(Z)$ = difference between vertical σ_{\max} and σ_{\min} at depth z under center of tire

$\sigma_{\max}(Z)$ = maximum vertical stress at depth z under center of tire

VESYS PAVEMENT PERFORMANCE MODEL

The VESYS computer model was developed by FHWA in cooperation with other agencies.^[70] Several versions of the VESYS computer program have been developed which consider the elastic, viscoelastic, plastic, and fatigue

properties of the pavement materials. The program includes models to predict pavement distress in terms of fatigue as well as low-temperature cracking, rutting, and roughness.

The fatigue cracking is predicted using a probabilistic Minor's hypothesis. The criterion for fatigue cracking is based on fatigue resulting from the tensile strain at the bottom of the asphalt-bound layer. It is given as follows:

$$C_q(t) = n_q/N_q \quad (17)$$

where

- $C_q(t)$ = increment to the crack index resulting from a repetition of loads in the q-th incremental analysis period
- n_q = the number of axle loads applied to the pavement in the q-th incremental analysis period
- N_q = the number of loads to failure under temperature and strain conditions of the q-th time interval.

$$N_q = K_{1q} (1/\epsilon_q)^{K_{2q}} \quad (18)$$

where

- ϵ_q = radial strain response
- K_{1q} and K_{2q} = material fatigue properties

The crack index at any time is obtained by the summation of the incremental crack indices for previous incremental analysis periods. A crack is initiated at the bottom of the asphalt-bound layer when the expected value of the crack index equals one. The expected area cracked in square feet per 1,000 square feet is further calculated.^[70]

The rut depth is determined using the viscoelastic-plastic layer theory and the repeated-load laboratory testing. The wheel load is represented by a

haversine pulse, while the flexible pavement deflection response curve due to the n-th load repetition takes the form of a haversine pulse with an unrecoverable portion. The permanent deformation is represented for each incremental analysis period as:

$$R_p(n) = R \times f(n) \quad (19)$$

$R_p(n)$ = permanent deformation at load repetition n

R = peak deflection response of pavement surface as a function of load duration and temperature

$f(n)$ = a monotonically decreasing function of the number of previously applied loads

The integration of equation 19 for various layers over the expected number of load repetitions yields the accumulated rut depth. Therefore, the rut depth is the summation of the permanent deformations of all layers.

11. GENERALIZED MODULUS BACKCALCULATION PROCEDURES

A key requirement of this study is to be able to take the output of pavement instrumentation under known loadings and convert it to appropriate layer moduli. The instrumentation to be used includes strain gauges, pressure cells, and deflection sensors. The conversion will be made using calculations made with linear elastic or nonlinear elastic theory. In either case, a search routine is needed to minimize error between the measured reading (stress, strain, or displacement) and the computed value. In the search routine, the solution is the set of layer moduli which produces the best fit between measured and calculated values.

A growing body of knowledge already exists in this area with regard to the backcalculation of layer moduli under nondestructive test loading (NDT), such as with the falling weight deflectometer (FWD). The aim is to match measured surface deflections with those calculated using assumed layer moduli. For more than 2 decades, the matching process has been trial and error, with few rules to guide the analyst. In recent years several automatic search routines have been developed which minimize error between measured and calculated deflection bowls. One such routine is the CHEVDEF routine; the other is the generalized backcalculation procedure.^[71, 72, 73] The generalized procedure has great potential for assisting in this project. The details of this procedure are given below. It has already been used to backcalculate layer moduli from multidepth deflectometer data, and it can easily be modified to process stress or strain profiles.^[74]

The ultimate goal of the backcalculation process from NDT results is to estimate the pavement material properties. The procedure is to find the set of parameters which corresponds to the best fit of the measured deflection bowls. The best fit is achieved by minimizing the error between the measured and calculated deflection bowls. The objective function can therefore be written as:

$$\text{minimize} \quad \epsilon^2 = \sum_{i=1}^S \left[\frac{W_i^m - W_i^c}{W_i^m} \right]^2 W_{e_i} \quad (20)$$

where

ϵ^2 = squared error

W_i^m = measured deflection at sensor i

W_i^c = computed deflection at sensor i

s = number of sensors

W_{e_i} = user supplied weighing factor for sensor i

Equation 20 can be written simply as

$$\text{minimize} \quad \epsilon^2 = \sum_{i=1}^s \left[1 - \frac{W_i^c}{W_i^m} \right]^2 W_{e_i} \quad (21)$$

Different techniques are available for minimizing the objective function expressed in equation 21. The unknown variables are those required to compute the surface deflection, W_i^c :

$$W_i^c = F_i (X_j) \quad (22)$$

where

X_j = unknown variables $j = 1$ to n unknowns

Any solution to equation 21 calls for a solution of equation 22, obtained numerically in most cases by running a separate program (such as the BISAR, or CHEVRON computer program in the case of linear elasticity and ILLI-PAVE in the case of nonlinear elasticity). The number of calls depends on the minimization algorithm used. For example, the CHEVDEF program calls the deflection computation program $(N_{\text{LAYER}} + 1) * \text{ITER} + 1$ times for each bowl to be analyzed, where N_{LAYER} is the total number of layers for which moduli are to be determined, and ITER is the number of iterations.^[71] Generally, the pattern search technique requires numerous calls of the deflection computation program for each measured bowl, which can be inefficient when a large number of bowls are to be analyzed for a single project, as is frequently the case. This drawback is overcome in this system by generating, ahead of time, a

databank containing deflection bowls for the expected range of moduli and using the 3-point Lagrange interpolation technique to compute the deflection bowl for any set of unknown values within the expected range. After the generation of the databank, the deflection computer program is no longer required.

In the case of linear elasticity, the computed deflection, W_i^c , at sensor i (or radial distance r_i ,) can be expressed as follows:

$$W_i^c = f_i (E_k, \nu_k, h_k, r_i, 0) \quad (23)$$

where

E_k, ν_k = modulus of elasticity and Poisson's ratio of layer k (k = 1 to n layers)

h_k = thickness of layer k

0 = other variables, such as pressure, contact area, radius, and interface conditions

In the backcalculation, all variables except E_k are either assumed or known, and the moduli are the only variables to be backcalculated.

In the case of linear elasticity and a circular contact area, equation 23 can be written as:

$$W_i^c = \frac{p}{E_{sg}} f_i \left[\frac{E_1}{E_{sg}}, \dots, \frac{E_k}{E_{sg}}, \dots, \frac{E_n}{E_{sg}} \right] \quad (24)$$

where

p = pressure (psi)

E_{sg} = subgrade modulus of elasticity

Equation 24 represents a unique property of linear elasticity in that the deflection is (1) linearly related to the load level, (2) inversely proportional to the subgrade modulus, and (3) a function of the modular ratios.

Using equations 21 and 24, it is possible to obtain a direct solution for the subgrade modulus, E_{sg} . To minimize the squared error of equation 21 with regard to E_{sg} requires that its derivative with regard to E_{sg} be zero, as follows:

$$2\varepsilon \frac{\partial \varepsilon}{\partial E_{sg}} = \sum_{i=1}^S 2 \left[1 - \frac{W_i^c}{W_i^m} \right] - \left[\frac{1}{W_i^m} \frac{\partial W_i^c}{\partial E_{sg}} \right] W e_i = 0 \quad (25)$$

and, from equation 24

$$\frac{\partial W_i^c}{\partial E_{sg}} = \frac{\partial}{\partial E_{sg}} \left[\frac{P}{E_{sg}} f_i \left(\frac{E_k}{E_{sg}} \right) \right] \quad (26)$$

For the sake of clarity, the term $f_i (E_k/E_{sg})$ is replaced by f_i in the equations below:

$$\frac{\partial W_i^c}{\partial E_{sg}} = -\frac{P}{E_{sg}^2} f_i + \frac{P}{E_{sg}} \frac{f}{\partial E_{sg}} (f_i) \quad (27)$$

When the ratio E_k/E_{sg} is kept constant, i.e., at a particular set of modular ratios in the data base, the second term in equation 27 is zero; therefore, equation 27 can be written as:

$$\frac{\partial W_i^c}{\partial E_{sg}} = -\frac{W_i^c}{E_{sg}}$$

substituting back into equation 25 yields:

$$\sum_{i=1}^S \left[1 - \frac{W_i^c}{W_i^m} \right] \left[\frac{W_i^c}{W_i^m} \frac{1}{E_{sg}} \right] W e_i = 0 \quad (28)$$

using equation 24 to substitute back for W_i^c yields

$$\sum_{i=1}^S \left[1 - \frac{pa}{E_{sg}} \frac{f_i}{W_i} \right] \left[\frac{pa}{E_{sg}} \frac{f_i}{W_i} \right] W_{e_i} = 0 \quad (29)$$

This equation simplifies to:

$$\frac{1}{E_{sg}} \left[\frac{p^2}{E_{sg}} \right] \sum_{i=1}^S \left[\frac{E_{sg}}{pa} - \frac{f_i}{W_i} \right] \left[\frac{f_i}{W_i} \right] W_{e_i} = 0 \quad (30)$$

Normalizing equation 30 with regard to f_1 yields:

$$\sum_{i=1}^S \left[\frac{E_{sg}}{p} - \frac{f_i}{f_1} \frac{1}{W_i} \right] \left[\frac{f_i}{f_1} \frac{1}{W_i} \right] W_{e_i} = 0 \quad (31)$$

This equation leads to:

$$E_{sg} = \frac{p \sum_{i=1}^S \frac{f_i}{f_1} \frac{W_{e_i}}{W_i^2}}{\sum_{i=1}^S \frac{f_i}{f_1} \frac{W_{e_i}}{W_i}} \quad (32)$$

Although equation 32 can be simplified, this normalized form is preferred for data processing. Equation 32 provides a direct method for estimating subgrade modulus E_{sg} from the data base of normalized (f_i/f_1) deflection values. This data base, as is demonstrated below, is built from multiple runs of the BISAR program.^[29] Each run corresponds to set of modular ratios E_k/E_{sg} . Therefore an E_{sg} can be calculated for each set of $f_i(E_k/E_{sg})$. To decide which solution minimizes error, it is necessary to calculate squared error associated with each set of modular ratios. Equation 33, an expanded version of equation 21 is used:

$$\epsilon^2 = \sum_{i=1}^S \left[1 - \frac{p f_i}{E_{sg} W_i} \right]^2 W_{e_i} \quad (33)$$

E_{sg} is the particular solution of equation 32 corresponding to the given modular ratio, and p is the actual pressure under which the W_i^c value was calculated. By locating the minimum squared error from equation 33, a

seed value of E_{sg} is selected and the corresponding seed values of E_{EASE} and $E_{SURFACE}$ are calculated. These seed values are used as input to the pattern search routine.

12. REFERENCES

1. D. A. Anderson, P. Sebaaly, N. Tabatabaee, R. Bonaquist, and C. Churilla, Pavement Testing Facility-Pavement Performance of the Initial Two Test Sections, Final Report No. FHWA/RD-88/060, Federal Highway Administration, Washington, DC, 1988.
2. Department of Main Roads, Pavement Accelerated Loading Facility (ALF). Design, Construction and Development - Mechanical and Structural Aspect, New South Wales, Australia, February 1985.
3. Organisation for Economic Cooperation and Development, Full-Scale Pavement Tests, Paris, 1985.
4. D. J. VanVurren, "Pavement Performance in the S12 Road Experiment, An AASHTO Satellite Test Road in South Africa," Third International Conference on the Structural Design of Asphalt Pavements, Volume I Proceedings, 1972.
5. P. Ullidtz and B. Christian, "Laboratory Testing of a Full-Scale Pavement: The Danish Road Testing Machine," Transportation Research Record 715, Transportation Research Board, Washington, DC, 1979.
6. R. Dempwolf, and P. Sommer, "Comparison between Measured and Calculated Stresses and strains in Flexible Road Structures," Third International Conference on the Structural Design of Asphalt Pavements, Volume I Proceedings, 1972, pp. 786-794.
7. Organisation for Economic Cooperation and Development, Strain Measurements in Bituminous Layers, Paris, 1985.
8. D. A. Anderson, W. P. Kilaeski, and R. F. Bonaquist, Fourth Cycle of Pavement Research at the Pennsylvania Transportation Research Facility. Vol. 1. Construction and Operation of the Pavement Durability Research Facility, Final Report No. FHWA/PA 84/023, Federal Highway Administration, Washington, DC, 1984.
9. J. F. Potter, H. G. Mayhew, and A. P. Mayo, Instrumentation of the Full Scale Experiment on A1 Trunk Road at Conington, Huntingdonshire, Report LR 296, Road Research Laboratory, 1969.
10. J. T. Christison, K. O. Anderson, and B. P. Shields, "In Situ Measurements of Strains and Deflections in a Full-Depth Asphaltic Concrete Pavement," Proceedings of the Association of Asphalt Paving Technologists, Vol. 47, 1978, pp. 398-433.
11. Applications Note 290-1 Practical Strain Gauge Measurement, Hewlett-Packard Company, Palo Alto, California, May 1987.
12. Thompson, "On the Electro-Dynamic Qualities of Metals," Transactions of the Royal Philosophical Society, London, No. 146, 1956, pp. 649-751.

13. E. C. Eaton, "Resistance Strain Gauge Measures Stresses in Concrete," Engineering News Record, No. 107, October 1931, pp. 515-616.
14. A. Bloach "New Methods for Measuring Mechanical Stresses at Higher Frequencies," Nature, No. 136, August 1935, pp. 223-224.
15. T. G. Beckwith and N. L. Buck, Mechanical Measurements, Addison Wesley Publishing Company, 1969.
16. L. J. Weymouth, J. E. Starr, and J. Dorsey, "Bonded Resistance Strain Gauges," Experimental Mechanics, Vol. 6, No. 4, April 1966, p. 19A.
17. Semiconductor Strain Gauges, Bulletin 102, BLH Electronics, Canton, Massachusetts, 1985.
18. S. F. Brown, "State-of-the-Art Report on Field Instrumentation for Pavement Experiments," Transportation Research Record, 640, Transportation Research Board, Washington, DC, 1977, pp 13-28.
19. P. Ulidtz, Pavement Analysis, Elsevier Press, 1987.
20. Dynatest 8000 FWD Test System, Dynatest Consulting, Inc., Ojai, California.
21. Pressure, Strain and Force Measurement Handbook and Encyclopedia, Omega Engineering, Inc., Stamford, Connecticut, 1987.
22. A. J. G. Klomp and T. W. Niesman, "Observed and Calculated Strains at Various Depths in Asphalt Pavements," Proceedings, Second International Conference on the Structural Design of Asphalt Pavements, University of Michigan, 1967, pp. 671-688.
23. M. Muhtalla, personal communication.
24. R. H. Ledbetter, J. L. Rice, H. H. Ulery, F. W. Kearney, and J. B. Gambill, Multiple Wheel Heavy Gear Load Pavement Tests, Vol. IIIA, Technical Report S-71-17, U.S. Army Engineer Waterways Experiment Station, Vicksburg, Mississippi, November 1971.
25. "Bison Model 4101A," Bison Specifications, Bison Instruments, Inc., Minneapolis, Minnesota.
26. W. J. Horn and R. H. Ledbetter, Pavement Response to Aircraft Dynamic Loads, Vol 2, U.S. Army Engineer Waterways Experiment Station, Vicksburg, Mississippi, Technical Report S-75-11, June 1975.
27. E. T. Selig, "Soil Strain Measurement Using Inductance Coil Method," in Performance Monitoring for Geotechnical Construction, ASTM STP 584, American Society of Testing Materials, Philadelphia, Pennsylvania, 1975, pp. 141-158.
28. R. Addis, personal communication, 1988.

29. BISAR, Computer Program User's Manual, Amsterdam, Koninklijke Shell Laboratorium, 1972.
30. P. E. Sebaaly, Dynamic Models for Pavement Analysis, Ph.D., Dissertation, Department of Civil Engineering, Arizona State University, May 1987.
31. E. T. Selig, "A Review of Stress and Strain Measurement in Soil," Proceedings on Soil-Structure Interaction, Tucson, Arizona, 1964.
32. A. C. Torry, and R. W. Sparrow, "The Influence of the Diaphragm Flexibility on the Performance of an Earth Pressure Cell," Journal of Scientific Instruments, No. 44, 1967, pp. 781-785.
33. J. Dunnicliff, Geotechnical Instrumentation for Monitoring Field Performance, John Wiley & Sons, Inc. 1988.
34. R. Collins, K. J. Lee, G. P. Lily, and R. W. Westmann, "Mechanics of Pressure Cells," Experimental Mechanics, Vol. 12, No. 11, 1972, pp. 514-519.
35. P. E. Fossberg, "Load Deformation Characteristics of Three-Layer Pavements Containing Cement Stabilized Base," University of California, Ph.D. Thesis, 1970.
36. T. Kallstenius, and W. Bergau, "Investigation of Soil Pressure Measuring by Means of Cells," Proceedings of Royal Swedish Geotechnical Institute, No. 12, 1956.
37. K. R. Peattie and R. W. Sparrow, "The Fundamental Action of Earth Pressure Cells," Journal of Mechanics and Physics of Solids, Vol. 2, 1954, pp. 141-155.
38. A. C. Whiffin and S. A. H. Morris, "Piezoelectric Gauge for Measuring Dynamic Stresses Under Roads," The Engineer, No. 213, April 27, 1962, pp. 741-746.
39. S. F. Brown and B. V. Brodrick, "The Performance of Stress and Strain Transducers for Use in Pavement Research," Science Research Council, University of Nottingham, England, Research Report No. SFB/BVB/593.13, June 1973.
40. W. J. Horn, and R. H. Ledbetter, Pavement Response to Aircraft Dynamic Loads, Vol. 1, Technical Report S-75-11, U.S. Army Engineer Waterways Experiment Station, Vicksburg, Mississippi, June 1975.
41. Bulletin No. KG-1000A, Kulite Semiconductor Products Inc., Ridgefield, New Jersey.
42. P. F. Hadala, "The Effect of Placement Method on the Response of Soil Stress Gauges," Proceedings of the International Symposium on Wave Propagation and Dynamic Properties of Earth Materials, The University of New Mexico Press, Albuquerque, New Mexico, 1967, pp. 255-263.

43. E. T. Selig, "Soil Stress Gage Calibration," Geotechnical Testing Journal, Vol. 3, No. 4, American Society of Testing Materials, Philadelphia, Pennsylvania, December 1980, pp. 153-158.
44. Technical Bulletin 4501E, Schaevitz Engineering, Pennsauken, New Jersey, 1986.
45. Mark Products, Inc., Houston, Texas.
46. T. Scullion, "Using the Multidepth Deflectometer to Verify Modulus Backcalculation Procedures," First Symposium on NDT of Pavements and Backcalculation of Moduli, Baltimore, Maryland, June 1988.
47. T. J. Seebeck, Evidence of the Thermal Current of the Combination Bi-Cu by Its Action on Magnetic Needle, Royal Academy of Science, Berlin, 1822-1823, p. 265.
48. Manual on the Use of Thermocouples in Temperature Measurement, American Society for Testing and Materials Committee E-20, 1981.
49. Temperature Measurement Designer's Guide, Thermo Electric Co., Inc., Saddle Brook, New Jersey, 1988.
50. Omega Complete Temperature Measurement Handbook and Encyclopedia, Vol. 26, Omega Engineering, Inc., Stamford, Connecticut, 1988.
51. Gordon Temperature Measurement, Gordon Company, Richmond, Illinois.
52. Practical Temperature Measurements, Application Note 290, Hewlett Packard Company, Palo Alto, California.
53. Linear Products Databook, Analog Devices, Inc., Norwood, Massachusetts, 1988.
54. Operator's Manual: AD590 Temperature Sensor, Omega Engineering, Inc., Stamford, Connecticut, 1987.
55. B. J. Dempsey, W. A. Herlache, and A. J. Patel, Environmental Effects on Pavements--Theory Manual, Volume 3, FHWA/RD-84/115, Federal Highway Administration, Washington, DC, 1985.
56. R. L. Berg, G. L. Guymon, and T. C. Johnson, Mathematical Model to Correlate Frost Heave of Pavements with Laboratory Predictions, Interim Report No. FHWA-RD-79-71, Federal Highway Administration, Washington, DC, 1980.
57. S. J. Liu, and R. L. Lytton, "Rainfall Infiltration, Drainage, and Load-Carrying Capacity of Pavements," Transportation Research Record 993, Transportation Research Board, Washington, DC, 1984, pp 28-35.
58. Two-Probe Density Gauge Model 2376, Instruction Manual, Troxler Electronics Lab, North Carolina.

59. R. J. Lascarno, "Field Calibration of Neutron Meters Using a Two Probe Gamma Density Range," Soil Science, June 1986.
60. C. J. Phene, G. J. Hoffman, and S. L. Rawlins, "Measuring Soil Matric Potential Insitu by Sensing Heat Dissipation within a Porous Body: I. Theory and Sensor Construction," Soil Society of America Proceedings, Volume 35, 1971, pp 27-33.
61. B. T. Kulakowski and D. R. Luhr, "Effects of Different Tire Sizes and Pressures on Pavement Performance," Pennsylvania Transportation Institute, University Park, PA, 1988 (ongoing research).
62. M. C. Chi, "Analysis of Dynamic Truck Tire-Pavement Interaction," M. S. paper in Mechanical Engineering, The Pennsylvania State University, December 1987.
63. G. Magnusson, "Measurement of Dynamic Wheel Load," VTI Report No. 279A, Linkoping, Sweden, 1987.
64. C. A. Lysdale and R. R. Hegmon, Wheel Force Transducers, Report No. FHWA/RD-80/133, Federal Highway Administration, Washington, DC, May 1979.
65. B. G. Rauhut and T. W. Kennedy, "Characterizing Fatigue Life for Asphalt Concrete Pavements," Transportation Research Record 888, Transportation Research Board, Washington, DC, 1982.
66. G. M. Dorman and C. T. Metcalf, "Design Curves for Flexible Pavements Based on Layered System Theory," Highway Research Record 71, Highway Research Board, 1965.
67. Documentation of the Asphalt Institute's Thickness Design Manual, No. 14 (RS-14), 7th edition, The Asphalt Institute, College Park, Maryland, 1964.
68. F. Finn, C. L. Saraf, R. Kulkarni, K. Nair, W. Smith, and A. Abdullah, Development of Pavement Structural Subsystems, NCHRP No. 291, Transportation Research Board, Washington, DC, December 1986.
69. ILLI-PAVE: A computerized pavement analysis program provided by the Transportation Facilities Group, Department of Civil Engineering, University of Illinois at Urbana-Champaign.
70. W. J. Kenis, Predictive Design Procedures. VESYS User Manual--An Interim Design Method for Flexible Pavements Using VESYS Structural Subsystem, Final Report No. FHWA-RD-77-154, Federal Highway Administration, Washington, DC, January 1978, pp. 128.
71. A. J. Bush, Nondestructive Testing of Light Aircraft Pavements, Phase II. Development of the Nondestructive Evaluation Methodology, Report No. FHWA/RD-80/911, 1980.

72. J. Uzan, R. L. Lytton, and F. P. Germann, "General Procedures for Backcalculating Layer Moduli," First Symposium on NDT of Pavements and Backcalculation of Moduli, ASTM, Baltimore, July, 1988.
73. J. Uzan, T. Scullion, C. H. Michalek, M. Parades, and R. L. Lytton, "A Microcomputer Based Procedure for Backcalculating Layer Moduli from FWD Data", Texas Transportation Institute Research Report 1123-1, July, 1988.
74. T. Scullion, T. Uzan, J. Yazdani, and P. Chan, "Field Evaluation of the Multidepth Deflectometer," Texas Transportation Institute Research Report 1123-2, September 1988.